Spring 2004

Microdischarge Arrays

Wenhui Shi
Old Dominion University

Recommended Citation

Shi, Wenhui. "Microdischarge Arrays" (2004). Doctor of Philosophy (PhD), Dissertation, Electrical & Computer Engineering, Old Dominion University, DOI: 10.25777/40yk-0p53
https://digitalcommons.odu.edu/ece_etds/132

MICRODISCHARGE ARRAYS

by

Wenhui Shi
B.S. July 1987, Changchun Institute of Optics & Fine Mechanics

M.S. August 1998, Old Dominion University

A Dissertation Submitted to the Faculty of
Old Dominion University in Partial Fulfillment of the
Requirement for the Degree of

DOCTOR OF PHILOSOPHY

ELECTRICAL ENGINEERING

OLD DOMINION UNIVERSITY
May 2004

Approved by:

Karl H. Schoenbach (Director)

Ravindra P. Joshi (Member)

Gilbert R. Hoy (Member)

Linda Vahala (Member)

ABSTRACT

MICRODISCHARGE ARRAYS

Wenhui Shi
Old Dominion University, 2004
Director: Dr. Karl H. Schoenbach

Microhollow cathode discharges (MHCDs) are DC or pulsed gas discharges between two electrodes, separated by a dielectric, and containing a concentric hole. The diameter of the hole, in this hollow cathode configuration, is in the hundred-micrometer range. MHCDs satisfy the two conditions necessary for an efficient excimer radiation sources: (1) high energy electrons which are required to provide a high concentration of excited or ionized rare gas atoms; (2) high pressure operation which favors excimer formation (a three-body process). Flat panel excimer sources require parallel operation of MHCDs. Based on the current-voltage characteristics of MHCD discharges, which have positive slopes in the low current (Townsend) mode and in the abnormal glow mode, stable arrays of MHCD discharges in argon and xenon could be generated in these current ranges without ballasting each MHCD separately. In the Townsend range, these arrays could be operated up to pressures of 400 Torr. In the abnormal glow mode, discharge arrays were found to be stable up to atmospheric pressure. By using semi-insulating silicon as the anode material, the stable operation of MHCD arrays could be extended to the current range with constant voltage (normal glow) and also that with negative differential conductance (hollow cathode discharge region). Experiments with a cathode

geometry without microholes, i.e. excluding the hollow cathode phase, revealed that stable operation of discharges over an extended area were possible. The discharge structure in this configuration reduces to only the cathode fall and negative glow, with the negative glow plasma serving to conduct the discharge current radially to the circular anode. With decreasing current, a transition from homogenous plasma to self-organized plasma filaments is observed. Array formation was not only studied with discharges in parallel, but also with MHCD discharges in series. By using a sandwich electrode configuration, a tandem discharge was generated. For an anode-cathode-anode configuration, the excimer irradiance, recorded on the axis of the discharge, was twice that of a single discharge. The extension of this basic tandem electrode structure to multiple electrode configurations permits the generation of high-irradiance excimer sources.

ACKNOWLEDGMENTS

I would like to express my appreciation and gratitude to my advisor, Dr. Karl H. Schoenbach, for his guidance and continuous support on my study. I would like to thank Dr.Gilbert R. Hoy, Dr. Linda Vahala, and Dr. Ravindra P. Joshi for serving on my dissertation committee.

I am grateful for the valuable discussions with Dr. Ahmed El-Habachi, Dr. Mohamed Moselhy, Dr. Chungqi Jiang, Dr. Robert Stark, Dr. Frank Leipold, and Dr. Sunao Katsuki. I also would like to thank Shu Xiao, Abdel-Aleam Mohamed and Ron Bentley for their help and cooperation during the course of this dissertation.

I extend many thanks to Dr. Jack Bufton for his patience and hours of guidance on the editing of this manuscript. I also thank my colleagues and friends for their help.

My gratitude is devoted to my wife, Lan Luo, for the love and support she has provided through my academic endeavors. Finally, I would like to thank my parents for their love and inspiration during the completion of this dissertation.

TABLE OF CONTENTS

APPENDIX

LIST OF TABLES

LIST OF FIGURES

CHAPTER I

INTRODUCTION

Increased need for Ultraviolet (UV) radiation sources in established markets and many new applications for UV emission are producing innovations in UV radiation sources. For several years, excimer molecules of rare gases have attracted great interest because of their ability to generate UV radiation. Excimer UV radiation is quasi-monochromatic radiation and wavelengths can be selected by changing gases. Excimer UV lamps based on dielectric-barrier discharges, are known and commercially available [1]. Recently, another possible realization of a UV emission source is a microhollow cathode discharge (MHCD) in the pressure range up to atmospheric pressure [2-6].

Microhollow cathode discharges (MHCD) are characterized by hollow structure scaled to several hundreds of micrometer in the cathode. The main advantage of this type of electrical discharge is that an non-equilibrium plasma up to atmospheric pressure can be established in an economic and reliable way. Much effort continues toward understanding the complex processes involved in this miniaturized hollow cathode discharge due to the possible commercial importance of this system. Recent investigations showed that MHCDs convert electrical energy into UV radiation with efficiency up to 20% in pulse mode [7]. In spite of these advantages, microhollow cathode discharges have suffered from the difficulty of being scalable to large areas. Most of the work on microhollow cathode discharge is based on single discharges. This produces a small radiation

---

Journal Mode used in this thesis is *Journal of Applied Physics.*

source ranging up to several millimeters in diameter. In this paper we report studies into the generation of microhollow cathode discharge arrays. This research is motivated by applications such as lighting, sterilization, environmental pollution control, laser, thin film deposition, material processing and ozone generation [8].

1.1 Ultraviolet (UV) radiation

Ultraviolet radiation is a small portion of the electromagnetic radiation with wavelengths ranging between visible spectrum (400 nm – 700 nm) and X-rays (10 nm – 100 nm). Ultraviolet light is roughly defined in boundaries (100 nm – 400 nm), in which there are four regions in terms of applications and properties (Table 1). The four regions are: **near (UV-A)**, **mid (UV-B)**, **deep (UV-C)** and **far (VUV).**

The "near-UV" is the region from 315 to 400 nm; the "mid-UV" is from 280 to 315 nm. The "deep-UV" from 200 nm to 280 nm is highest quantum energy part of the UV spectrum for which the atmosphere is transparent. The VUV (vacuum ultraviolet) or far-UV light, which is the portion from 100 nm to 200 nm, obtains its name because air strongly absorbs radiation at wavelengths below about 190 nm. As a result, experiments with VUV radiation can usually only be performed in a vacuum or in gases such as argon or nitrogen.

Because of its high photon energy (3 to 12 eV), UV radiation can initiate chemical reactions, break molecular bonds, or modify surfaces in specific ways.

As the wavelength becomes shorter, the absorption coefficients of most substances increase considerably, so that UV radiation is completely absorbed in a very thin surface layer. For the application of photo-lithography in semiconductors: the shorter the wavelength, the smaller the dimensions.

Table 1: Wavelength ranges of UV radiation

Classification	**Wavelength λ**	**Quantum Energy**
UV – A	315 – 400 nm	3.1 – 3.9 eV
UV – B	280 – 315 nm	3.9 – 4.4 eV
UV – C	200 – 280 nm	4.4 – 6.2 eV
VUV	100 – 200 nm	6.2 –12.4 eV

1.2 UV Sources

UV light is available from a variety of sources, including naturally occurring UV light, UV lamps, and UV lasers. Ultraviolet (UV) light is contained in the range of wavelengths produced by the sun. UV light from the sun is abundant, but most UV light is absorbed by the ozone layer or reflected back into space so only a small amount reaches the surface of the earth. UVA radiation plays important role in the generation of photochemical smog and also in fading and damaging to plastics, paints and fabrics. UVC is totally absorbed by ozone and other gases, and does not reach the earth's surface. Only 1% of solar radiation is within the UVB band, and most of this is absorbed by ozone. UV radiation from the sun cannot be easily or economically harnessed for the applications that have practical value.

One of the most important UV sources available today is the low-pressure glow discharge in a mercury/rare gas mixture [9]. Under optimum conditions, the mercury lamps can convert electrical energy into UV with surprisingly high efficiency. About 60-70% of the electrical input power is radiated at 253.7nm and roughly 10% at 184.9 nm. This source is utilized in fluorescence lighting to generate visible light. However, these optimum discharge conditions can be maintained only at fairly low electrical power densities of less than 100 mW/cm^3 for the plasma column and at very low mercury vapor pressures of about 1 Pa. The UV output of these lamps can reach about 0.2W/cm of discharge column. If a higher photon flux is required, different discharge conditions such as higher power density and gas pressure must be chosen. Arc discharges, which are operated at medium pressure (about 10^5 Pa), can generate much higher UV intensity with less efficiency (4 to 6%). One of the most promising UV sources for high photon flux is the excimer source.

1.3 Excimer UV sources

The term “excimer” comes from organic photochemistry as an abbreviation for an **EXCI**ted dim**MER**. An excimer is a complex with weakly bound excited states of molecules that under normal conditions do not process a stable ground state.

In an excimer complex, the interaction of the ground states of two closed-shell systems (atoms or molecules) is usually repulsive except for a weak long-range van der Waals or electrostatic interaction. But the interaction of an excited state with the same fragments of the ground state can form a strong chemical bond. The transition from bound excited state to continuum defines an excimer emission system. Excimers are unstable molecular complexes which occur only under extreme conditions, such as those temporarily existing in a special type of gas discharge. Typical examples are the molecular bonds between two rare gas atoms (Ar^*_2, Kr^*_2, Xe^*_2) or between a rare gas atom and a halogen atom (ArF^*, $KrCl^*$, $XeCl^*$). The asterisk (*) indicates the presence of an electronically excited molecular complex (excimer). Among the most striking properties of the excimer complex is that they disintegrate typically within less than a microsecond and, while they are decaying, give off their binding energy in the form of UV radiation. The advantage of an excimer UV source over other UV lamps is that the excimer radiates UV in only a very narrow band. Excimer sources allow selective, intensive UV radiation at specific wavelengths. Fig 1.1 shows the narrow-band emission spectra of different UV sources: xenon excimer (172 nm), krypton chloride (222 nm), and xenon chloride (308 nm). Since there are many known excimers, a gas mixture can be chosen for practically every required wavelength range.

Excimer UV sources are found to have strikingly high efficiency. Several theoretical models predicate efficiencies up to 70% [10, 11, 12]. Osram Sylvania has recently announced its latest excimer discharge lamps reaching efficiency

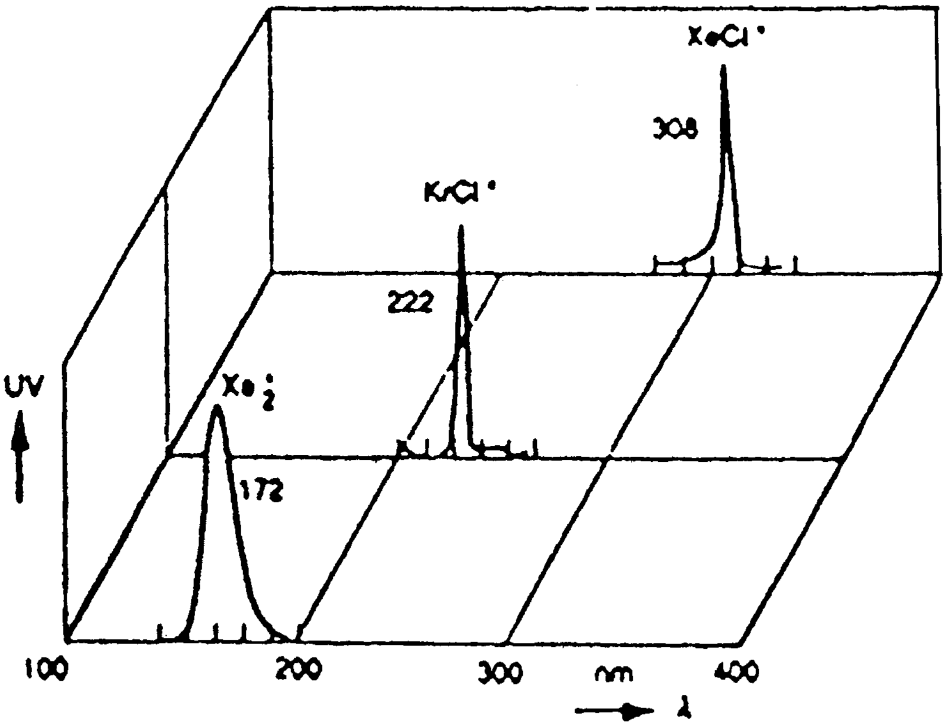

Fig 1.1 Emission spectra of excimer UV sources. [1]

40% [13]. The absence of radiation trapping and absorption is the main reason for this high efficiency. Due to a lack of stable ground state, reabsorption is absent in excimer discharge.

Besides the required UV radiation, excimer sources produce little visible and infrared radiation. The temperature of conventional excimer discharge lamp stays below 80 ^{0}C [13]. Therefore, heating of the irradiated material is largely avoided, and the lamp can be used to process heat-sensitive substrates.

Another advantage of excimer sources is their flexibility in shape. Besides the cylindrical discharge geometry, plane and other special curved or faceted geometries are possible. In many cases, the geometries of the excimer source are adapted to the object being irradiated.

1.4 Applications of Excimer UV Sources

1.4.1 UV curing

UV curing, the process of converting a liquid to a solid, by exposure to UV light, has become an established alternative to conventional drying [14, 15, 16]. The UV-curing properties are achieved by adding a so-called photoinitiator to the basic substances. When irradiated with UV light, the photoinitiator gives off free radicals, thereby starting the polymerization process in seconds. In addition to fast processing and improved product quality, a major advantage of UV curing is that no solvents are used and consequently emissions of volatile organic compounds (VOCs) are avoided. Excimer sources used in UV curing offer many benefits over conventional UV lamps. They are able to precisely match the photoinitiator absorption spectrum. Low temperature operating makes them more suitable in some applications. Furthermore, the scalability to large area and high photo flux can speed the curing process.

1.4.2 Surface processing

The cleaning and forming of material surfaces with excimer UV sources is an increasingly critical cutting edge technology. The UV/Ozone cleaning process provides a fast, low-cost method for providing organic-free surfaces prior to contaminant sensitive processes. UV removal of organic contaminants is mostly used in the glass cleaning process to manufacture liquid crystals. However, this technique is also increasingly applied in the fields of semiconductor and opt-electronic products because of easy handling and its excellent cleaning effect, ideal for thin film deposition where superior adhesion to the substrate is required, UV/Ozone cleaning can provide the final ultra-clean surface by removing residual layers of oils, condensed volatiles, and carbon traces in a matter of minutes. In the etching process of crystalline Quartz, the UV/Ozone cleaner can significantly reduce the quantity and size of surface pyramids and defects resulting from the asymmetric etching characteristics of the material [17]. The resulting "smoother" and more uniform surface produces a reliable starting point for subsequent critical processes.

Depositing metallic, dielectric or semiconductor layers is one of the most striking applications for excimer UV sources. Work on thin metal deposition with excimer UV sources was carried out at ABB research center [1, 18]. Photolytic processes can be used to obtain a thin palladium nucleation by selective photon dissociation of palladium film. Only a few simple and economical stages are needed to obtain a metal pattern on any substrate. Low temperature deposition of silicon dioxide and silicon nitride films was obtained by irradiating silane/nitrous oxide/ammonia mixtures.

1.4.3 Decontamination and sterilization [19, 20, 21, 22]

The threat of biological hazards, both natural and man-made, has created unprecedented challenges for public health institutions and hospitals, as well as for national defense. These biohazards demand fast and effective decontamination techniques. Conventional techniques, which rely on chemicals and/or extreme heat, are not suitable in many situations. Ultraviolet (UV) light can sterilize by causing DNA damage. Besides the UV radiation, the high energy radicals generated in excimer plasma sources can quickly overwhelm the natural defenses of living organism, leading to their destruction. Furthermore, scientists have observed that bacterial cell membranes sometimes rupture when exposed to plasma. This may be caused by charged particles attaching to the outer surface of the cell and inducing an electrostatic force that can overcome the tensile strength of the cell's membrane, rupturing it. Those effects can make excimer UV sources be more effective in many decontamination applications [14, 15, 16,17].

UV and Vacuum Ultraviolet (VUV) radiation are also currently used in toxic waste (e.g. CFC's, PCB's, dioxin's, trichloroethylene) destruction in air/water streams by photo-oxidation. Heat-sensitive medical tools that would be destroyed by the high temperatures of steam autoclaves are sterilized by UV/Ozone without damage. Compared with ethylene oxide, a toxic gas often used for low-temperature decontamination, plasmas are also advantageous because their decontamination processes do not leave toxic residues.

CHAPTER II

EXCIMER FORMATION

Excimer emission is based on the formation of excited molecular complex (excimers) and the transition from the bound excimer state to a repulsive state. The wavelength of the emitted photon depends on the gas used to generate excimers. A variety of different gases have been used for the generation of excimer emission over a wide wavelength range. Both rare gas and rare gas halides have been thoroughly studied for the excimer generation. Examples of rare gas excimers are Xe_2^*, Ar_2^*, Kr_2^*, Ne_2^*, and He_2^*, and examples of rare gas halides are $XeCl^*$, ArF^*, KrF^*, and $XeBr^*$. These excited complexes dissociate in less than a microsecond and give off their binding energy in the form of UV and VUV radiation during the decay. Most of these excimers radiate narrow bandwidth UV light. Table 2.1 shows a wide selection of UV to visible wavelengths that can be obtained from different excimers.

2.1 Conditions for excimer formation

The excimer can be classified into three cases: (1) bound covalent; (2) Rydberg; and (3) charge transfer excimer states [23]. Covalent bonding occurs when a pair of electrons shares a bond orbital that is distributed over two atoms. Group II homonuclear molecules such as Hg_2, Mg_2 provide examples of this type of binding. The rare gas excimer such as Xe_2 is an example of Rydberg molecular state. The Rydberg orbitals are diffuse and have relatively little molecular bonding or anti-bonding characteristics. The rare gas halide excimer such as XeCl is a charge transfer excimer.

For the rare gases, the main excimer formation can be described by:

$$Rg^* + Rg + Rg \rightarrow Rg^*_2 + Rg \qquad (2.1)$$

where, Rg is a rare gas atom, Rg^* is an excited atom state, and Rg^*_2 is a rare gas excimer.

The principal reaction in rare gas halides is

$$Rg^+ + X^- + Rg \rightarrow RgX^* + Rg \qquad (2.2)$$

or

$$Rg^* + X_2 \rightarrow RgX^* + X \qquad (2.3)$$

where RgX^* represents a rare gas halide excimer, Rg^+ a positive rare gas ion, X^- a negative halogen ion.

Table 2.1 Wavelengths of Excimer Sources

Wavelength (nm)	Species	Authors	Reference
126	Ar_2	Huges et al. (1972)	[24]
146	Kr_2	Hoff et al. (1973)	[25]
172	Xe_2	Koehler et al. (1972)	[26]
175	ArCl	Waynant (1977)	[27]
193	ArF	Hoffman et al. (1976)	[28]
222	KrCl	Murray and Powell (1976)	[29]
249	KrF	Ewing and Brau (1975)	[30]
282	XeBr	Searles and Hart (1975)	[31]
305	XeCl	Ewing and Brau (1975)	[30]
351	XeF	Brau and Ewing (1975)	[32]
502	HgBr	Parks (1977)	[33]
558	KrO	Powell et al. (1974)	[34]
540	XeO	Powell et al. (1974)	[34]
558	ArO	Huges et al. (1976)	[35]
558	HgCl	Parks (1977)	[33]

The reactions in Eqs (2.1- 2.3) shows that to form excimers, atoms and molecules must first be brought to an excited state or ionic state. The atoms and molecules can be excited or ionized by high-energy electrons through collisional energy transfer. When fast electrons collide with atoms or molecules, they will transfer their kinetic energy to heavy particles or ionize them. The excimers are generated by means of a three-body process where the excited atom reacts with two atoms that are generally in the ground state. As for any three-body process, the rate increases with pressure, making high-pressure operation mandatory for efficiency excimer generation. Excimer formation mainly depends on these two conditions: a) high-energy electrons which can excite the ground state atoms to an upper level; and b) relatively high pressure which makes three-body collision more favorable.

Fig 2.1 shows part of the potential energy level diagram of xenon with the different possible emissions, which represent a typical excimer gas [36]. The spectral behavior of radiation in xenon shows a pressure dependence. At low pressure, excimer formation is less likely, and therefore, resonant radiation (147nm) dominates the spectrum. When the pressure increases, the first continuum that peaks at 150 nm results from excimer molecules at high vibrational levels. At higher pressure, the vibrational relaxation of excimers is faster than their optical decay. Transitions from the lowest vibrational states of excimers are responsible for the generation of the second continuum at 172 nm.

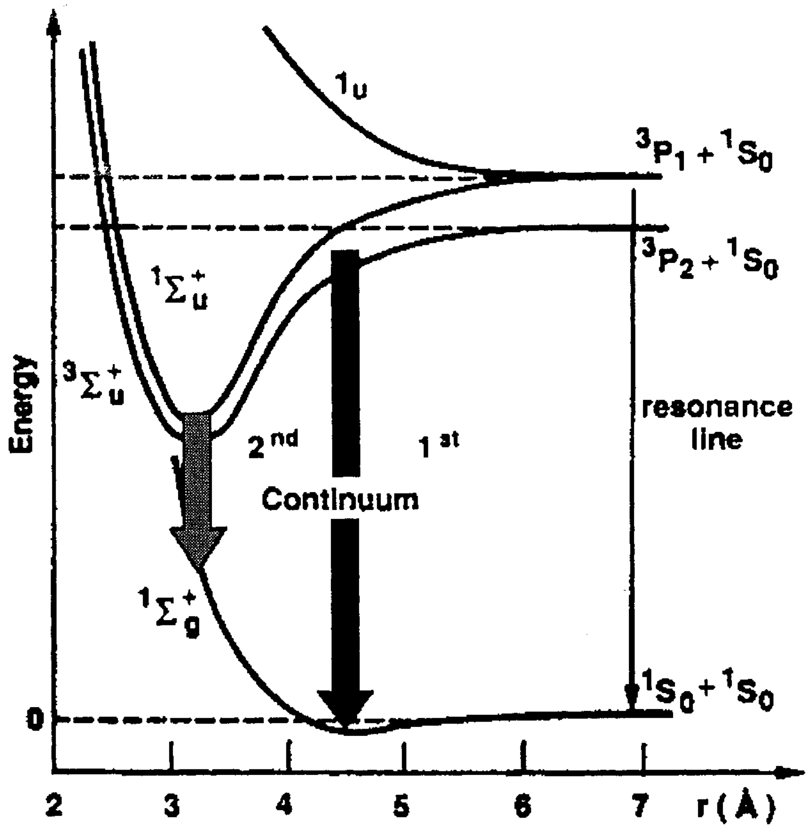

Fig 2.1 Energy level diagram of Xenon [36].

2.2 Excimer formation kinetics

The kinetics of excimer systems are rather complex, involving several ground state atomic and molecular species, several ionic species, and a large number of excited atomic and molecular species. A schematic diagram (Fig 2.2) shows the main kinetic process leading to the formation of the Xe_2^* excimer [37]. A mechanism of selectively populating the excimer levels, viewed as a sequence of collisional energy exchange, was reviewed by Lorents [38] and later was improved by Werner et al. [39]. The main kinetics pathway they describe can be simplified into three major processes: a) production of excimer precursors, eg, excited atoms and ions; b) excimer formation; and c) excimer decay and loss. Following sections briefly review these kinetics processes for rare gases.

2.2.1 Production of excimer precursors

As shown in equation 2.1, the primary reacting species for excimer formation are excited atoms. The precursor states are rapidly and efficiently produced by radiation, an electron beam, or a discharge. All the excitation methods provide high-energy electrons which transfer their kinetic energy as excitation energy to the atoms and molecules. These electrons either ionize or excite the gas atoms, depending on the electron energy, according to the following reactions

$$e^- + RG \rightarrow RG^+ + 2e^- \qquad (2.4)$$

$$e^- + RG \rightarrow RG^* + e^- \qquad (2.5)$$

$$e^- + RG \rightarrow RG^{**} + e^- \qquad (2.6)$$

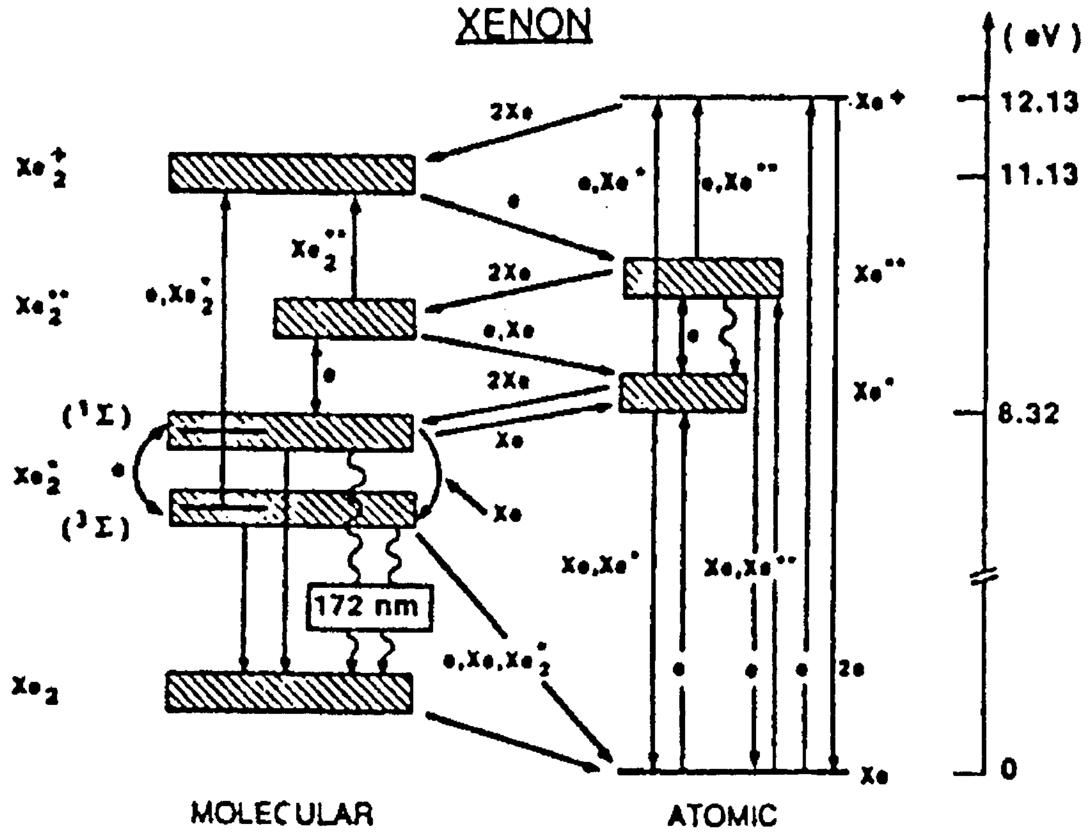

Fig 2.2 Main kinetic process to the formation of Xe_2^* excimer [37].

where e^- is an electron, RG^+ is the rare gas ion, RG^* is the rare gas excited state ($^3P_1$ & $^3P_2$), and RG^{**} is the higher lying state. The generated secondary electrons will have a mean energy of five to seven electron volts depending on the gas [23]. According to ref [40], the energy for producing an ion pair is similar for all the heavier noble gases (approximately 24 eV).

The conversion of electron energy to different species varies depending on the rare gas and on the excitation mechanism. RG^{**} and RG^+ will play a big role in populating the RG^* state. At higher pressure RG^{**} will also populate excimer RG_2^* in three-body association reactions given by,

$$RG^{**} + 2\,RG \rightarrow RG_2^* + RG\,. \qquad (2.7)$$

Typical rate constants for these reactions are $10^{-32}cm^6s^{-1}$ [41, 42, 43].

2.2.2 Excimer formation

The major excimer formation mechanism is achieved via three-body association reactions of excited gas atoms RG^* and buffering gas atoms given by

$$RG^*(^3P_1) + 2RG \rightarrow RG_2^*(^1\Sigma_u v>>0) + RG \qquad (2.8)$$

$$RG^*(^3P_2) + 2RG \rightarrow RG_2^*(^3\Sigma_u v>>0) + RG \qquad (2.9)$$

This is the principal process producing diatomic molecules in the upper vibrational states. The rate constants of this reaction are 10^{-32} cm^6s^{-1} for Ar, 2.5 ~8.5 × $10^{-32}cm^6s^{-1}$ for Xe [23]. In order to efficiently generate excimers the process rate should be higher than that of the resonance radiative decay of the RG^* states, which is the dominant process at low pressure,

$$RG^* \rightarrow RG + h\nu_0 \qquad (2.10)$$

where $h\nu_0$ is the resonance radiation.

2.2.3 Excimer decay mechanisms

The excimer radiative decay also shows a pressure dependency as mentioned earlier. The 1st continuum which corresponds to the decay of high vibrational energy levels of $^1\Sigma_u$ and $^3\Sigma_u$ excimer molecules is more pronounced at lower pressures. This result is due to increased likelihood of optical emission over relaxation of high vibrational levels, since collisions with the buffer gas are reduced as gas density decreases. The 1st continuum is described by

$$RG_2^*(^1\Sigma_u v>>0 \text{ or } ^3\Sigma_u v>>0) \rightarrow 2RG + h\nu_1 \qquad (2.11)$$

where $h\nu_1$ is the 1st continuum radiation, $RG_2^*(^1\Sigma_u v>>0 \text{ or } ^3\Sigma_u v>>0)$ describes the excimer molecules at high lying vibrational levels.

At higher gas densities, the 2nd continuum optical output increases since the vibrational relaxation rate is higher than that of the first continuum emission process. The relaxation processes populate lower vibrational energy levels and are followed by longer wavelength emission (second continuum) according to

$$RG_2^*(^1\Sigma_u v>>0 \text{ or } ^3\Sigma_u v>>0) + RG \rightarrow RG_2^*(^1\Sigma_u v\approx 0 \text{ or } ^3\Sigma_u v\approx 0) + RG \qquad (2.12)$$

and

$$RG_2^*(^1\Sigma_u v\approx 0 \text{ or } ^3\Sigma_u v\approx 0) \rightarrow 2RG + h\nu_2 \qquad (2.13)$$

where $h\nu_2$ is the 2nd continuum radiation, and $RG_2^*(^1\Sigma_u v\approx 0 \text{ or } ^3\Sigma_u v\approx 0)$ is the excimer molecule at lower vibrational energy levels.

Decay rates of the two excimer states ($^1\Sigma_u$ $^3\Sigma_u$) are appreciably different. The lifetime of the triplet state (~ μs) is several orders of magnitude longer than that of the singlet state (~ ns), contributing to fluorescence decay according to the fractional populations of the triplet and singlet states. At low pressure the decay rate is low and rises with increasing pressure to an asymptotic value. For xenon, this asymptotic value is $6 \pm 1 \times 10^7$ s^{-1} [23]. This value can be derived by assuming that complete population equilibrium exists between the triplet and singlet excimer states. The inverse of the decay time then becomes

$$\frac{1}{\tau} = \frac{3}{4} \cdot \frac{1}{\tau_3} + \frac{1}{4} \cdot \frac{1}{\tau_1} \cong 5.2 \times 10^7 s^{-1} \quad , \qquad (2.14)$$

where ¾ and ¼ are fractional populations of the triplet and singlet states, and τ_3 and τ_1 are triplet and singlet lifetimes. The lifetimes τ_3 and τ_1 are respectively about 0.1±0.05 μs and 5.5±1.0 ns [44].

In addition to the excimer radiative decay, excimer density can be reduced through several other processes, such as Penning ionization, photon ionization, super-elastic collision, and quenching by neutral atoms.

2.3 Excimer excitation techniques

2.3.1 Electron-beam excitation

When a high energy electron beam traverses a high pressure gas, the incident electrons scatter off the nuclei and electrons, transferring energy to the electrons in the gas and creating excited atoms and secondary electrons. In a high electron density plasma, the secondary electrons rapidly relax by electron-electron and electron-atom collisions to a non-Maxwellian distribution that has a mean energy of a few electron volts [23]. If a sufficiently high density of electrons and excited atoms are generated in the excimer gas, excimer radiation can be generated.

An electron beam is typically generated through devices which consist of a pulsed high voltage power supply and a vacuum diode. Electrons from the cathode are accelerated to the anode through a dc potential on the order of 0.2 to 2 MV. The electron-beam enters the gas through a foil “window”, which can be made of thin sections of aluminum, stainless steel, titanium, or aluminized plastics. Somewhere between 5% and 50% of the electron-beam energy is deposited in the cavity gas [23]. Compared with discharges, electron beams eliminate problems of stability and have the ability to achieve higher pulse energies. The disadvantages are beam pinching, diode closure and foil heating [23].

2.3.2 Gas discharge excitation

Compared with electron beams, discharges offer the potential for higher pumping efficiency and higher average power. By using carefully controlled discharges, it is possible to pump the metastable levels directly by electron impact with very high efficiency. Unlike the bulky apparatus associated with e-beam excitation, discharge excitation systems are relatively compact and easy to operate at high repetition rate.

Electrons can be generated in an electric gas discharge. The electron energy in a gas discharge depends on many parameters. The key parameters are the applied electric field, E and gas density. The parameter E/n, the reduced electrical field, is the dominant factor which determines electron energy. The higher the reduced field strength, the more energetic the electrons. Primary requirements for efficient discharge excitation are the initiation and maintenance of a spatially uniform, stable, high-voltage discharge in the excimer gas at high pressures. In the following paragraphs several examples of discharge excited excimer sources are described.

2.3.2.1 Barrier Discharges

Barrier discharges, sometimes referred to as dielectric-barrier discharges or silent discharges, are characterized by the presence of at least one insulating layer which is in contact with the discharge and is located between two planar or cylindrical electrodes connected to an ac power supply. It is a special non-equilibrium discharge that can be operated at approximately atmospheric pressure. When an electrical field is applied to the two electrodes, a displacement current flows through the dielectric and a space charge is accumulated on the dielectric surface. Due to the space charge, the electric field is intensified and a breakdown occurs. Electrons generated by the breakdown propagate in the gap and avalanche to produce high space charge and self-propagating electron streams. These developing discharge channels (filaments) are quenched by surface charge on the dielectric which grows in a few nanoseconds. Conditions can be established in these microdischarges that lead to excimer formation. Microdischarges have a typical radius of the order 0.1 mm and a lifetime of less than 10 ns. The discharge is maintained by applying an alternating high voltage operating at frequencies between 50 Hz and several hundred KHz. A commercial excimer lamp based on barrier discharge has reached an efficiency of 40% [13].

2.3.2.2 Glow discharges

Excimer formation can also be observed in direct current glow discharges at relatively low pressure [45,46]. In these glow discharges, typically operated at a pressure below 30 Torr, more vibrational energy levels are populated and the excimer spectra are much wider than those obtained at atmospheric pressure. Glow discharges extend all the way from the B→X transition to the D→X transition and reach UV outputs of 1.9 kW at 222 nm and 1.1 kW at 308 nm with efficiencies in the range of 10 – 15% [47]. Sinusoidal voltages of 10 kV amplitude or short pulses of 20 ns to 10 ns duration are used with repetition frequency up to 100 kHz.

One of the major obstacles in generating high pressure glow discharge is glow-to-arc transitions (GAT). The GAT, the development of a highly conductive channel which shorts out the glow discharge, generally develops during the cathode fall. In recent studies [48, 49, 50] stable atmospheric glow discharge have been generated by using a plasma cathode. By using a plasma source (microhollow cathode discharge or corona discharge) as a cathode, the cathode fall can be reduced or even eliminated. Efficiencies greater than 50% for conversion of electrical power into VUV light have been observed in this discharge [50].

Another type of microdischarge for excimer generation is microhollow cathode discharge (MHCD). MHCDs are direct current, high-pressure, non-equilibrium gas discharges. They will be discussed in detail in the following chapter.

CHAPTER III

MICROHOLLOW CATHODE DISCHARGE

3.1 Hollow cathode discharge

Hollow cathode discharges (HCD) are gas discharges between a cathode with some hollow structures, and an arbitrarily shaped anode. The first report on hollow cathode discharge was published by Paschen in 1916 [51]. For many years, the applications of hollow cathode discharge have been limited to spectroscopy and laser applications. Only recently has interest in the HCDs increased significantly, and this is due to progress in the miniaturization of hollow cathode discharge geometries [2-6].

3.1.1 Hollow cathode effect

When a plane cathode in a glow discharge is replaced with a hollow structured electrode, the negative glow is inside the hollow structure for a specific range of operating condition [52]. For these conditions, at a constant current the voltage is found to be lower than for a plane cathode and, at constant voltage, the current is found to be orders of magnitude larger. This effect is called the “Hollow cathode effect”. The hollow structure can be either cylindrical or slit-shaped as shown in Fig. 3.1. There is no restriction on the anode shape. The characteristics of the discharge are strongly dependent on the cathode geometry, electrode material, and operating conditions.

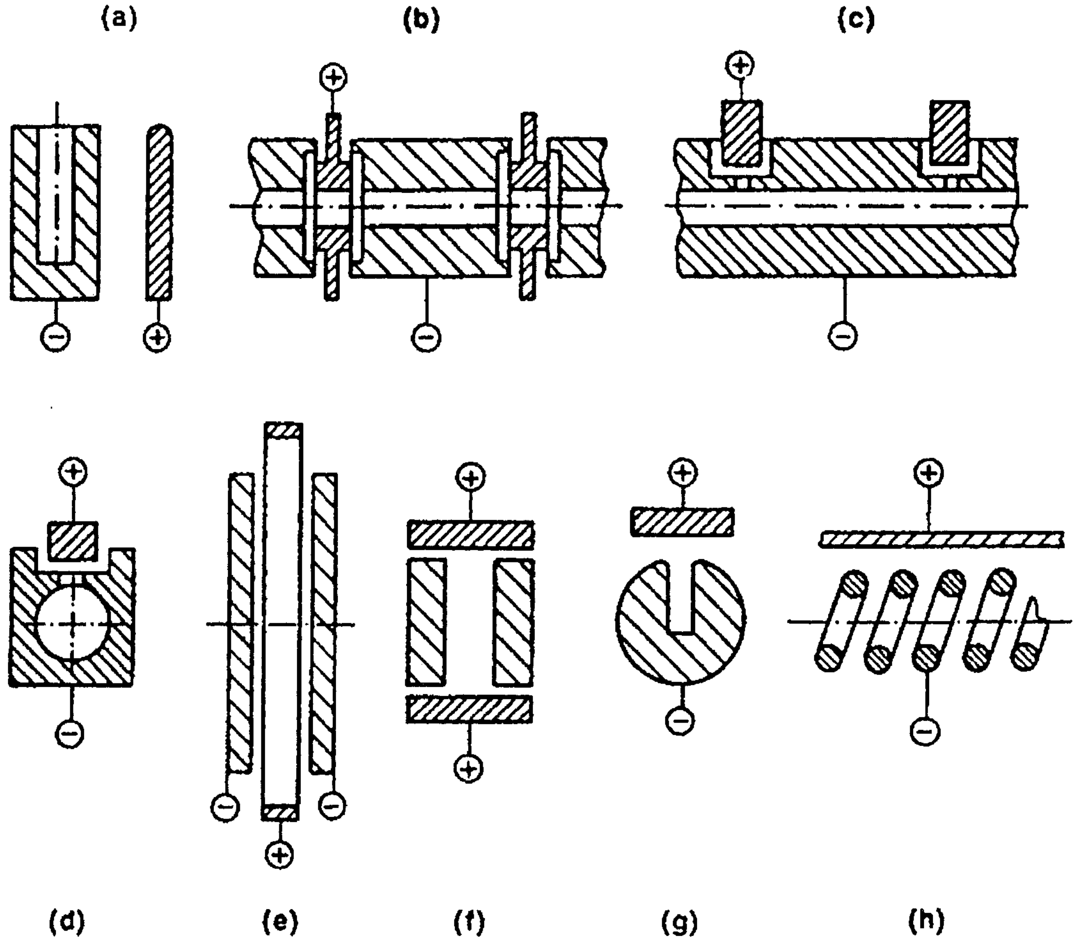

Fig 3.1 Hollow cathode geometries [52].

3.1.2 Mechanisms of hollow cathode effect

Schaefer and Schoenbach [52] have listed several mechanisms contributing to the hollow cathode effect: pendular electrons; secondary electrons; photons and metastables; multi-step processes; and sputtering. The main mechanism responsible for discharge current enhancement is believed to be the “pendel effect”.

a) Pendel effect occurs when electrons which have crossed the negative fall are reflected at the opposite cathode and change the potential distribution of the negative fall. These electrons further enhance the ionization rate in the negative glow and significantly influence the electron energy distribution function (EEDF) in the hollow cathode plasma.

b) Because the cathode fall in a hollow cathode can be significantly thinner than that in a plane cathode, the probability for charge-transfer collisions is reduced. Due to the higher average ion velocity at the surface, the second electron emission rate increases for a hollow cathode.

c) Photons and metastables generated in the negative glow inside the hollow glow have a better chance to hit the cathode surface due to the structure, which increases the electron emission rate of the cathode.

d) Multi-step excitation and ionization processes, contributing to the increase of discharge efficiency, are more likely in the hollow cathode because of the higher plasma density.

e) The confined structure of the hollow cathode leads to a higher density of sputtered atoms of cathode material with lower ionization potential. A sputtering process generates a vapor pressure of cathode metal on the inside wall of the hollow cathode.

3.1.3 Lower and upper limits of hollow cathode discharge

A hollow cathode discharge develops only when the mean free path for collisional ionization is comparable to the hole dimensions. This condition limits the hollow cathode discharge scaling with the product of pressure, p, and hollow cathode diameter, D. The lower limit of pD for the hollow cathode effect is determined by the loss of "Pendel" electrons, which reach the opposite cathode wall and are removed from the discharge. This lower limit of pD for which a hollow cathode discharge can be sustained was given by Helm [53] as

$$pD = \frac{\ln f^{-1}}{<\sigma> n_0} \tag{3.1}$$

with n_0 being the gas density at a pressure 1 Torr, f a loss factor, and $<\sigma>$ the average collision cross section. This cross section is defined as the sum of elastic and inelastic cross sections for the cathode fall and negative glow, divided by the cathode hole diameter. The minimum value of pD is 0.026 Torr cm for argon discharge [2].

The upper limit of pD is less well defined. It is on the order of 10 Torr cm as quoted in ref [54]. Recent experimental studies performed at Old Dominion University show the hollow cathode discharge upper limit is approximately pD<5 Torr cm [3]. The upper limit for hollow cathode discharge can be established by using the condition that the sum of the lengths of the two opposite cathode falls and the negative glow becomes greater than the cathode hole diameter. The cathode fall thickness for plane cathode is, according to Aston [55]:

$$d_{an}= B^*/p +B/J^{1/2} \tag{3.2}$$

where B* and B are constants depending on gas and electrode material, and J is the current density. The width of the negative glow corresponds to the range of electrons that have been accelerated by a potential difference equal to the cathode drop. Assuming that this distance scales linearly with 1/p, the upper limit in pD for hollow cathode discharges can be obtained by

$$pD=2B^* + 2pB/J^{1/2} +l_0p_0 \tag{3.3}$$

where l_0 is the negative glow length at pressure p_0= 1 Torr. The upper limit given by this model was much smaller than the experimentally obtained value 5 Torr cm. For the argon hollow cathode discharge, the upper limit obtained from this model is 1.1 Torr cm [3].

3.2 Microhollow cathode discharge

Hollow cathode discharges in a cylindrical/spherical geometry were shown to obey a similarity law [56, 57]. In this law, the sustaining voltage V scales with pD and I/p as

$$V= V(pD, I/p) \tag{3.4}$$

where I is discharge current. This law indicates that hollow cathode discharges with same pD values have similar characteristics. According to this law, by keeping the pD value constant, higher pressure operation can be achieved by reducing the cathode diameter. By reducing the hole size to the order of 100 μm, microhollow cathode discharges can be operated up to atmospheric pressure according to the experimentally obtained pD upper limit of pD of 5 Torr cm.

Hollow cathode discharge with smaller diameters in the range of hundreds of micrometer are referred as “Microhollow Cathode Discharge” (MHCD). Recently MHCD has attracted great interest because of the possibility that they can be used to generate DC high-pressure non-equilibrium plasmas, and intense UV and VUV radiation [2-6]. MHCDs in xenon were shown to have an internal efficiency for excimer emission at 172 nm (output UV optical power to input electrical power) in the range of 6-9% [4].

3.2.1 Voltage-current characteristics of MHCDs

The voltage-current (V-I) characteristic of microhollow cathode discharges shows three distinct ranges of operation: Townsend mode, hollow cathode mode, and abnormal glow mode. Fig 3.2 shows the V-I curves in argon discharges and a schematic sketch of three modes.

a) **Townsend Discharge mode**: The resistive V-I characteristic at low current, with an exponential increase in current with voltage, indicates that the discharge in this mode is a Townsend discharge. A schematic sketch of this mode is shown in Fig 3.2 (left). “Townsend discharge”, is a glow discharge which follows the path defined by the vacuum electrical field. During this phase the electron and ion densities are too small to induce a space-charge field. The geometric field dominates over the space-charge field. The plasma column develops on the cathode opening axis.

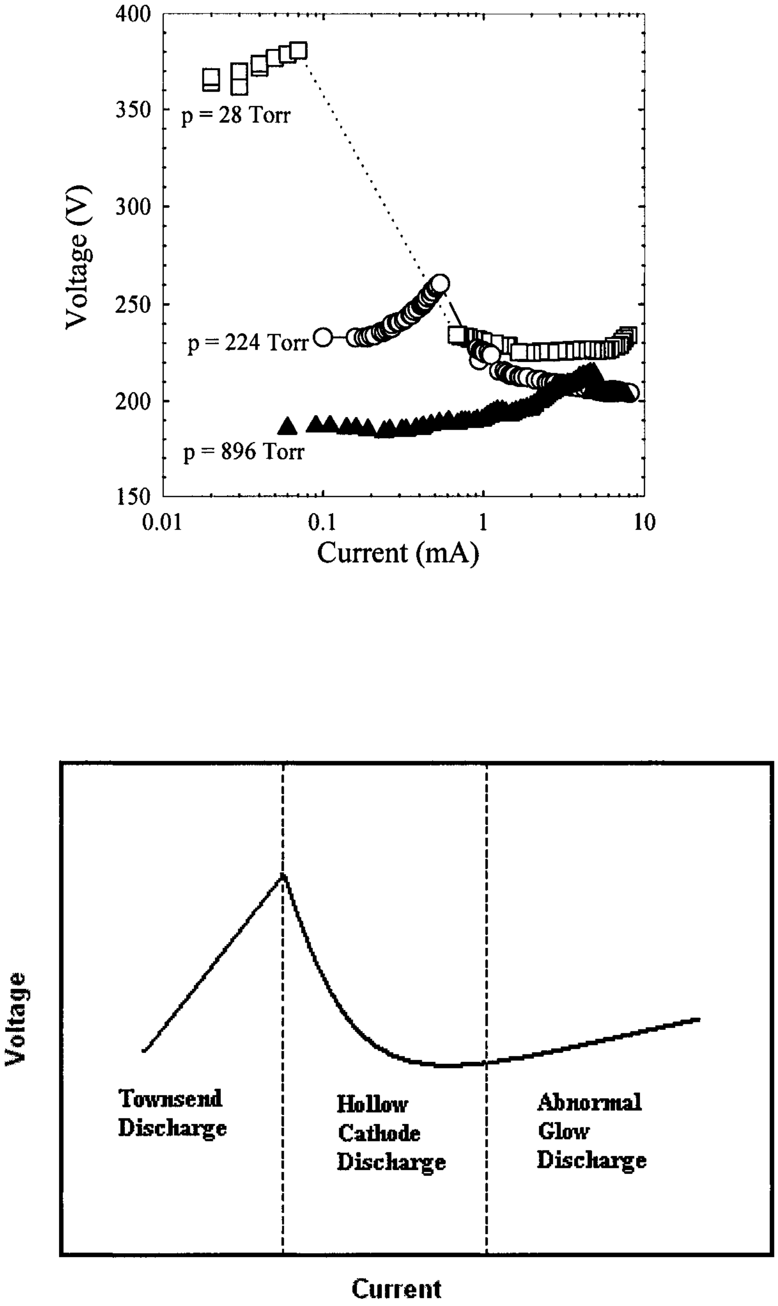

Fig 3.2 V-I characteristics of hollow cathode discharges [48].

b) **Hollow cathode discharge mode**: Because of their smaller mass, electrons have much higher mobility than ions. Electrons are quickly transported to the anode, leaving a growing (ionic current) ion space charge on the axis of the hollow cathode. With increase of current, there are more electrons and ions generated in the cathode gap, and the conductivity of the discharge column inside the electrode cavity increases. The increase of ion space charge density produces an increase in the space-charge field to values on the same order as the vacuum field. The electric field begins to become distorted. It changes from mainly axial to a more radial-oriented field at the cathode as shown in Fig 3.3 (right). The formation of this strong radial field at the cathode perimeter causes a fraction of electrons generated through ion impact at the cathodes to gain such energy that they oscillate through the axis region, unloading much of their energy through ionizing collisions. The hollow cathode discharge mode leads to an increase in current and a simultaneous decay in voltage, i.e. a negative differential conductivity.

c) **Abnormal glow discharge mode**: With further increase in current, the discharge expands until it covers the entire cathode surface. Any increase in current then requires an increase in voltage. The hollow cathode discharge transits to an abnormal glow discharge mode, which is shown in the V-I characteristics of the discharge at high current in Fig. 3.2. These operational modes were also seen in modeling results [58].

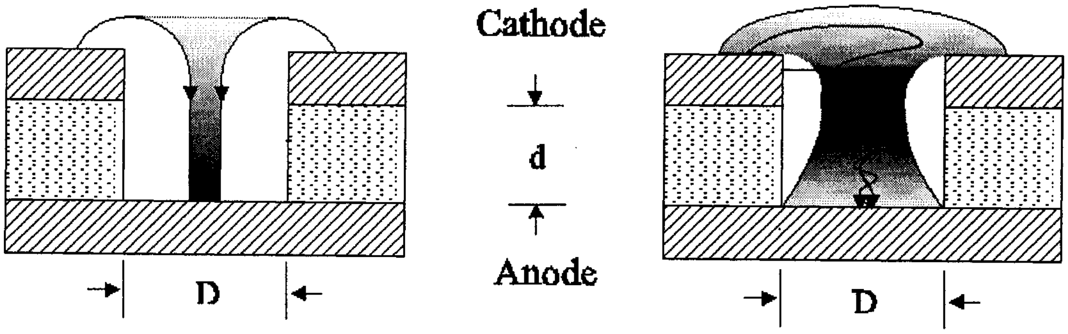

Fig 3.3 Schema of hollow cathode discharge.

3.2.2 Excimer emission from MHCD

In DC operation, the vacuum ultraviolet (VUV) radiant power of a single xenon MHCD operating at a forward voltage of 220 V and currents exceeding 2 mA reaches values between 6% and 9% of the input electrical power [4]. Figure 3.4 shows the wavelength spectrum for MHCD for several xenon pressures. The excimer efficiency, defined as the ratio of optical power in the spectral range of excimer emission to the electrical power, was measured as 6% for flowing argon [59]. Pulsed measurements in 20 ns duration xenon discharges show the efficiency reaching 20% [59].

3.2.2 Microhollow Cathode Discharge Arrays

Industrial applications of microhollow cathode discharge excimer lamps generally require higher total optical power levels than are achievable with single microhollow cathode discharge. The optical power of a single xenon discharge reaches approximately hundred mW (at efficiency of 6% - 9%), consequently, the operation at kW optical power level would require an array of more than 10^4 discharges.

If operated in discharge modes where the current-voltage characteristic has a positive slope, the discharges can be arranged in parallel without individual ballast [2]. For discharge modes where the current-voltage characteristic has a negative slope (i.e., the hollow cathode discharge mode) or is flat (normal glow discharge mode) it is possible to generate arrays of discharges by using distributed resistive ballast [60].

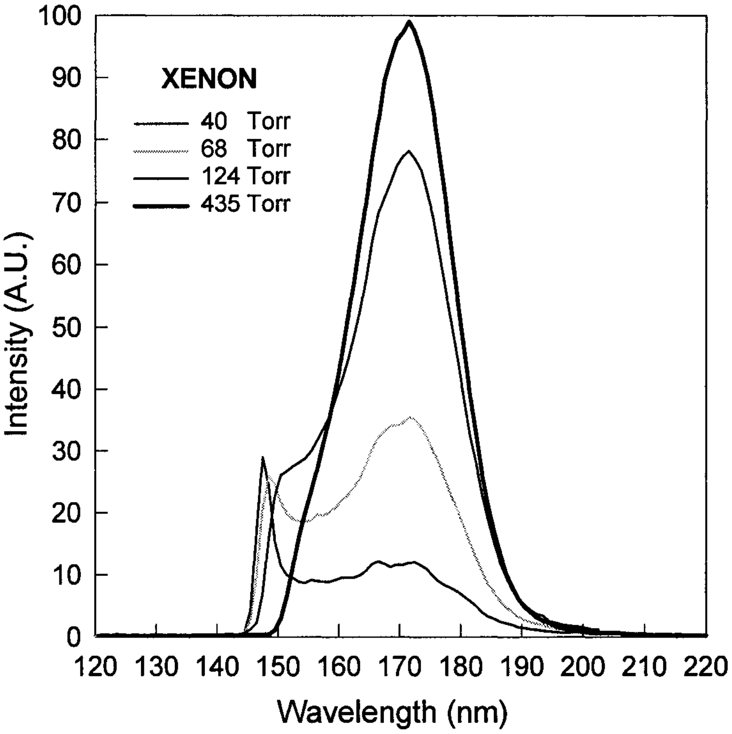

Fig. 3.4 Spectrum of microhollow cathode discharge for different xenon pressures [6].

CHAPTER IV

EXPERIMENT SETUP

The experimental investigation of microhollow cathode discharges requires sample preparation. Diagnostics, which are used to study these discharges, include current-voltage characteristics, discharge imaging, and the measurement of excimer UV radiation.

4.1 Sample preparation

4.1.1 Electrode and dielectric material

The typical microhollow cathode sample used in the experiment consists of three layers: two metal foils and one dielectric spacer. We assume that the electrode material and dielectric play minor roles in the physics of the discharge. Molybdenum was selected as the electrode material because of its high melting point (2610^0 C). Pure molybdenum (99.95% metal basis) foils with thickness of 100 μm and 250 μm were used in our samples. High purity (99.5%) alumina ceramic (Accumet Engineering Corp.) was used as the dielectric spacer. High thermal conductivity (27 W/mK) and high dielectric constant (9.9) make alumina a good dielectric for microhollow cathode discharge. We used alumina with a thickness of 250 μm. The two electrode layers were glued to the alumina sheet with Epoxy H20E, a two-component conductive adhesive. The reason for choosing Epoxy H20E was its high operating temperature stability and thermal conductivity. The epoxy was cured in a oven at a temperature of 180^0 C for ten minutes either before or after the hole was drilled.

4.1.2 Laser Drilling

To achieve stable high-pressure operation, the hollow cathode hole size should be on the order of 100 μm. Holes of such small size were drilled by means of a KrF excimer laser (OPTex, Lambda Physik). The wavelength of this laser was 248 nm. Pulse repetition rate could be as high as 200 Hz. The highest energy per pulse was 22.9 mJ. The beam size at the near field was 7X4 mm and the laser beam is shaped by means of a telescope which consists of two cylinder lenses. The changeable mask was mounted in the laser path and then imaged on the work piece. The ratio between the size of mask and the image was chosen to be 15:1. By controlling the hole size of mask, we could drill the desired hole size on work piece from 50 μm to 250 μm. It normally took less than 1000 shots to drill though a piece of Molybdenum with thickness of 100 μm, and less than 2000 shots for a piece of alumina with thickness of 250 μm. The holes on the three layers were drilled separately, and the layers were then aligned and glued together. The advantage of drilling separately was that no obvious taper along the hollow was created. But aligning of such small holes was time consuming. Three layers consisting of two 100 μm molybdenum layers and one 250 μm alumina layer could be drilled through by applying more than 8000 laser shots. This saved the trouble of alignment at the expense of a conical shaped hole. Then, the sample was cleaned with an ultrasonic cleaner for ten minutes to remove debris generated through laser drilling.

4.1.3 Sample conditioning

Sample conditioning is a critical step in getting stable and reproducible result from the discharge. The purpose of conditioning is to remove the tips around the hole and the impurities on the surface by the plasma. The way to condition is to run the discharge at low pressure (<100 Torr) with a noble gas (argon or xenon) and a current around 2 to 3 mA for half an hour. Then, the discharge is turned off and the chamber is left evacuated overnight at 5×10^{-5} Torr. It was proven that conditioning could increase excimer radiation efficiency from xenon discharges by at least one order of magnitude.

4.2 Electrode Geometries

Several electrode geometries have been used in experiments of single discharge and discharge arrays. The typical configuration for a single discharge with electrical circuit is shown in Fig 4.1. The diameter of the opening is on the order of 100 μm. Because the anode shape plays a minor role in the characteristics of MHCD, it can be either opened or closed.

A simplified microhollow cathode array geometry is shown in Fig 4.2 (a). There is a 10 by 10 hole array on the cathode foil. The hole size is about 100 μm and the distance between holes is 250 μm. The anode is a planar molybdenum foil and the dielectric is a 250 μm thick alumina layer with a large square opening under the cathode hole arrays.

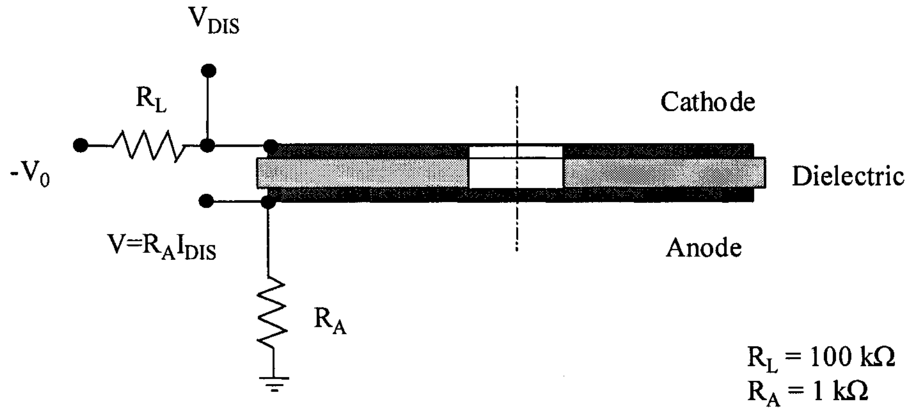

Fig 4.1 Typical configuration of single MHCD [3].

Whereas the three-layer sample was used as standard geometry, other geometries have also been studied. These include geometries where one of the electrodes was semi-insulator and served as ballast. Another one was built with a fourth layer to limit the cathode surface. Closed cathode geometry blocked one end of cathode hole and left the anode open.

The distributed ballast sample we used was a four-layer structure [60]. A sixteen-hole array sample (Fig 4.2 (b)) was machined with 500 μm diameter holes separated around 1 mm. A mica sheet with thickness of 200 μm was used as the dielectric between cathode and anode. The cathode is a molybdenum foil with 100 μm thickness. The holes were drilled through cathode and dielectric layers. The anode was a high resistivity (1200 Ω cm) silicon wafer with 300 μm thickness. The silicon anode was glued with a copper sheet by means of a conductive adhesive (EPO-TEK H20E).

The covered cathode sample we used was a four-layer geometry as shown in Fig 4.2 (c). In addition to the three layers (cathode, dielectric and anode) for the typical configuration in Fig 4.1, there was one more dielectric layer on top of the cathode. This dielectric layer was an alumina sheet with thickness 250 μm and the hole size was about 150 μm. Two multi-hole samples (one 5 by 5 array, one 10 by 10 array) were machined with the same layer geometry as Fig 4.2 (c). The separation between holes was 250 μm as shown in Fig 4.2 (d).

In the single closed microhollow cathode sample (Fig 4.2 (e)), there was a hole with diameter 500 μm through the anode, dielectric and cathode. The cathode (500 μm thickness) was covered with another molybdenum foil. Because

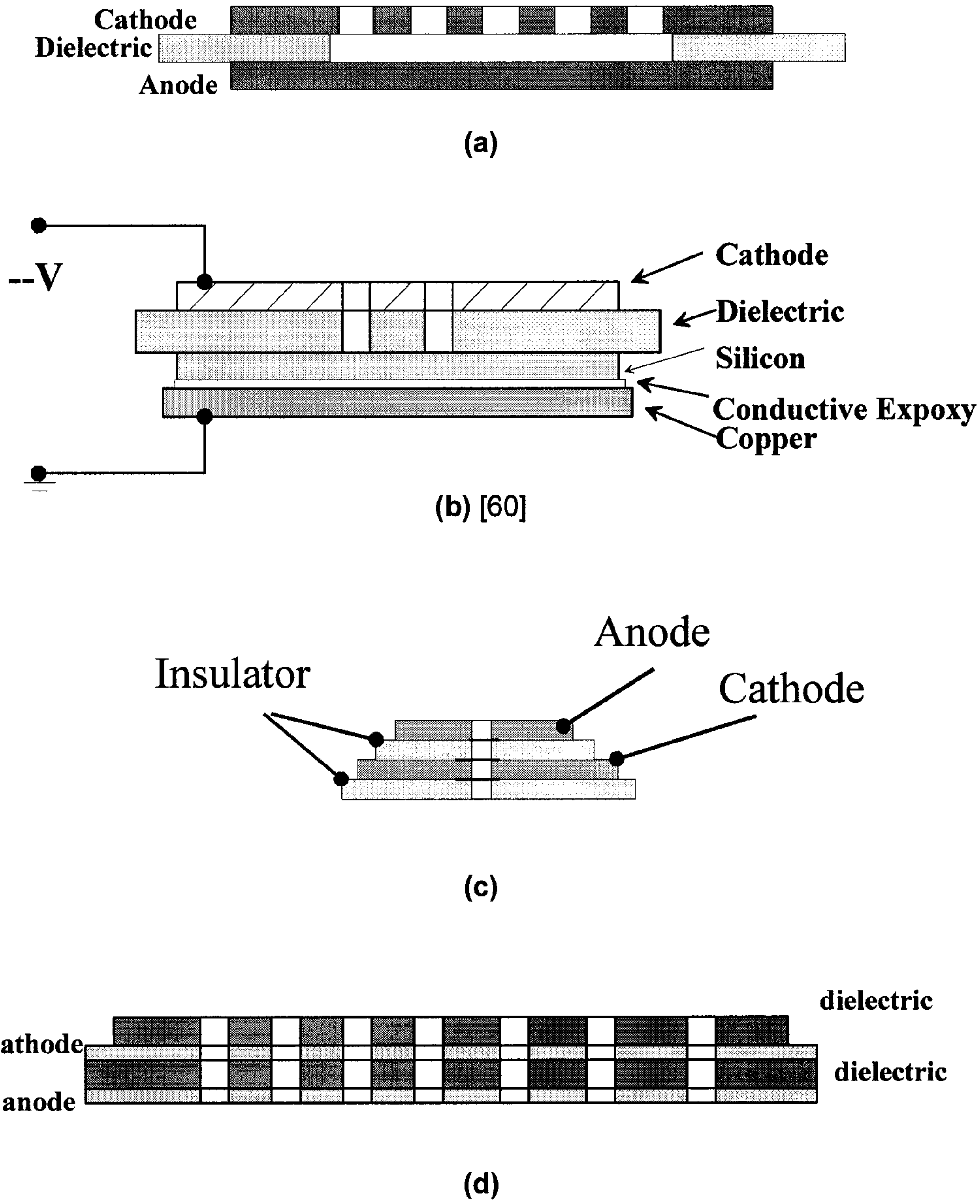

Fig 4.2 MHCD electrode geometries.

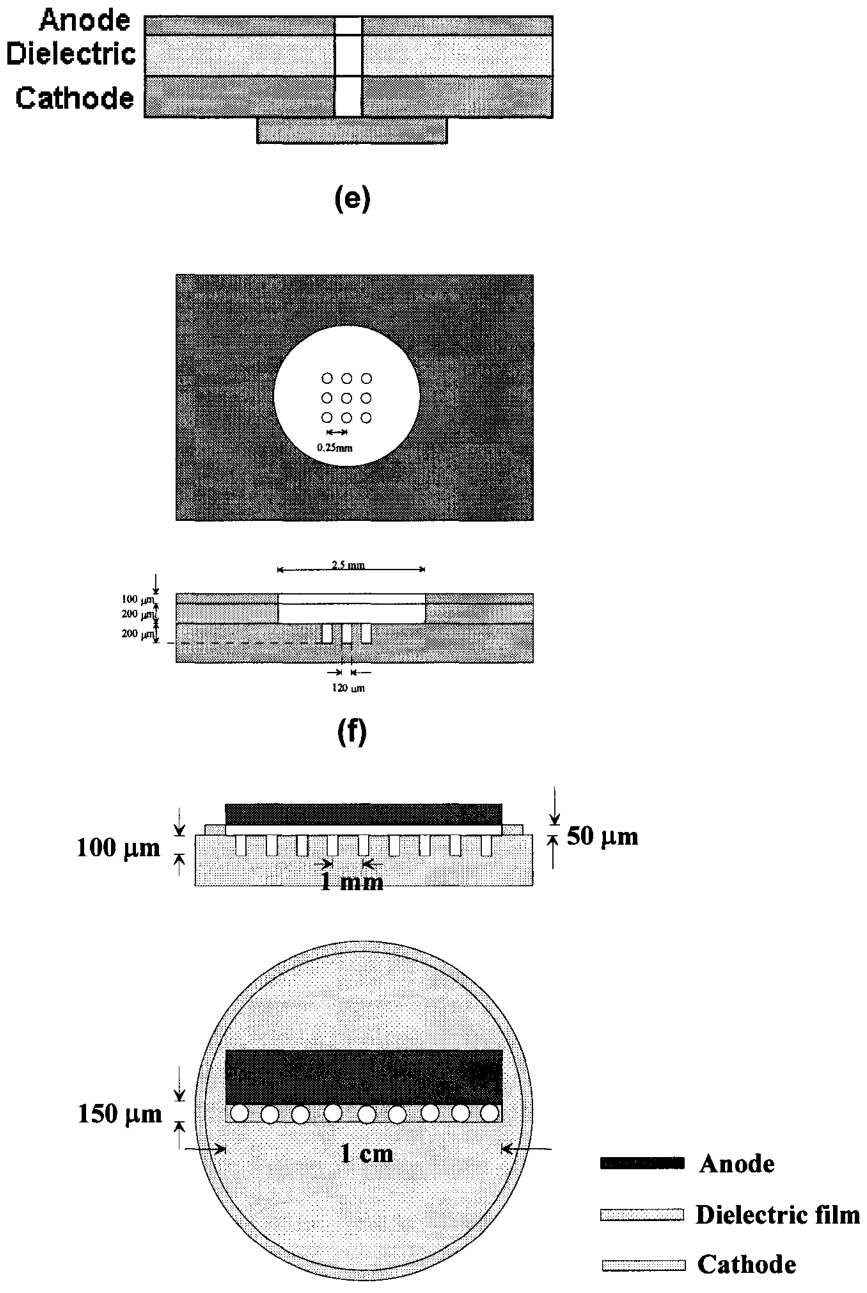

(e)

(f)

(g) [61]

Fig 4.2 Continued

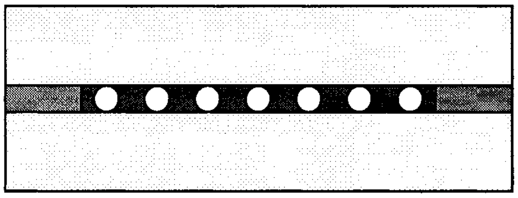

(h)

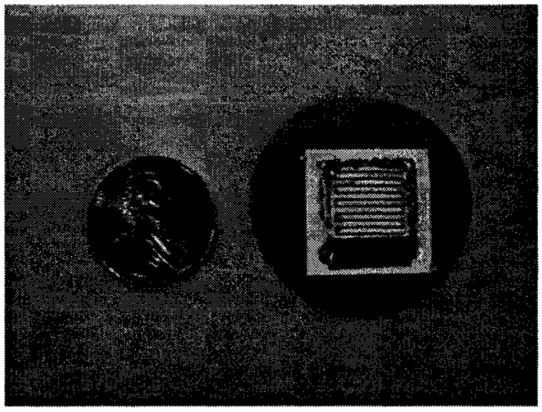

(i)

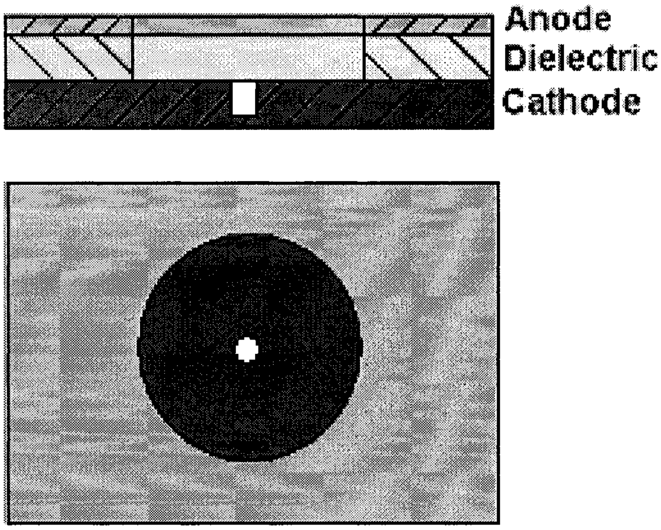

(j) [69]

Fig 4.2 Continued

of the blocking foil, the cathode was a closed cylinder in this geometry. Drilling part way through a thick material was another way to make this a closed (limited in surface area) cathode.

A 3x3 array of closed microhollow cathodes with diameter 120 μm, 200 μm depth and 250 μm hole separation, was fabricated on a thick molybdenum sheet (Fig 4.2 (f)). Both the anode and dielectric were attached to this hollow cathode array with a 2.5 mm diameter opening. The dielectric was a mica sheet with thickness 200 μm and the anode was a 100 μm thick molybdenum foil.

A two-layer structure provided by University of Minnesota [61] was used to generate a plasma string (Fig 4.2 (g)). A layer of alumina with thickness of about 50 μm was coated on a molybdenum substrate. A slit of the alumina coating, 150 μm in width and 1 cm in length, was removed by drilling with the KrF excimer laser. Along the slit, 9 holes with separation 1 mm were drilled to a depth of about 100 μm. Then a piece of molybdenum foil was aligned along the slit as anode. A similar geometry is shown in Fig 4.2 (h). However, in this sample the anode(s) was placed at both ends of the line of holes.

A 10x10 array pattern was created with a layer structure similar to Fig 4.2 (f). There were 10 lines with length 1 cm arranged in parallel fashion. Each line had 10 holes in it. Fig 4.2 (i) shows the photo of this sample alongside a penny for scale.

The cross section of the cathode boundary layer geometry is shown in Fig 4.2 (j). The cathode consisted of a molybdenum foil, 250 μm thick, with a microhole of 100 μm diameter and 100 μm depth in the center. A 250 μm thick layer of alumina was placed on top of the cathode, coaxial to the hole. The diameter of the opening on the alumina was 1.5 mm. A molybdenum anode was placed, again with a thickness of 100 μm, on top of the dielectric, with the same opening as the dielectric. In other samples, a planar cathode replaced the cathode and hole combination. Various diameter values of the ring-shaped anode and alumina were fabricated.

In order to study the series operation of microhollow cathode arrays, we used a three-electrode system, which allowed us to generate two discharges in series, i.e., a "tandem" discharge. The electrode geometry (Fig 4.3) consisted of three molybdenum foils with thickness of 250, 100, and 250 μm, separated by mica sheets of 200 μm thickness. A 250 μm diameter hole was drilled mechanically through the five layers. It was possible to have the outer electrodes serve as cathodes with the inner electrode serve as the common anode or the other way around.

4.3 Discharge chamber and vacuum system

A schematic of the discharge chamber is shown in Fig. 4.4. The main body of the chamber was a six-way cube crossing (cu6-0275 Kurt J. Lesker). The CF flanges were used to connect the chamber with a pressure gauge, gas cylinder and vacuum system. The microhollow cathode sample was connected to the electrical circuit through an electrical feed-through. A flange was made to attach the chamber with an evacuated monochromator or imaging system. The window in the flange was an MgF_2 glass with high transmittance in the VUV

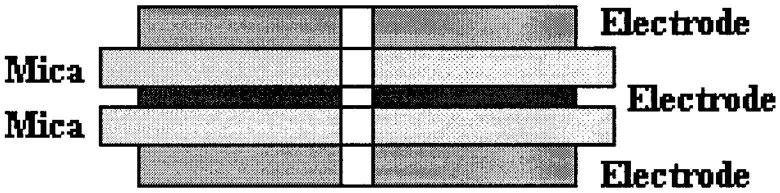

Fig.4.3 Electrode geometry of tandem discharge [67].

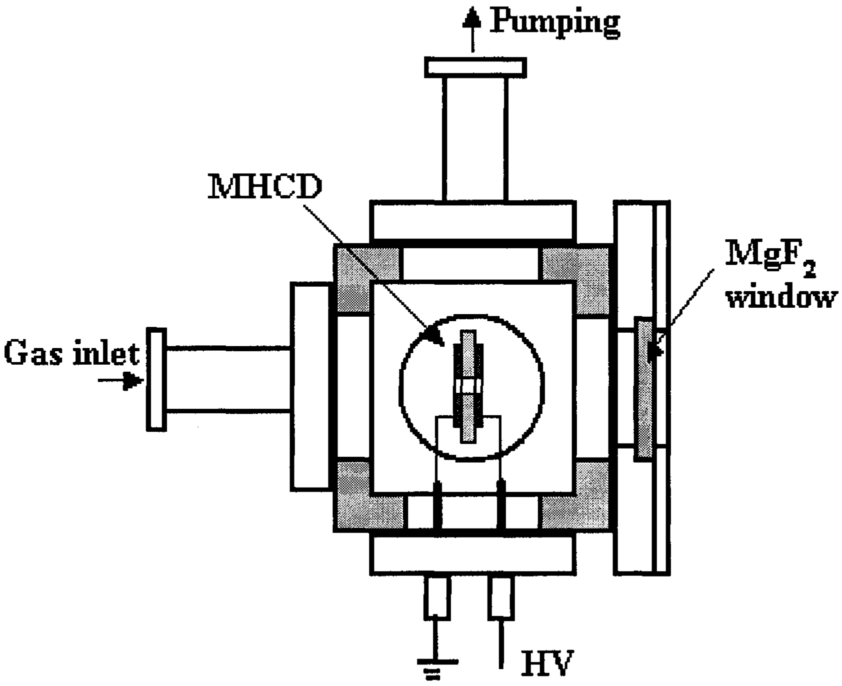

Fig 4.4 Schematic diagram of vacuum chamber.

range (~ 80% at 172 nm). The other ports in the cube were sealed by CF view ports with regular glass. The visible image of discharge could be seen through these windows.

The vacuum system consisted of a mechanical vacuum pump (Alcatel CE 2005) and a turbomolecular pump (Alcatel ATP100). With this vacuum system the chamber could be evacuated to a pressure of $5*10^{-5}$ Torr. A wide range pressure gauge (KJL 902056, Kurt J. Lesker) was used to monitor the evacuating chamber. A diaphragm manometer (KJL 912022) was used to control the gas pressure.

4.4 Electrical measurement setup

The electrical circuit is shown in Fig 4.1. The high-voltage V_0 was supplied by a Glassman High Voltage Supply (0 to 5 KV, 0 to 60 mA). The R_c resistor of 100 kΩ was used to limit the discharge current. The R_{CVR} resistor of 1 kΩ was used as current-monitoring resistor. The discharge voltage is the difference between V_1 and V_2. The dc voltages were measured using two digital multimeters.

4.5 Spectroscopy Setup

Spectral measurements were performed using a 0.5 m McPherson scanning monochromator, model 219, with a grating of 600 G mm^{-1} blazed at 150 nm. The discharge chamber with an MgF_2 window was mounted directly at the inlet of the monochromator as shown in Fig 4.5. The spectrally resolved radiation

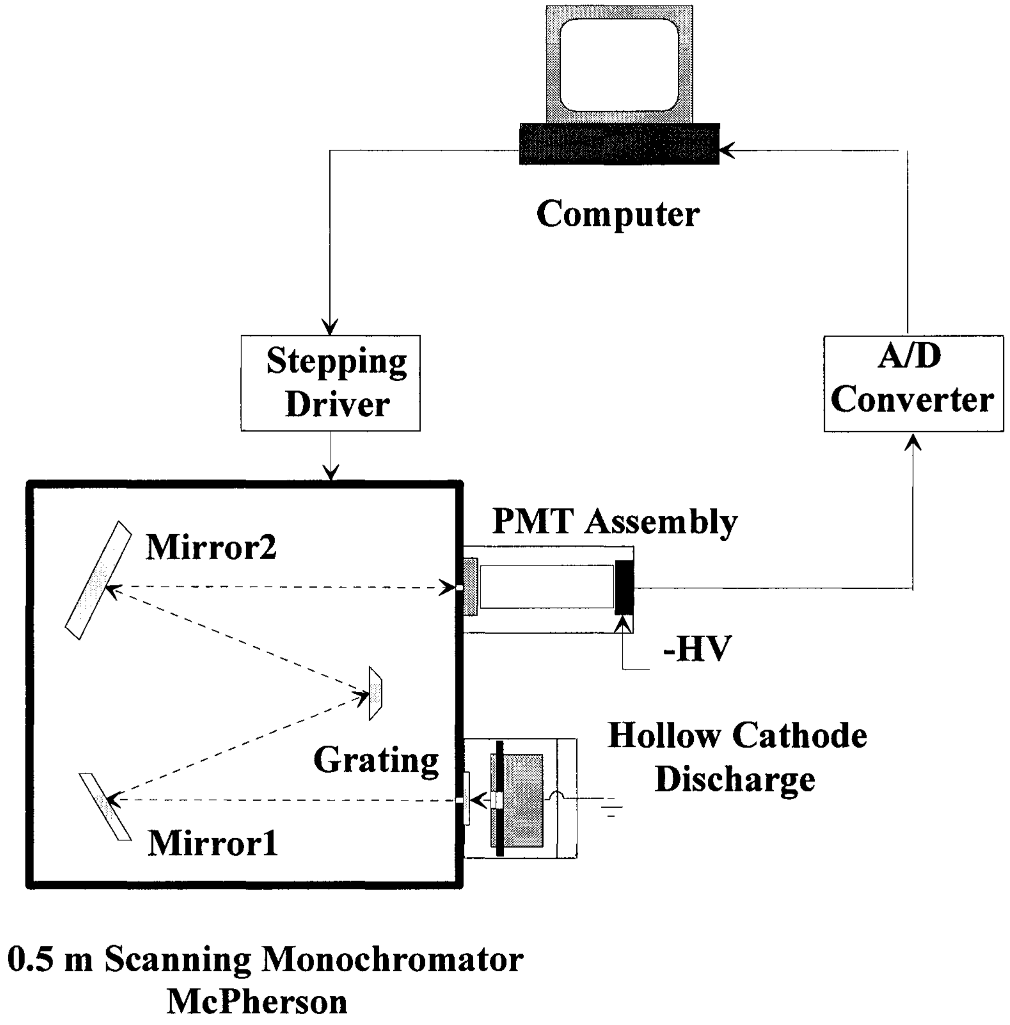

Fig 4.5 Schematic diagram of VUV spectroscopy system [63].

at the exit slit was detected with a photomultiplier tube (PMT: Hamamatsu model R375) after conversion to visible light, centered around 425 nm. The sodium salicylate scintillator had an absolute quantum efficiency of 65% between 40 and 340 nm [62]. This arrangement allowed detection at wavelengths below the 160 nm cutoff of the PMT response. The entire system, including the monochromator, the space between the source and the entrance slit, and the space between exit slit and scintillator was evacuated to a pressure of less than 45 mTorr. With slit openings of 600 μm, the instrument resolution was ~ 2nm full-width-at-half-maximum (FWHM). The scanning process was computerized using an A/D converter and a stepper drive scan controller.

A 0.2 m McPherson monochromator (Model 234/302) was used in spectral measurements. This monochromator covered a spectral range from 50 nm to 300 nm with a concave holographic grating (1200 grove/mm, blazed at 150 nm).

4.6 Optical imaging setup

4.6.1 Visible imaging system

The visible image of discharge was recorded end-on by means of a microscope with a CCD camera. The CCD camera was focused on the sample through one of the view ports of the vacuum chamber. The microscope was a VAM 450 microscope system, parfocal zoom: 0.7X – 4.5 X. The CCD was a Panasonic Model GP-KR222. The image taken by the CCD camera was recorded by means of a video capturer program (Snappy 4.0, Play,Inc).

4.6.2 VUV imaging system

In addition to spectral measurements and visible imaging, we measured the spatial distribution of the excimer source by means of an UV imaging system as shown in Fig 4.6. Excimer radiation was separated from all other radiation by using a UV filter with a peak transmittance of 24% at a wavelength of 170.9 nm and a FWHM of 26.8 nm. The UV image was recorded using an RS Princeton Instruments ICCD-MAX intensified charge coupled device (CCD) camera. The ICCD-MAX used a proximity focused microchannel plate (MCP) image intensifier fiber coupled to CCD array. The discharge chamber was mounted directly with the imaging tube. A silica lens in the imaging tube was used to focus the discharge to the MCP of the ICCD camera. The UV filter was mounted on a wheel filter holder. The ICCD camera was mounted on the other end of the tube. The imaging tube was evacuated to the mTorr range to minimize absorption of the VUV radiation.

4.7 Absolute power measurements

Excimer radiation can be measured in two ways as described in Ref [63]. The first method is based on comparing the discharge emission with that of calibrated UV source (e.g. a mercury vapor lamp with line emission at 184.9 nm and a deuterium lamp with continuum emission from 160 to 400 nm), the other method uses a radiometer measurement.

It is assumed that the calibrated source is a point source, and the emission is isotropic. The calibrated source was mounted the same position as the discharge chamber. The relation between the photomultiplier reading for emission power at a wavelength was determined.

A radiometer (IL 1400) with a calibrated detector (SED 185) was used in absolute power measurement. The responsitivity of the detector ranged from 160 nm to 240 nm with a peak at 185 nm. The total power was calculated by considering the distance, responsitivity, window transmittance and oxygen absorption in air.

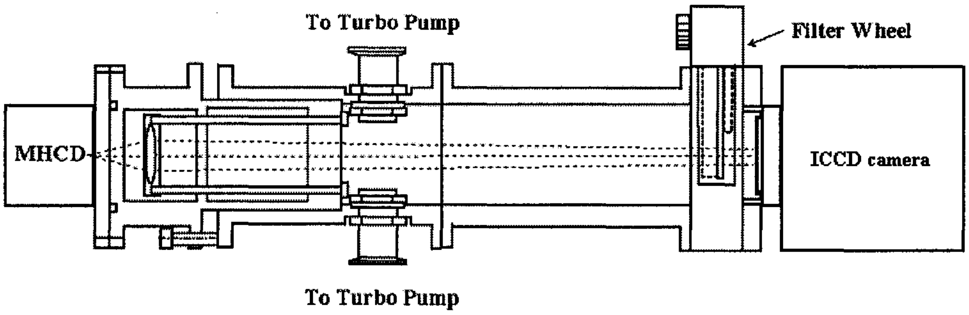

Fig 4.6 VUV imaging system

CHAPTER V

MICROHOLLOW CATHODE DISCHARGE ARRAYS

5.1 MHCD arrays in the Townsend mode

As shown in Fig 3.2, the operating current range of the Townsend discharge mode extends from sub-mA to several mA with increasing pressure. However, the slope (dV/dI) of I-V characteristic becomes less steep with increasing pressure. Parallel operation of the microhollow cathode discharge (MHCD) array without individual ballast for each discharge is possible in the Townsend discharge mode if there is a large operating current range and a steep positive dV/dI slope.

A 10 by 10 MHCD array (Fig 4.2a) was fabricated by means of laser drilling. It was shown that at pressures ranging between 200 Torr and 400 Torr in Xe, the discharges can be operated in parallel without individual ballast. The operating current ranges from 10 mA to 30 mA, corresponding to 100 μA to 300 μA per discharge. When the current increases to a value such that one or more discharges reaches the hollow cathode mode, the current through this discharge increases dramatically and that of the others quenches. The UV image along with a schematic diagram of the array geometry is shown in Fig 5.1. The operating currents for the Townsend discharge mode are 10 mA (100 μA/per hole) at 200 Torr, 14 mA (140 μA/per hole) at 300 Torr, and 26 mA (260 μA/per hole) at 400 Torr, respectively. The same sample has also been operated

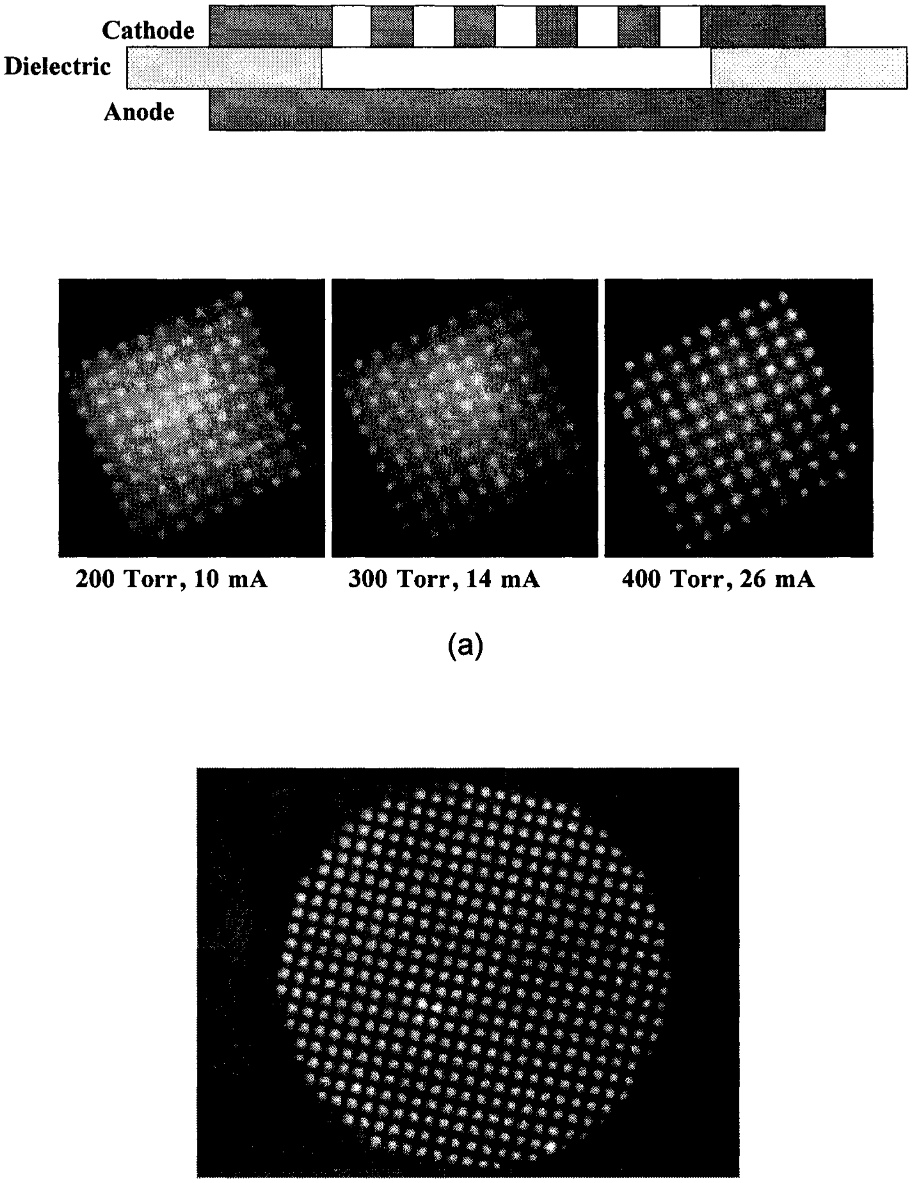

(a)

(b)

Fig 5.1 (a) Geometry of a three-layer electrode system and UV images of the discharge in Xe. (b) A photograph of an argon discharge (80 Torr, 8 mA) in a sample with stainless steel mesh as the cathode.

continuously over 24 hours at 8 mA (80 μA per discharge) in an argon discharge at a pressure of 70 Torr.

To simplify the manufacturing procedure of test samples, a metal mesh (stainless steel) obtained from Ted Pella Inc. was used to replace the metal foil drilled by laser. The mesh open space is 340 μm square, and the bar width is 200 μm. This sample worked well in argon at pressures of less than 100 Torr. A photograph of the discharges in argon is shown in Fig 5.1b.

Parallel operation in the Townsend discharge mode is limited to a low current and pressure range. During the ignition of the device, the supply voltage needs to be controlled to avoid that one of the discharges reaching the hollow cathode mode. On the other hand, the low operating current could be of advantage for long lifetime operation and low radiation density applications would not need cooling.

5.2 Parallel operation with distributed ballast [60]

Parallel operation of microhollow cathode discharges was achieved only at low pressure (< 400 Torr) when operated in the Townsend discharge mode (low current). Further increase of current results in transition from the Townsend discharge mode into the hollow cathode discharge mode, which has a negative I-V characteristic. In order to obtain parallel operation over the entire dc current range, particularly where the discharge I-V characteristic is flat or has negative slope, the discharges need to be individually ballasted. Individual ballasting is a reasonable approach for relatively small arrays. For large arrays, with thousands

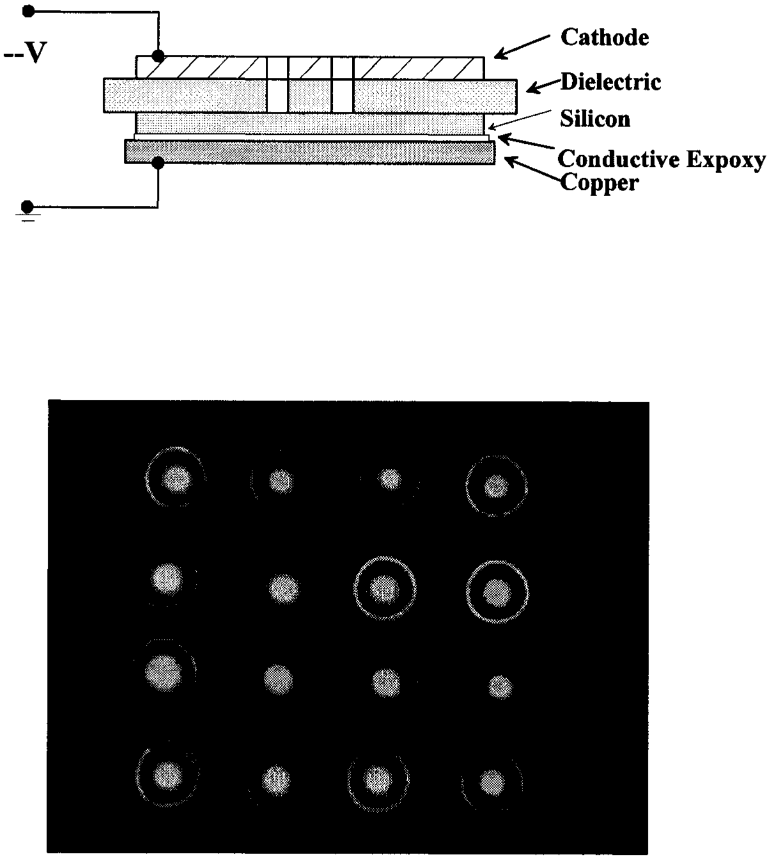

Figure 5.2 Distributed ballast electrode geometry and microhollow cathode discharge array operated in Ar [60].

of discharges, this is technically challenging and troublesome. Instead of ballasting each discharge by means of a resistor, we explored the use of distributed resistive ballast for stable operation of multiple discharges in flat panels [60]. B.G. Salamov et al. has reported that GaAs layer as a distributed resistor on the cathode stabilizes the atmospheric pressure discharge and prevents glows to arc transition [64]. Here we used a semi-insulating Si material as the anode to stabilize the hollow cathode discharges.

Parallel operation was demonstrated using a test sample with a distributed ballast electrode [60]. A cross-section of an electrode system with the anode made of semi-insulating silicon is shown in Fig 4.2 b. In order to obtain data on the optimum parameters of the resistive material required for stable operation of two parallel discharges, the distributed resistor was simulated by a network of two ballast resistors in series with the discharges, and a variable coupling resistor connecting the two discharges. Based on the experimental results, a semi-insulating silicon wafer of 300 μm thickness and resisitvity of 1200 Ωcm was chosen as the anode and connected to the electrode system by ohmic contact. A sixteen-hole array test sample was machined with 500 μm holes and a hole-separation of around 1 mm. An end-on photograph of dc discharges operating in Argon at pressure 28 Torr for this geometry is shown in Fig 5.2 along with a schematic diagram. The dc current can vary widely except for the restriction of electrical heating at the anode.

The advantage of distributed ballasting microhollow cathode discharge arrays is that the semi-insulating anode stabilizes the discharges. Parallel operation of MHCD arrays can be achieved through a wide current range (all three discharge modes). The fabrication of this device is technically simple. One drawback of this electrode geometry is energy dissipation in the semi-insulating electrode. Efficiency for conversion of electrical power to UV radiation is low because of the energy consumption at the electrode. Thus for large arrays, heat sinks will be needed to cool the device for long duration and efficient operation.

5.3 MHCD array in abnormal glow mode

Open microhollow cathode discharges exhibited negative ($dV/dI<0$) or flat resistive behavior for currents above the value needed for the Townsend discharge. Because of the open cathode geometry, the plasma extends out from the cathode hollow to the open surface when the current increases. In the current range, where the discharge stays in the normal glow mode, an increasing current leads to little change in voltage. Abnormal glow discharge sets in when the whole cathode surface is covered by the discharge. Beyond this threshold, the only way the total current can increase further is by applying higher voltage. In order to force the discharges to abnormal glow mode, the cathode surface has to be restricted to a smaller area. There are two ways to reduce the cathode area. One approach is to cover the cathode electrode surface with a dielectric layer, leaving the surface of the hollow as the only cathode. Another way is to close the cathode hole and leave the anode open.

5.3.1 Parallel operation in covered cathode geometry

The microhollow cathode surface was covered with a dielectric layer that had an opening that was the same size as the hollow cathode and was aligned to it(Fig 4.2 c). The cathode surface for the discharge was thus the circular surface inside the hollow. The test sample was fabricated in a dielectric/ metal/dielectric/metal system. A hole with 250 μm diameter was drilled through the four layers. The I-V characteristic of covered microhollow cathode discharge was measured at the various pressures in XeCl (Fig 5.3). Contrary to the uncovered microhollow cathode discharge, the covered cathode discharge has a distinct resistive behavior, except for low currents. The differential resistance (dV/dI) of the discharge in this mode is on the order of kΩ. The same I-V characteristics were observed in Ar and Xe discharges.

Given a four-layer electrode geometry, a picture of a twenty-five hole array discharge in xenon is shown in figure 5.4. Xenon, helium and argon were used in the experiments to determine the applicability of such structures for ballast free parallel operation. In argon stable, direct current discharges could be achieved up to a pressure of 200 Torr. In argon at 85 Torr, the voltage was 220 V and the current for 25 discharges was 5 mA (200 μA per discharge). In helium, the discharges could be operated up to 230 Torr, at approximately 200 V and currents of 6 mA (240 μA per discharge). In xenon, discharges could be operated up to 200 Torr at 350 V and current 40 mA (1.4 mA per discharge). At higher pressures, the instability of discharge prevented parallel operation.

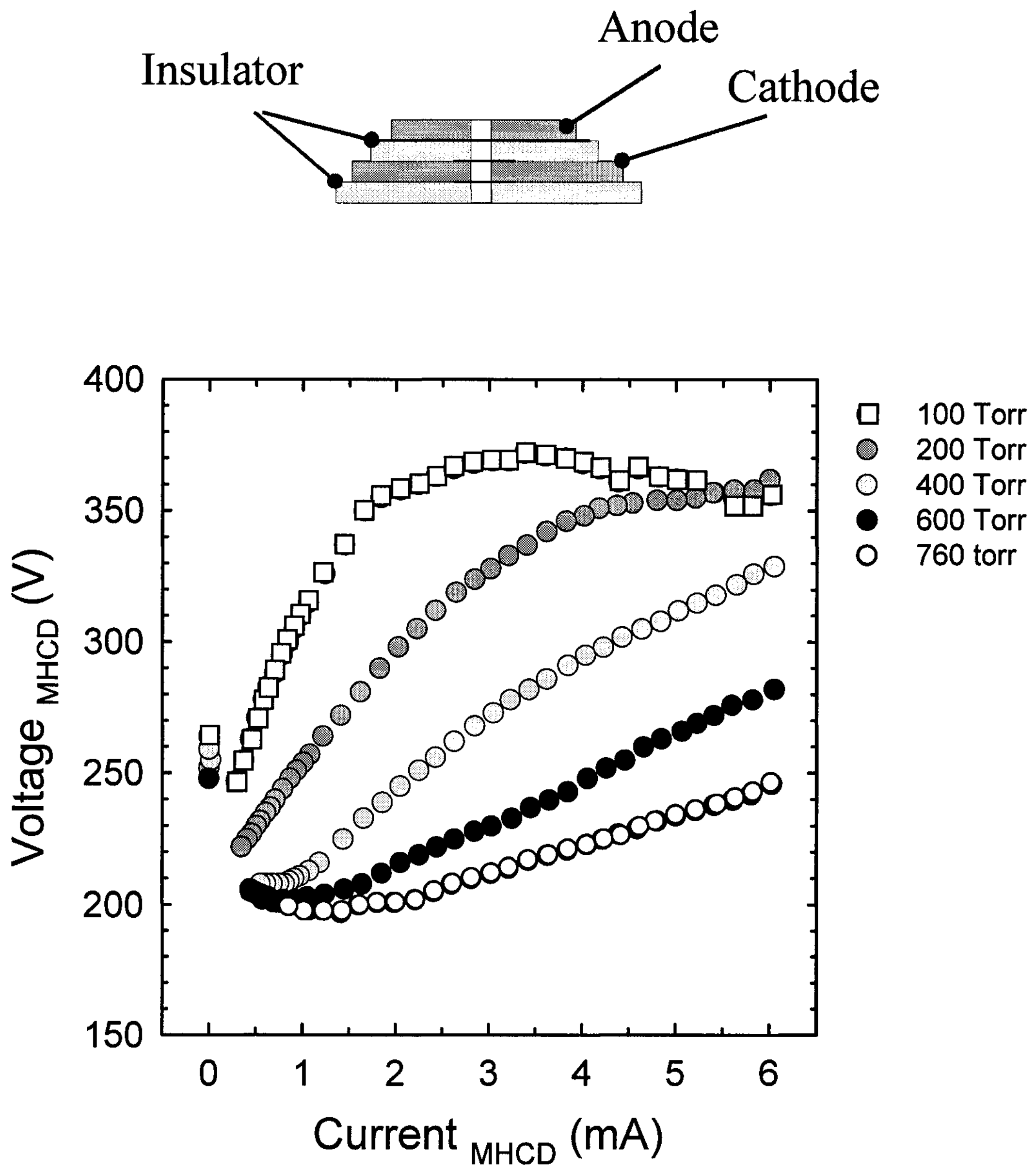

Fig 5.3 Covered cathode electrode geometry and I-V characteristics.

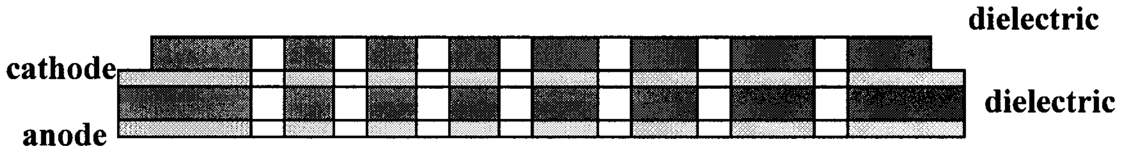

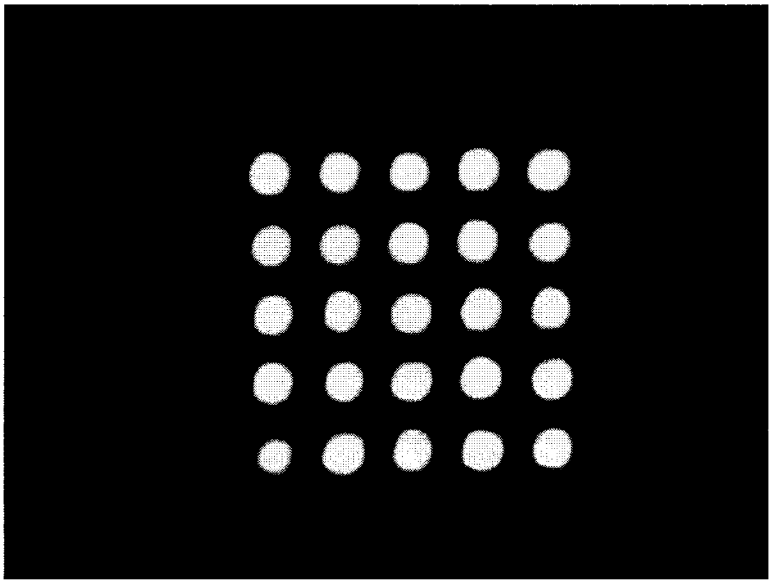

Fig 5.4 Covered cathode electrode geometry and photograph of parallel operation of MHCDs in xenon 200 Torr, 40 mA 350 V.

Several problems were encountered with this electrode geometry during lifetime testing of a hundred-hole array operating in argon. After operating for approximately 30 minutes at 10 mA, the surface of the dielectric layer was found coated with a thin layer of metal, and this layer added to the cathode area in addition to the original cathode surface. The discharge distribution tends to become inhomogeneous after a homogenous start (Fig. 5.5) because of the metal deposition. This means that some discharges become more intense at the expense of others. The reason for in-homogeneity could be the sputtering from the small cathode surface. Another problem with this cathode geometry is the difficulty in manufacturing. Laser-drilling through a four layer system with a total thickness of 400 μm was not possible with our laser system. The various electrode layers therefore needed to be aligned after drilling, a very cumbersome and time consuming task.

5.3.2 Parallel operation with closed cathode

Closed cathode microhollow cathode discharge was reported by Schoenbach et al in 1996 [2]. In their experiment, the highest operating pressure was 56 Torr because of the large cathode diameter (0.7 mm). They found that the slope of the current-voltage characteristic was positive over a wide range of currents. They were able to demonstrate parallel operation in this geometry by using a set of four discharges in “predischarge mode” (Townsend mode). Silicon microdischarge devices having inverted pyramidal cathodes were reported by J.G.Eden et al in 2001 [65]. The discharges exhibited high differential resistance

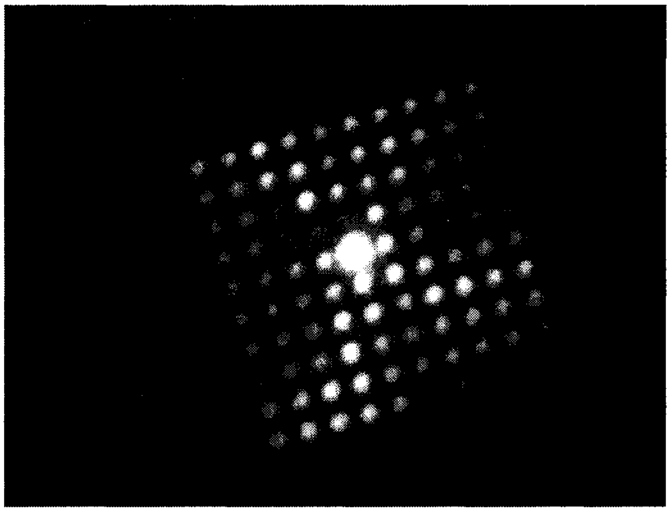

Fig 5.5 After operating a covered cathode sample in argon for 30 minutes, the discharge tends to become inhomogeneous.

(~ 2 X 10^8 Ω in Ne) up to pressure 1200 Torr. But the operating current was limited in to the μA range and lifetime was limited to several hours because of ohmic losses in the Si cathode.

In a closed cathode, the cathode surface is limited to the area of the cylindrical hole. When the current exceeds a certain value, the discharge is forced to become an abnormal discharge which has a resistive characteristic. The current-voltage characteristic of a single closed cathode discharge is shown in Fig 5.6. The test sample geometry is also shown in Fig 5.6. The cathode hollow structure is 500 μm in diameter and 500 μm in depth. The open end of the cathode hole is closed by a molybdenum foil. This test sample was operated in Xe gas at pressures of 100, 200 and 300 Torr. The I-V characteristic had distinct positive slopes for all the pressures tested. Because the plasma layer which covers the cathode surface reduces in size at higher pressure, higher currents are needed for the plasma to cover the same surface area. This is the reason that at high pressure the I-V curve turns positive at a higher current value. Reducing the hole diameter and depth will cause the onset of abnormal glow discharge at a lower current. Comparing our results with the results in ref 2 and ref 65, we found that the smaller the holes size, the higher the differential resistance of the discharge. This led to the possibility of placing the microdischarges side by side without ballasting each one.

In this side-by-side geometry, the radiation is mainly concentrated inside the hollow cathode. In order to prevent sputtering of the cathode hole, the current

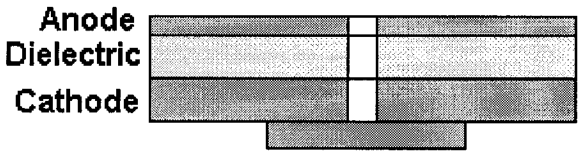

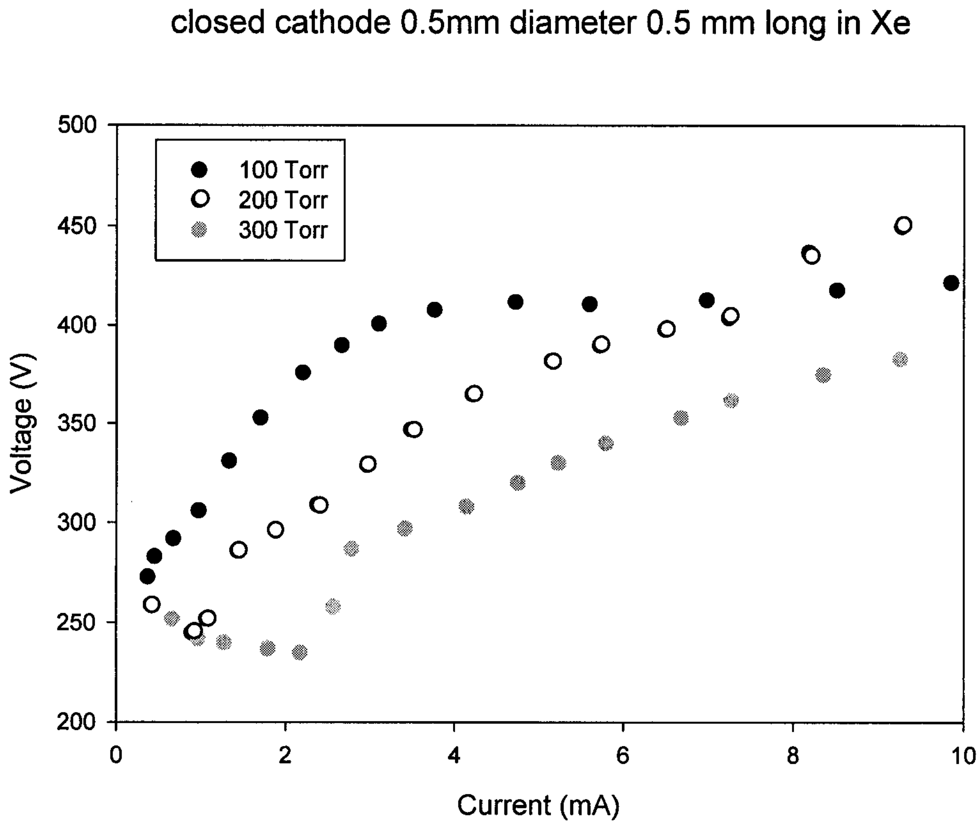

Fig 5.6 I-V characteristic of single closed cathode MHCD (cathode diameter 0.5 mm, length 0.5mm) in Xenon.

has to be limited to a small value. The irradiance of this UV source was constrained because of low current operation and small emitting area.

5.3.3 Limited cathode MHCD arrays

In published literature, most emphasis has been on emission from the hole area, but there is experimental evidence that the stability of the MHCD at high pressure supports a stable discharge area far exceeding that of the discharge hole. This area was shown for a single discharge with an open cathode hole to extend over several square millimeters, compared to the cathode hole area of 10^{-2} mm^2. This is more than a factor of hundred larger than the microhole area [6]. We studied the optical emission of a MHCD xenon plasma in the vacuum ultraviolet (VUV) and the visible spectrum as a function of current and gas pressure. We found that a disc-shaped 100 to 150 μm thick plasma layer (shown in Fig 5.7) extended from the hollow cathode to the planar cathode and had diameters up to 1 cm [66]. This layer is assumed to consist of the cathode fall and the negative glow of the high pressure glow discharge.

At constant pressure, the diameter of the plasma layer, d, increases with current, I. However, the spatially averaged current density J_t stays constant.

$$J_t = 4I/\pi d^2 \tag{5.1}$$

For xenon where the highest excimer efficiency was measured, at a pressure of 0.52 bar [3], the current density was 0.3 A/cm^2. The UV radiative power emitted from the source increases linearly with increasing current for hollow cathode and normal glow discharge modes. However, since the voltage across the discharge stays constant, the excimer efficiency is independent of current.

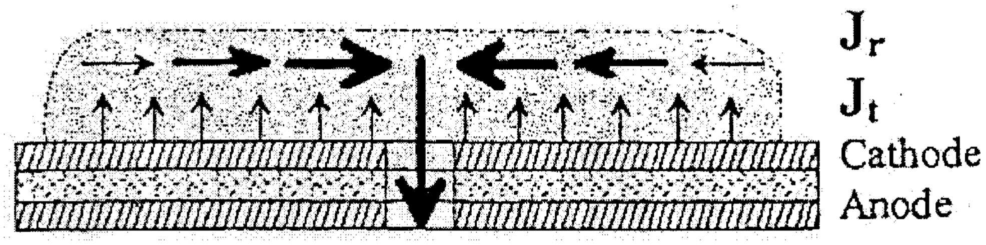

Fig 5.7 Plasma layer and current pattern of MHCD [66].

For constant current, the current density increases linearly with the squre of the pressure,

$$J_t = Cp^2 \tag{5.2}$$

where C is a constant (approximately 1 A/bar^2) and p is the pressure. A current density which is independent of the current that scales with the square of the pressure is typical for a normal glow discharge.

For a constant transverse (with respect to the cathode surface) current density J_t, the radial current density J_r increases with reduced distance r from the cathode opening according to

$$J_r(r) = \frac{J_t}{2t}\left(\frac{r_0^2}{r} - r\right) \tag{5.3}$$

where r_0 is the maximum diameter of the plasma layer and t is the thickness.

If we reduce the cathode surface to a small area at a constant pressure, the plasma layer will cover the whole cathode surface even at a low current value. Beyond this low, critical current value, the discharge becomes an abnormal discharge with a positive resistive characteristic. This permits us to operate arrays of MHCDs with limited cathode surfaces.

By connecting these uncovered cathode areas, coupling of the single microhollow cathode discharge to all others leads to a homogeneous ignition. The cathode fall areas, above a critical current, which is dependent on the microhollow density (ratio of number of holes per open cathode area for homogeneous distribution of holes), merge and form a homogeneous cathode fall layer, which is identical to the UV emitting layer. Merging of the cathode layers is identical to the transition into an abnormal discharge, and, consequently, is related to a resistive current-voltage characteristic (increasing voltage with increasing current). Fig 5.8 shows the geometry of a plasma UV light source with 3x3 closed cathode hole arrays in the center of a dielectric opening. The anode around the dielectric opening and all uncovered cathode areas are connected. An end-on photograph of this discharge in the visible for 400 Torr of xenon proves the discharge can be operated parallel in this geometry (Fig 5.8). The current was 10 mA, corresponding to approximately 1 mA per discharge.

By generating microdischarges along a line, the cathode fall and negative glow fill in the space between the holes and the dielectric, and generate a homogeneous line plasma source. The position of the anode is of minor importance, as long as the anode-cathode distance is not too large compared to the cathode hole diameter such that the voltage across the positive column becomes significant high respect to the cathode fall voltage. A possible anode is a metal foil, which is placed on top of the dielectric. Fig 5.9 shows the geometry of a plasma UV source with the anode placed along the line of microholes. The dielectric between the holes, along the line, is removed, allowing the expansion of the glow in the area between holes. The current-voltage characteristics of the line discharges are also shown in Fig. 5.9. The increasing voltage with current, above threshold current values (which increase with increasing pressure), are indicative of the resistive behavior of the discharges, a condition for parallel operation without individual ballast.

Photographs (Fig 5.10) show the development of the microdischarges obtained with the system shown in Fig 5.9. With increasing current, the intensity

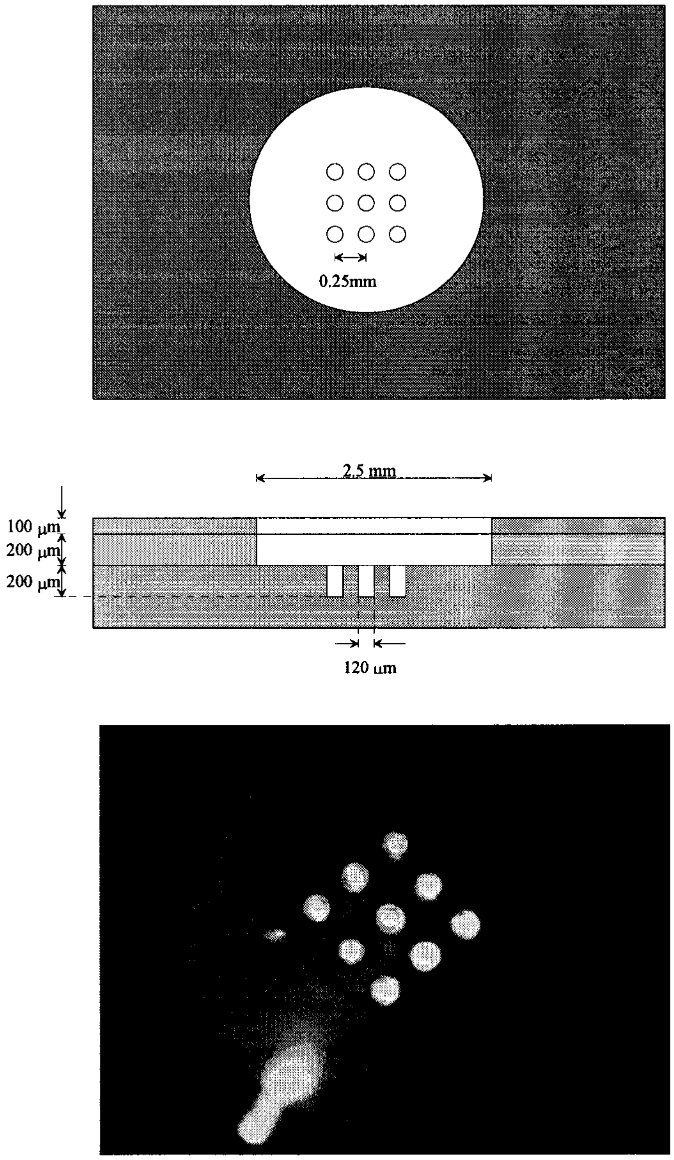

Fig 5.8 Limited cathode geometry and photograph of microdischarge array in visible.

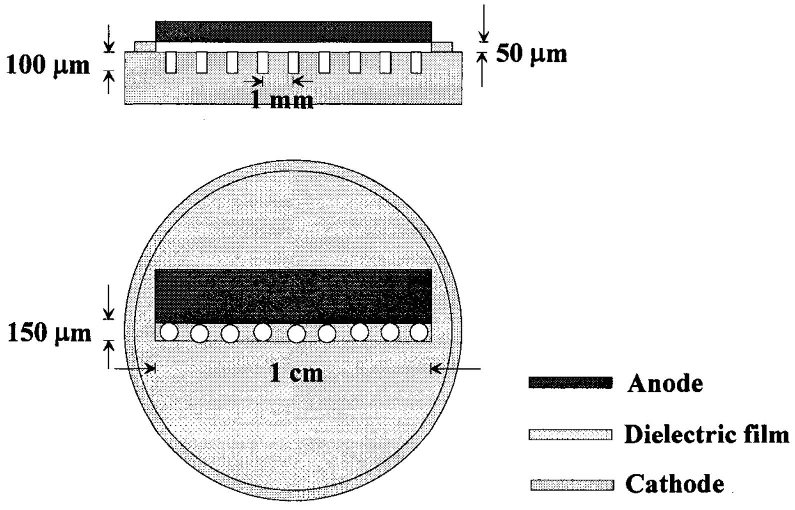

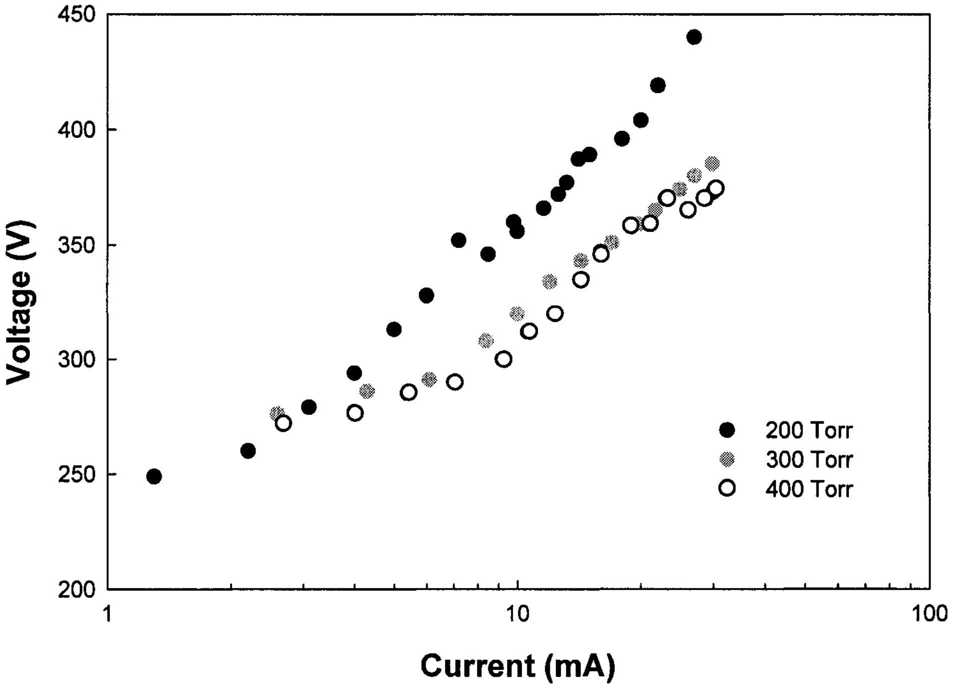

Fig 5.9 I-V characteristic of single array of closed cathode MHCDs [61].

of the light and the homogeneity of the light emitted from the plasma increases. The current per discharge ranges from approximately 300 μA to approximately 3 mA.

A similar hole geometry is shown in Fig 5.11, however here the anodes are placed at both ends of the line of holes. As in the previous geometry, the current- voltage characteristics have a positive slope, about 10 V/mA, with a threshold current, which is higher for higher pressure (Fig.5.11). The discharge array was operated at pressure of up to 450 Torr. This is approximately the pressure where excimer emission in xenon has the highest efficiency [4]. Fig 5.12 shows the development of the spatial distribution of the emission with increasing current.

The photographs of the string of discharges, taken in the visible spectrum, show highest intensities close to the anode at low current (Fig 5.11). With increasing current, however, the light emission becomes homogeneous over the entire length of the plasma string.

5.4 Spectral measurements

The microplasma, which extends over the cathode surface is a strong emitter of ultraviolet radiation. The emission spectrum for the plasma arrays generated with the electrode configuration as shown in Fig 5.8, is plotted in Fig 5.13. The 3 by 3 arrays with an opening about 2.5 mm in diameter on the dielectric and the anode was operated at 9 mA current in the pressure range from 100 Torr to 760 Torr. The discharge chamber was mounted directly on the

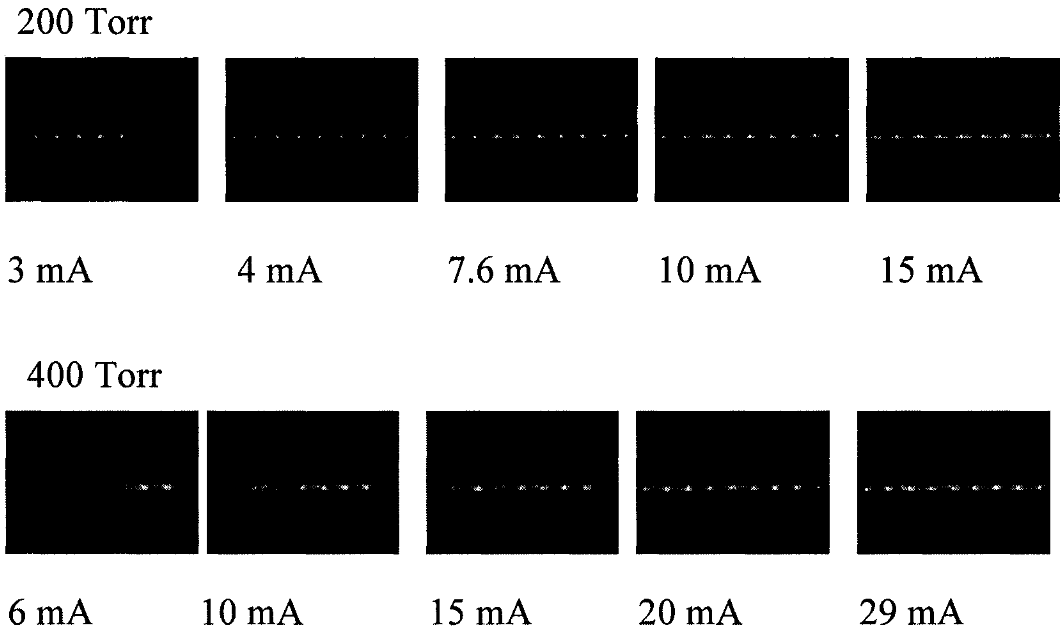

Fig 5.10 Photographs of MHCDs array in Xe.

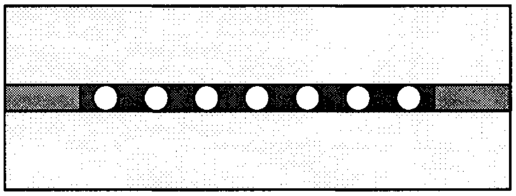

Long slit with 7 holes on cathode, and anode on the slit ends

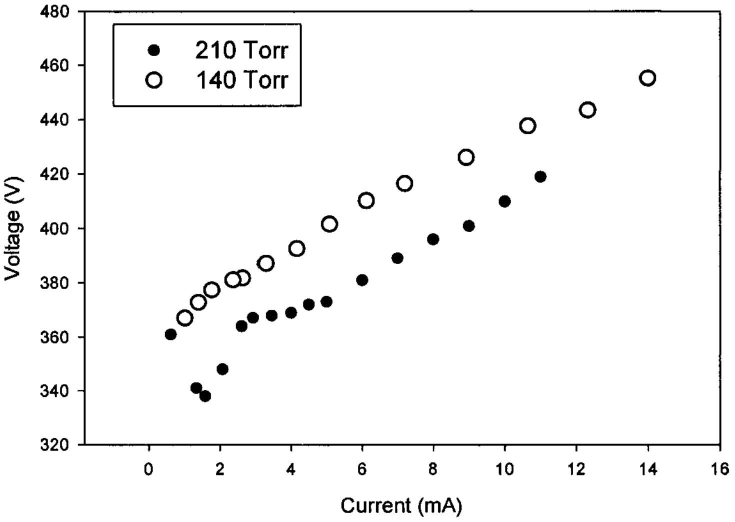

Fig 5.11 Top-view of a MHCD array with end anodes and I-V characteristics.

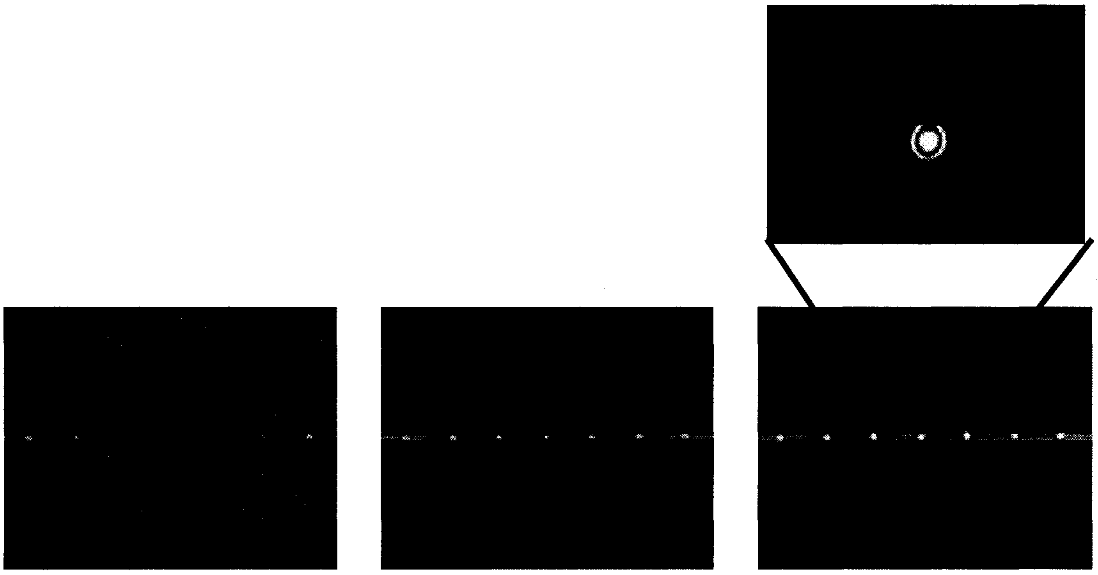

210 Torr, 8 mA **210 Torr, 10 mA** **210 Torr, 20 mA**

Fig 5.12 Photographs of MHCD array development with current.

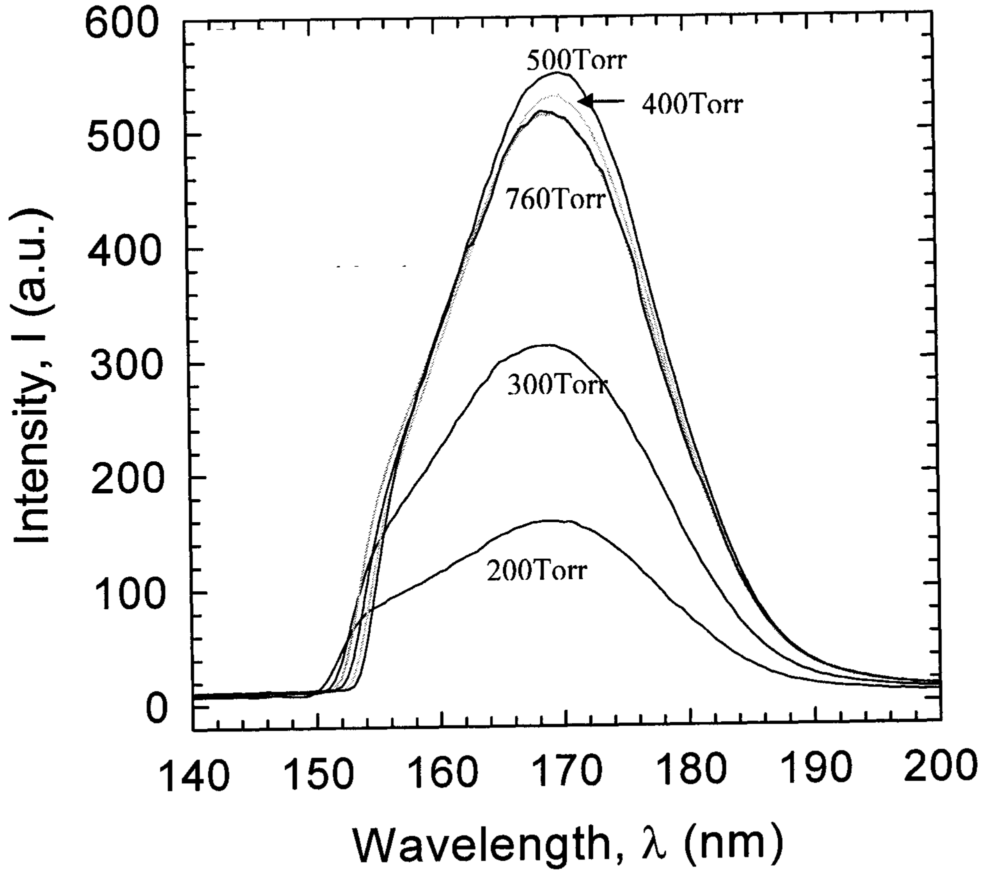

Fig 5.13. Spectrum of MHCD array in Xe.

monochromator and a LiF window was used to separate the high pressure discharge chamber from the evacuated spectrograph. The entrance slit of the monochromator was about 200 μm wide which corresponds to a spectral resolution of 0.5 nm. The measured spectrum is very similar to that of single MHCD as shown in Fig 3.4. At low pressure, there are some indications of the first continuum, which extends from the resonance line towards longer wavelength. The second excimer continuum peaking at 172 nm appears at higher pressures. At 500 Torr pressure, excimer radiation has the highest efficiency which is similar as that for the single open cathode MHCD [4].

5.5 Absolute power and efficiency measurement

The absolute UV power of a slit with ten MHCDs was measured by means of a photomultiplier (PMT) tube (Hamamatsu R1533). Both the sample and the PMT were attached to a vacuum tube in which a focus lens and UV filter are mounted. The UV radiation was focused on the PMT. The PMT was calibrated by means of a MHCD source with known UV power. The highest UV radiant power we obtained from this sample was about 370 mW at 600 Torr and 30 mA. The efficiency reached 10%, similar to a single MHCD. Figure 5.14 shows the absolute power of UV radiation versus discharge current, with xenon pressure being the variable parameter.

The intensity of the excimer emission depends on pressure and current. It reaches a maximum for pressure in excess of 400 Torr, as already shown in Fig 5.14. It increases with current up to a maximum value which depends on pressure. Consequently, the excimer efficiency, shown in Fig 5.15 has its maximum at low currents. It reaches 10 % for high pressure and currents below 10 mA (1 mA/discharge). The optimum pressure derived from the power measurement corresponds to the spectrum measurement result in the previous section.

The excimer radiation did not increase linearly with current, as shown in Fig 5.15. It reached a maximum when the whole string was covered by the plasma. Radiation saturated or even dropped at higher current. This means that in the abnormal mode the voltage increase does not cause the generation of more excimers. The additional power could either be converted in thermal energy or multiple ionization of the xenon atom, an effect which does not contribute to excimer generation.

5.6 Spatial distribution of excimer radiation

The spatial distribution of the line excimer source was recorded by means of vacuum imaging system with an ICCD camera. Photographs of plasma taken at 172 nm are shown in Fig 5.16. The plasma extended above the anode by about 2 to 3 mm, and expanded in width from the 0.2 mm wide slit to about 1 mm. The number of microdischarges which “turn on” increased with current.

However, when the current was increased beyond the value where all the discharges were excited, the excimer source changed. Instead of showing highest intensity values at the position of the microholes (spots in Fig 5.17) the plasma became homogenous. The total excimer power decreased from this point

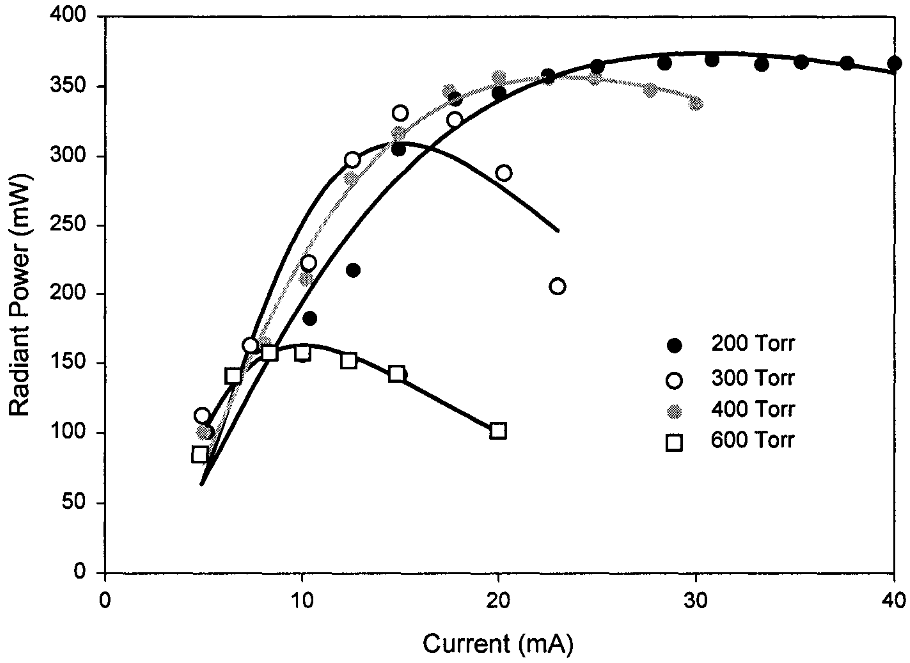

Fig 5.14 Radiant excimer power, versus discharge current with xenon pressure as variable parameter [61].

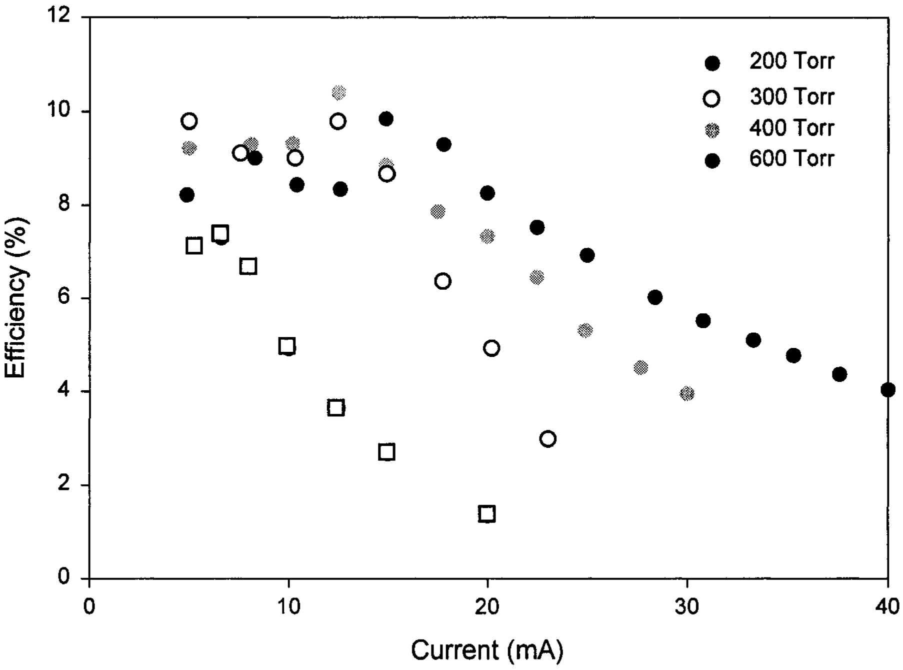

Fig 5.15 The corresponding values of the excimer efficiency: total optical power in UV divided by the electrical power [61].

on with current (Fig 5.18). The critical current for this transition was dependent on pressure. The lower the pressure, the lower the critical current (Fig 5.18).

By creating a pattern in the dielectric, which covers the cathode surface, an identical UV pattern is formed. An example is shown in Fig 5.19. The total current 60 mA corresponded to an average current per hole of 0.6 mA. The pressure was 200 Torr in Xenon. This pattern was formed on a flat surface with area 1 cm by 1cm.

5.7 Lifetime measurement

The sample lifetime was measured for different geometries operated in the three modes. In the Townsend discharge mode, a test sample with a geometry as shown in Fig 5.1 was continuously operated over 24 hours at 8 mA (80 μA per discharge) in 70 Torr Argon. No obvious damage was observed due to the small operating current. The sixteen-hole sample with distributed ballast (as shown in Fig 5.2) was operated at a current higher than 20 mA about twenty-four hours before there was a short circuit between cathode and anode. Increasing the operating lifetime of the sample requires cooling and lowering of the power density. For the covered cathode sample (Fig 5.4), the discharge distribution tends to become inhomogeneous after a homogeneous start. As shown in Fig 5.5, after 30 minutes operating time one discharge became more intense and the other discharges extinguished. The reason for this is that the current density on the small hollow area is high enough to cause strong sputtering. When the sputtered metal vapor deposits on the cover dielectric, it begins to serve as a

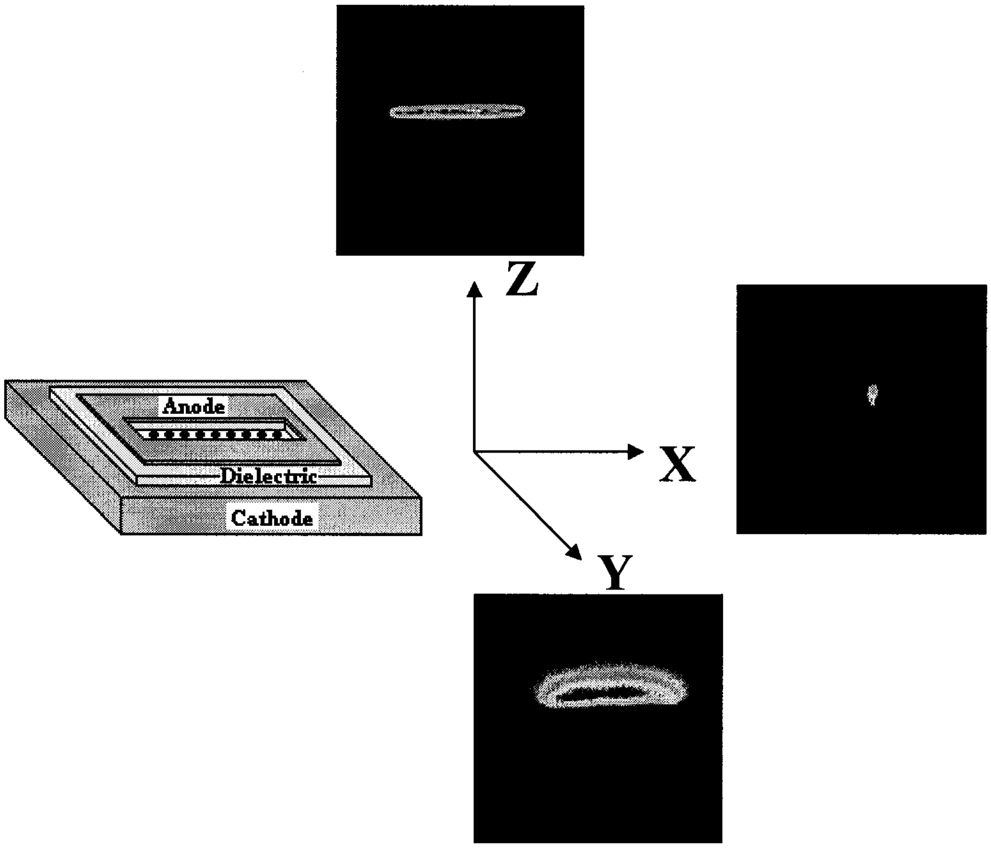

Fig 5.16 Plasma distribution of MHCD array obtained at 172 nm radiation.

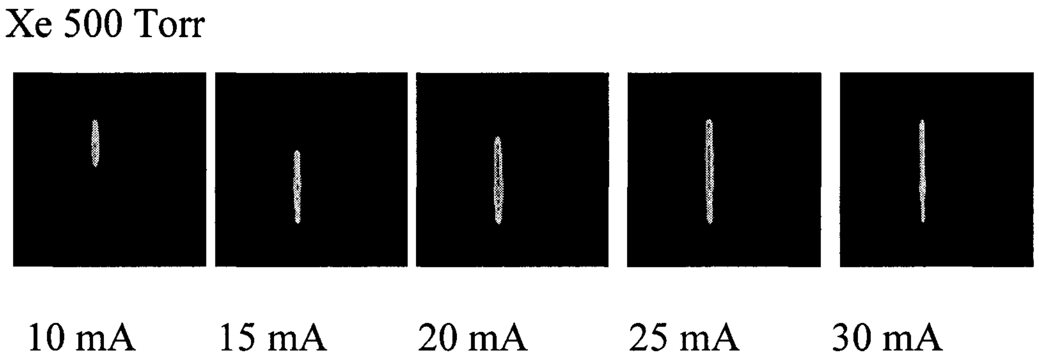

Fig 5.17 UV images of MHCD array development with current.

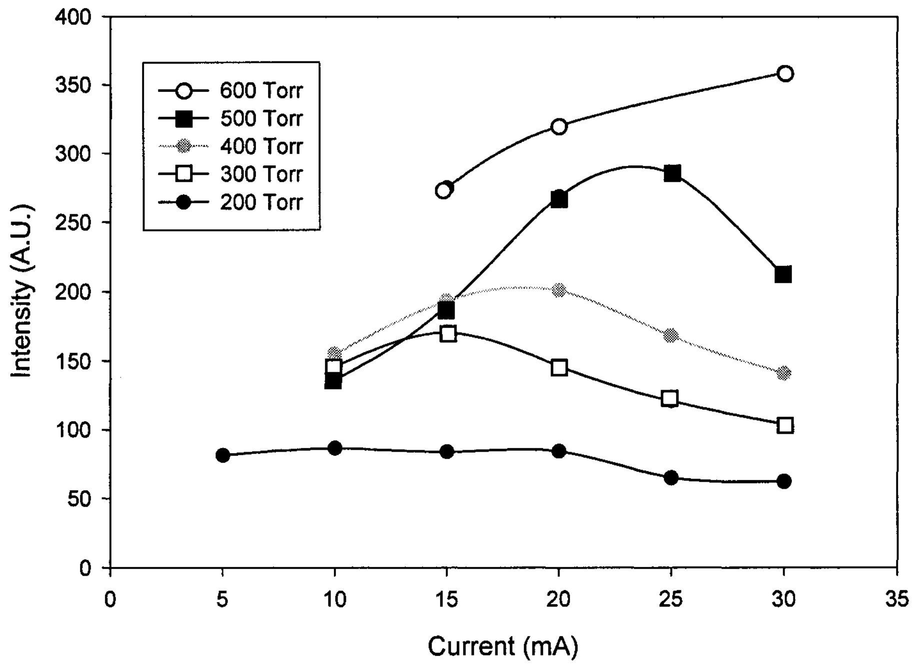

Fig 5.18 UV radiation intensity from MHCD array.

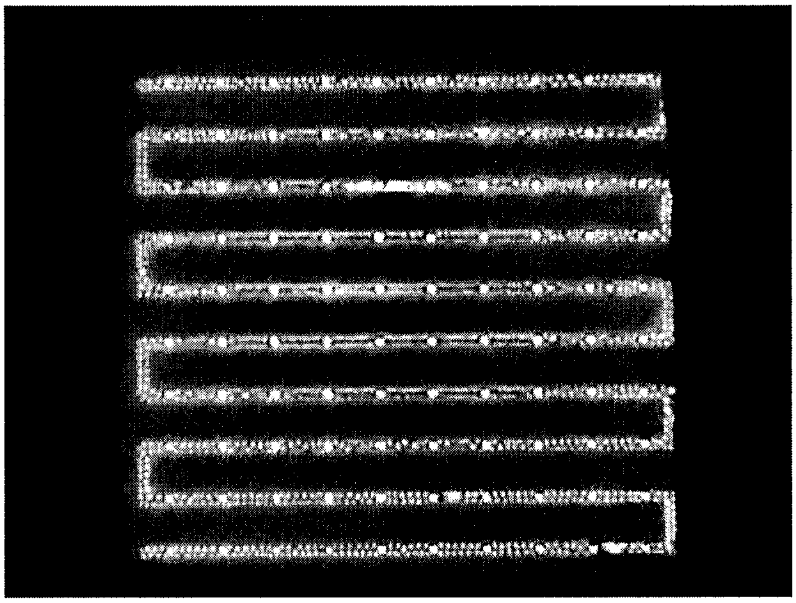

Fig 5.19 A 10mm by 10mm plasma pattern generated by MHCD arrays.

cathode. The deterioration of the size of the cathode due to dc sputtering is concomitant to the behavior of parallel operation in covered cathode discharges.

Because the cathode surface is much larger than the covered cathode, the current density in the system shown in Fig 5.8 is much less. The device does not deteriorate even after a long time of operation at optimum current. In order to determine the temporal development of UV radiation, the excimer emission from this geometry with 1 cm length and ten micro holes was recorded by means of an ICCD camera. The chamber was filled with 175 Torr Xenon, and the discharge was operating at 5 mA current. The discharge had homogenous plasma along the whole string. We observed that a very small leak of the chamber strongly effected the lifetime of UV radiation. By improving the vacuum chamber, the UV radiation lifetime was increased from 80% reduction in 3 hours to 30% reduction in the same period. Fig 5.20 plots the UV intensity versus time. The curve fitting for this data shows an exponential decay with rate 1.72 × 10^{-3} s^{-1}.

$$I = I_0 \exp(-1.72\times10^{-3}t) \tag{5.4}$$

where I represents the UV intensity, I_0 initial UV intensity and t the time in seconds.

5.10 Series operation of MHCDs[67]

The excimer radiation power of a discharge increases linearly with current [4]. However, the irradiance stays approximately constant due to the almost linear increase in the emitting area with current [6, 66]. One method to increase the radiant emittance is to increase the pressure, as was shown in xenon [66].

Some sections of 5.10 are extracted from publication "Series operation of direct current xenon chloride excimer sources" (A. El-Habachi, W. Shi, M. Moselhy, R. H. Stark, K. H. Schoenbach) where the candidate was co-author.

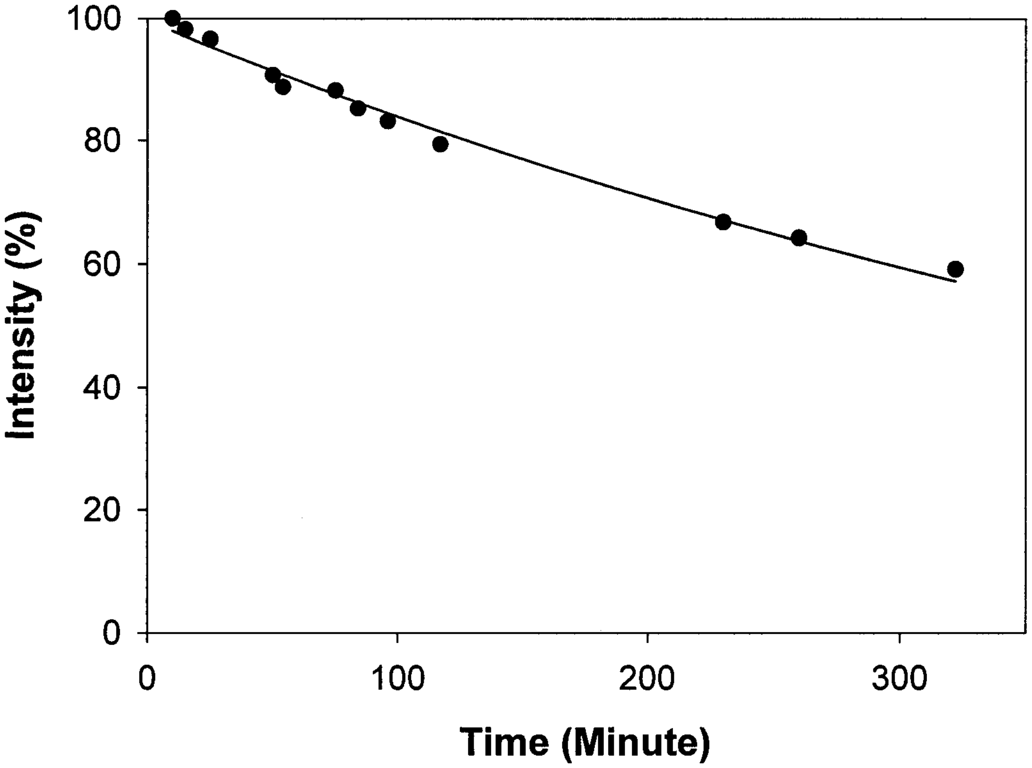

Fig. 5.20 Lifetime of MHCD array in Xe.

However, this is a relatively weak effect: the irradiance increases only 2 times when the pressure is increased from 200 to 760 Torr. Another way to increase the irradiance is based on the series operation of an array of these discharges. Since the excimer gas does not reabsorb the excimer radiation, the excimer irradiance generated by n discharge plasmas in series along the discharge axis is expected to be n times that of a single discharge.

We used a three-electrode system, which allows us to generate two discharges in series, i.e., a “tandem” discharge. These discharges were operated in XeCl mixtures, where the excimer wavelength is 308 nm, rather than in xenon. Xenon chloride has the largest stimulated emission cross section and excimer lifetime of the rare gas halides and is therefore the best candidate for exploration of excimer laser concept.

The electrode geometry consisted of three molybdenum foils of 250, 100, and 250 μm thickness separated by mica sheets of 200 μm thickness. A 250 μm diameter hole was mechanically drilled through the five layers. The geometry is shown in Fig 4.3. This electrode configuration allowed us to study both single discharges, with one electrode disconnected, and tandem discharges. The electrodes could be biased in any way: it was possible to have the outer electrodes serve as cathodes with the inner electrode being the common anode or the other way around.

5.10.1 Single discharge in tandem sample

By disconnecting one of the outer electrodes, a single discharge in this tandem electrode configuration could be explored. Two modes of the microhollow cathode discharge were observed in this case depending on the polarities of the remaining outer electrode and the inner electrode. With the outer electrode serving as the cathode the I-V characteristic of the discharge resembled that of a two-electrode microhollow cathode discharge as shown in Fig 3.2. However, when the outer electrode is the anode, the I-V characteristic resembled that of covered cathode microhollow cathode discharge as shown in Fig 5.3. Besides the I-V characteristics, the excimer source had a very different appearance for the two modes, the excimer source was confined to the electrode opening, whereas in the second case (the outer electrode cathode) it spread over the outer electrode surface.

Stable dc operation of MHCDs in a XeCl gas mixture of HCl, H_2, Xe, and Ne was achieved up to pressures of 1150 Torr. The excimer spectrum of XeCl radiation for the configuration where the inner electrode was the cathode is shown in Fig. 5.21 for various pressures. The main spectral feature is the XeCl excimer line at 308 nm corresponding to the B-X band. The internal radiative efficiency reached a maximum value of 3.2 % at a pressure of 1050 Torr. At this pressure, the radiant power was consequently 19 mW for a current of 3 mA and a sustaining voltage of 195 V. The spectral peak power at 308 nm was 5 mW/nm. For the a given input power this is higher by a factor of two, compared to xenon excimer emitters (with efficiency ~6%) [4], due to the small FWHM of the 308 xenon chloride line (4nm) vs that of the xenon line (24 nm). The center electrode was ring shaped with a limited surface given by the hole radius and the foil thickness. It was therefore expected that the discharge for this configuration at

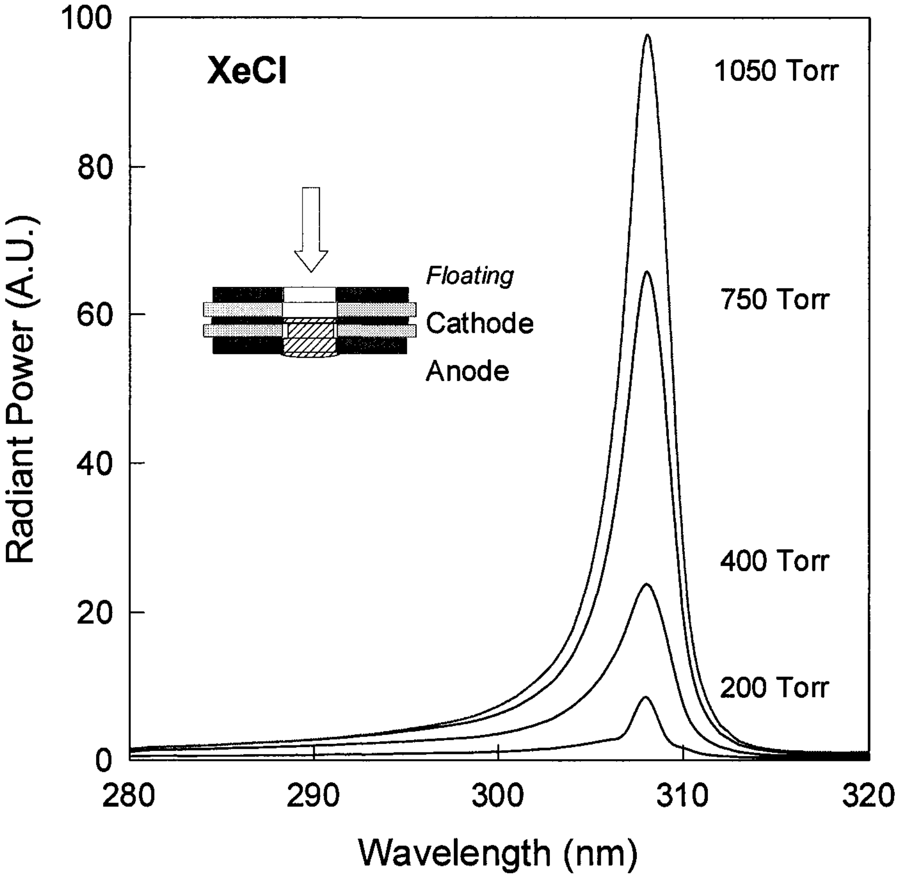

Fig. 5.21 Excimer spectra of a single discharge for various pressures. The arrow indicates the direction of observation [66].

high currents should be an abnormal glow where the voltage increases with current. The outer electrode had a much larger surface, which included the surface area of the outer electrode. In the configuration, where the outer electrode served as cathode, the cathode fall could expand over an almost unlimited area. The discharge in that case behaved as a normal glow discharge, with constant voltage at increasing current.

For the configuration where the inner electrode was the cathode, measuring the end-on emission from the opposite side gave the same value of radiant power. A similar pressure dependence of the excimer spectrum was obtained when the center electrode served as the anode. However, the values of the measured radiant power from the cathode side were higher than that recorded from the anode side.

These measurements indicate the radiation source locates at the cathode. In the case where the outer electrode was the cathode the excimer source expanded over the cathode surface outside the hole, whereas in the opposite case the excimer source was confined inside the electrode hole, probably close to the center electrode.

5.10.2 Tandem discharge

When the third electrode was also biased (rather than disconnected), two basic configurations were studied: one, where the outer electrodes were cathodes (insert in Fig 5.22), and the other where these electrodes were anodes (insert in Fig.5.23). The spectrum of each individual discharge and the tandem

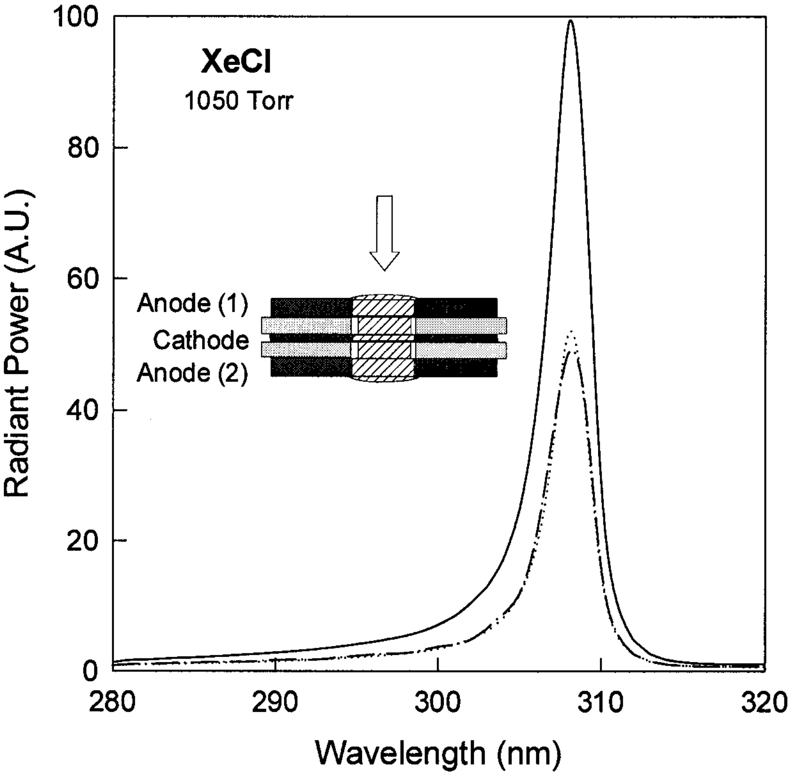

Fig. 5.22 Excimer spectra of single discharges between the center cathode and anode (1) (dotted line) and anode (2) (dash line), and the combined (tandem) discharge (solid line) [66].

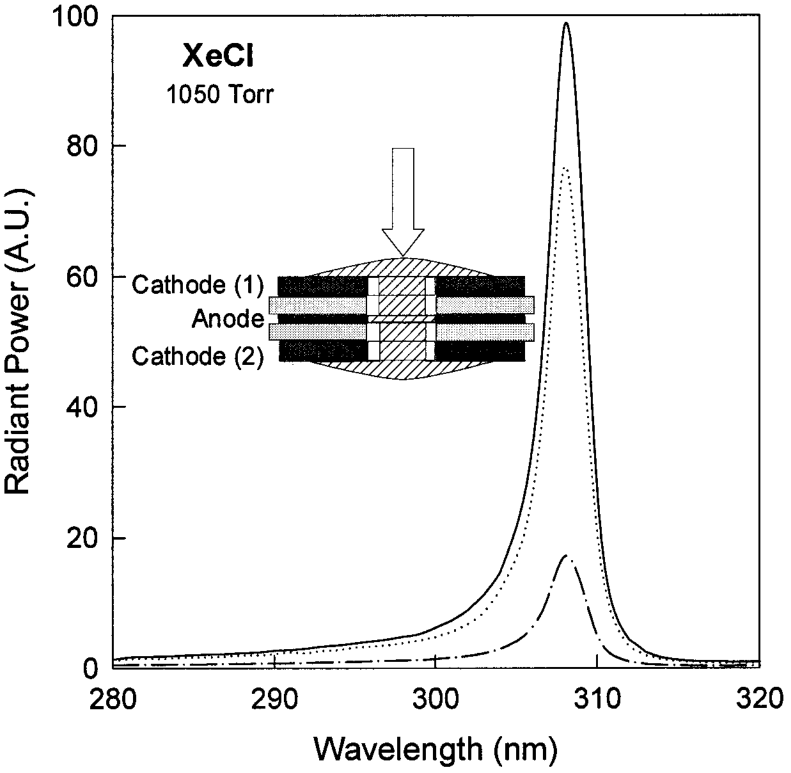

Fig. 5.23 Excimer spectra of single discharges between the center anode and cathode (1) (dotted line) and cathode (2) (dashed line), and the combined (tandem) discharge (solid line)[66].

discharge were recorded in both case. The spectral distribution was found to be the same as that of single discharges, however the amplitude was strongly dependent on the configuration.

Using the center electrode as cathode, two stable discharges with almost identical current were obtained between this electrode and the two outer anodes without individually ballast. The spectral emission of the two discharges was of the same magnitude, as shown in Fig. 5.22. The sum of the radiant power of the two single discharges was, as expected (because of the negligible absorption of the excimer radiation), identical to that of the tandem discharge.

For the case where the center electrode was the anode, the current of two discharges extending from this center electrode to the outer electrodes was not identical. In order to generate the same current in each of the two discharge branches the outer electrodes needed to be individually biased. The measured radiant power of the two individual discharges even for the same current drastically differed in this configuration due to different optical access. The radiant power for the discharge between cathode (1) and anode (insert in Fig. 5.23) was measured end-on from the cathode side where the plasma expanded over the cathode surface; consequently the total emission was recorded. The discharge between cathode (2) and anode was recorded from the anode side where only 20% of the radiation was observable (80% of the source extended over the outer cathode surface).

For tandem operation, with the center electrode being the cathode, the range of stable operation was limited to approximately 5 mA due to the onset of instabilities. These instabilities are possibly glow-to-arc transitions, which became more likely at higher cathode fall voltages. A way to increase the current range for stable operation is, therefore, to increase the cathode surface by using a thicker cathode foil. The anode area, as demonstrated by our experiments in the configuration where the outer electrode served as anode, did not limit the discharge stability, at least not in the current range of our measurements.

The resistive current-voltage characteristics of the microdischarges in the configuration where the center electrode with its limited surface served as the cathode, indicate the possibility of forming longitudinal arrays consisting of a multi-electrode sandwich structure with alternatively biased metal foils (electrodes). The extension of the basic three-electrode structure, used in our experiments, to a multiple sandwich structure, provided an electrode configuration, which resembled a multitude of basic anode-cathode-anode structures, rather than cathode-anode-cathode structures, where control of the discharges would require current control at all electrodes. In a multi-electrode configuration all the electrodes, anodes and cathodes, would be limited in surface area, due to the dielectric spacers between them. The electrodes at both ends could be covered with a dielectric to prevent normal discharges even at the end electrodes. Consequently, any of the discharges in this multi-electrode system would be abnormal, with a resistive discharge characteristic at higher currents, the condition for stable operation. Ballasting of the individual discharge does not seem to be required. The irradiance generated by such a discharge string on the axis of the hollow electrode configuration would for n discharges be n times that of a single discharge. This is due to the negligible reabsorption of excimer radiation in the excimer gas. Running these discharge strings in parallel will therefore allow us to generate more powerful flat panel excimer lamps compared to just using planar structures with single discharges arranged in parallel [60].

A second application for a string of discharges would be as an excimer laser medium. The input electrical power for a single discharge is on the order of Watt. The volume of the cathode fall and negative glow, where most of the electrical energy is dissipated is assumed to be less than or at most equal to the volume of the cathode opening. For a 250 μm thick, 100 μm diameter cathode hole the cathode hole volume is 1.9×10^{-6} cm^3. The power density in this plasma will therefore exceed 500 kW/cm^3. The typical fluorescence lifetime, τ, of the XeCl excimer is 11 ns [68], and the photon energy, hν, is 4 eV. If we assume that 90% of this power density will be used to overcome losses (volume losses and the loss in the form of the laser output), the spontaneous power density is:

$$P_s = 50 \text{ kW/cm}^3 = (h\nu/e)(N_2/\tau) \tag{5.5}$$

Consequently the upper state density, N_2, is 8.59×10^{14} cm^{-3}. The small signal gain coefficient is:

$$k = (N_2 - g_2N_1/g_1)\sigma_{se} \tag{5.6}$$

Assuming that the lower state is empty ($N_1 = 0$), and using the cross section for XeCl stimulated emission, σ_{se}, of 4.5×10^{-16} cm^2 [9], the small signal gain coefficient will be 0.38/cm.

With such gain conditions, lasing should be achievable if sufficient discharges are placed along the line of sight. The advantages of such a laser, besides operating cw, would be its size which is expected to be in the mm range (dependent on the number of discharges in series), the low sustaining voltage, which is comparable to that of a single discharge voltage, approximately 200 V, and the possibility of creating an array of microlasers by placing them in parallel similar to the lamp structure explored before [60].

5.10.3 Plasma column

In addition to the tandem discharges, multiple discharges in electrode geometries with larger distance separations (several mm) were studied. A three-electrode sample was made as shown in Fig 5.24. In this geometry, the third electrode was placed at a distance of 1.6 mm with respect to the other two. All of the holes on the electrodes were aligned by using a He-Ne laser. When the voltage was applied as shown in Fig 5. 24, a plasma column could be established in XeCl gas along the axis through the holes at pressures of up to 1000 Torr. The discharge was first established through the MHCD sample. The plasma column between the large distance electrode was generated when the voltage applied to the third electrode exceeded a threshold value (normally 30-50 V depending on pressure). Similar results are reported ref 48 and ref 49.

To study the scalability, another hollow cathode sample was stacked on the three-electrode geometry as shown in Fig 5.25. The distance was also 1.6 mm. This experiment indicates that long plasma columns can be established by stacking hollow cathode test samples.

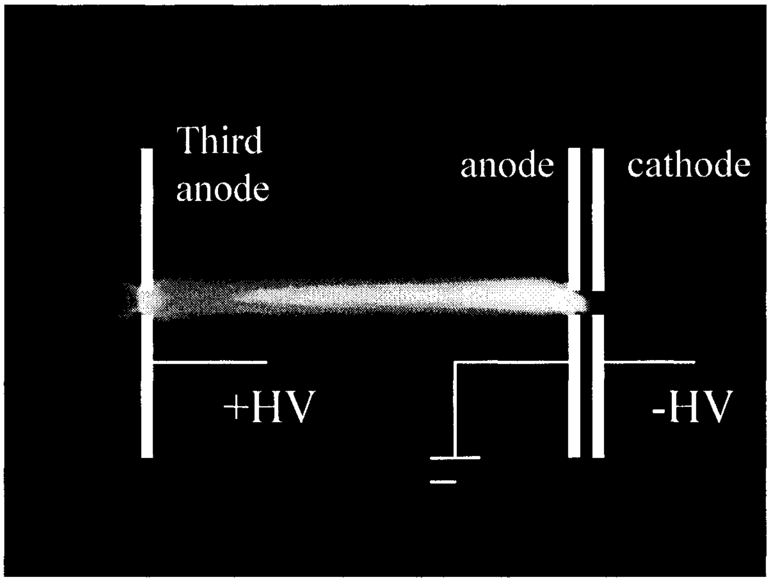

Fig 5.24 Plasma column through a MHCD and a third electrode.

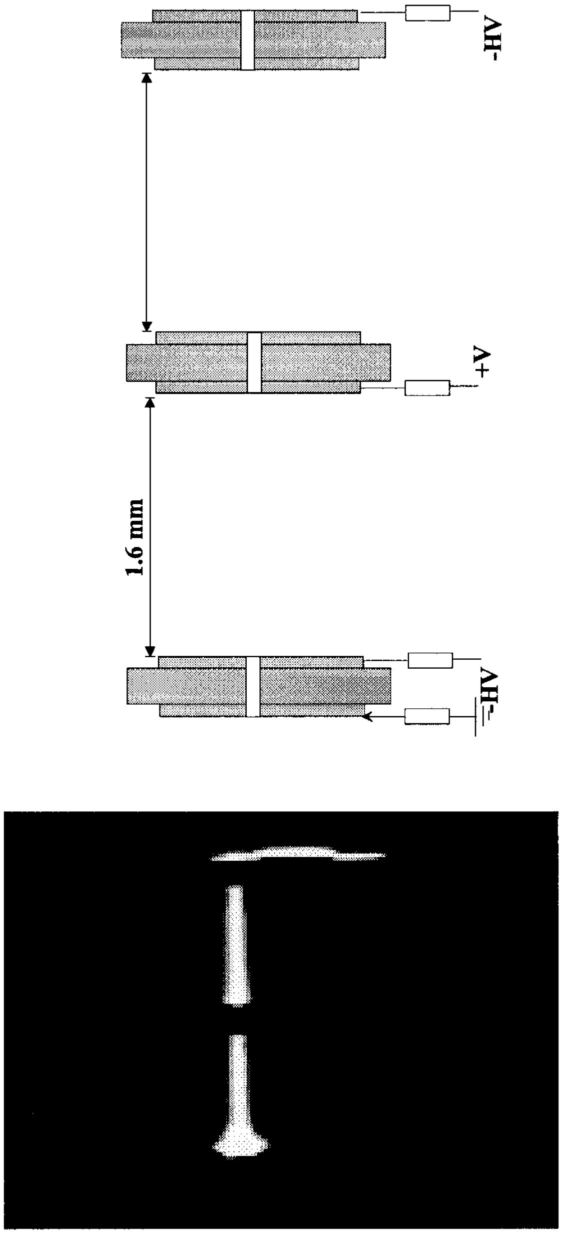

Fig 5.25 Plasma column through three stacked MHCDs.

CHAPTER VI

SELF-ORGANIZATION IN CATHODE BOUNDARY LAYER MICRODISCHARGES [69]

The use of electrodes containing microholes has allowed us to generate stable direct current gas discharges at high pressures [2-6]. Various electrode configurations of microhollow cathode discharges were described in pervious chapters. In geometries such as the open cathode and limited cathode where the cathode surface area was not restricted to the interior surface of the hole but extended over the planar area, we observed that the cathode fall extends into the surface area outside the hole as current increases. The expansion of the plasma layer over the planar cathode surface outside the cathode hole is dependent on pressure. The diameter of plasma layer is reduced with increasing pressure [66]. The external parameters, which determine the DC excimer emission, are (in addition to the electrode geometry) pressure and current. Because of the emphasis on excimer emission, the research in this field has focused on optimization of the use of these discharges as excimer lamps by varying current and pressure. The excimer power increases linearly with current, and irradiance increases linearly with pressure. The design of a high power excimer lamp consequently requires high pressure and high current operation. The opposite range of operation, i.e. low pressure and low current, has not had the same attention as the high pressure, high current regime.

Most of the sections in Chapter VI are extracted from publication “Self-organization in cathode boundary layer microdischarges” (Karl H. Schoenbach, Mohamed Moselhy, and Wenhui Shi) where the candidate was co-author.

6.1. Experiment and results for CBL discharge

In order to explore excimer discharges in the low current, low pressure regime we used an electrode configuration as shown in Fig. 4.2(j). The cathode consisted of a molybdenum foil, 250 µm thick, with a microhole of 100 µm diameter and 100 µm depth in the center. The hole was generated by means of laser drilling, and was therefore slightly conical. A 250 µm thick layer of alumina was placed on top of the cathode, coaxial to the hole. The diameter of the opening was 1.5 mm. A molybdenum anode again with a thickness of 100 µm was placed on top of the dielectric, with the same opening as the dielectric. As a fill gas we used xenon at pressures varying from 50 to 130 Torr. The discharge was operated in a direct current mode, and DC voltage and current were recorded. The discharge plasma was observed end-on in the visible spectrum range using a CCD camera.

When the discharge was operated at pressures of approximately 128 Torr and at relatively high current (> 1mA), the plasma was not only generated in the microhole, but also covered the planar cathode surface outside the hole (Fig 6.1(a)). Further increase current the discharge operated in abnormal glow mode. In the low-pressure case, at 128 Torr, this effect could be observed at a current of 6 mA as shown in Fig. 6.1 a. However, when the current was reduced below 1 mA for 128 Torr pressure, the plasma structure changed completely. Patterns consisting plasma filaments developed symmetrically around the center as shown in Fig. 6.1 b, c, d. The patterns were well expressed at higher current, and

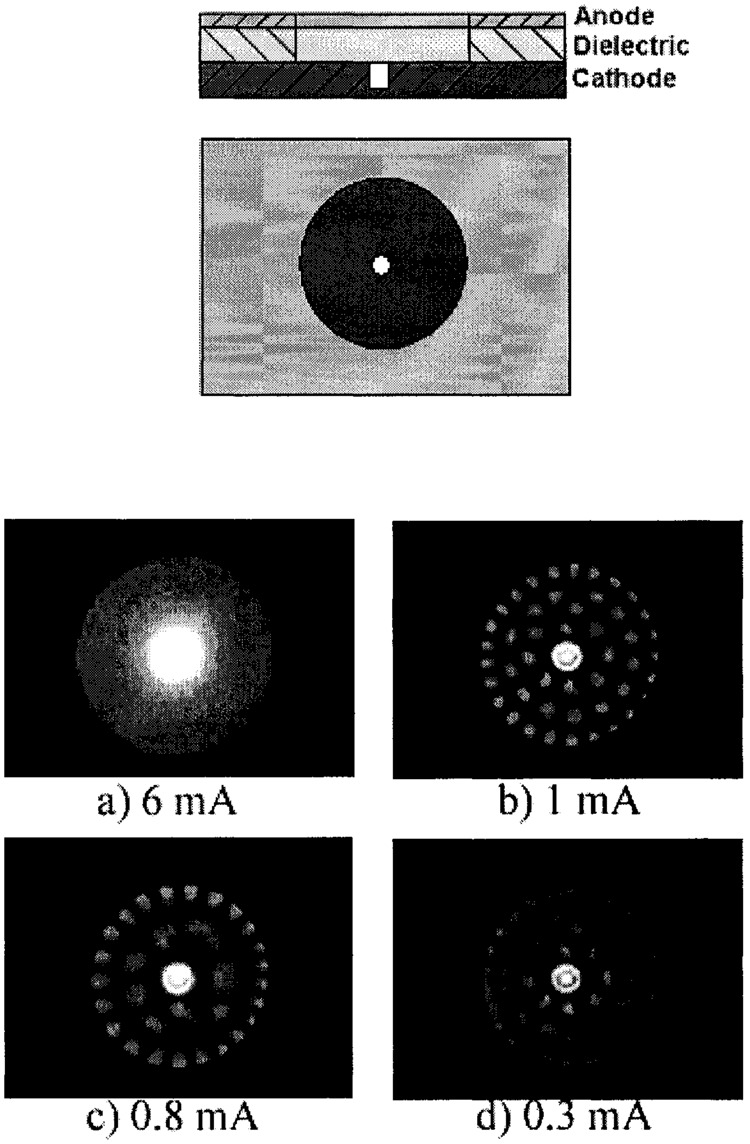

a) 6 mA

b) 1 mA

c) 0.8 mA

d) 0.3 mA

Fig 6.1 Sample geometry and the spatial plasma distribution in microhollow cathode discharges observed end-on for various discharge currents. The gas was xenon at a pressure of 128 Torr [69].

became more blurry at lower current, until the discharge extinguished at approximately 0.3 mA.

In the formation of these patterns, the microhole did not seem to play an important role. We therefore replaced the cathode by a flat layer of molybdenum without a microhole. The simpler electrode geometry allowed us to generate discharge structures similar to the one containing the center hole. The diameter of the dielectric and anode opening with flat cathode was varied from 0.75 mm to 3.5 mm. In addition, we explored discharges with rectangular shaped anodes and found that the basic phenomena are not dependent on the shape of the anode opening. For fill gas we have again used xenon at pressures varying from 75 Torr to 760 Torr. The discharge plasma was observed end-on in the visible spectrum range, as before, using a CCD camera with a microscope lens. In some cases a VUV imaging system was used to observe the plasma emission at the wavelength of xenon excimer emission. The imaging system consisted of an Intensified CCD camera (ICCDMAX provided by Princeton Instruments), an optical filter with a peak transmission of 24% at 170.9 nm and a full width at half maximum (FWHM) of 26.8 nm, and a Mg_2F lens.

The DC current-voltage characteristics for discharges in a circular electrode geometry with a cathode diameter of 0.75 mm are shown in Fig. 6.2 for four pressure values. These characteristics show several distinct regions. At low current, and pressures higher than 400 Torr, voltage stays constant, indicating the presence of a normal glow discharge (region I). This region was not found in the low-pressure range. At the current threshold value, which shifts with

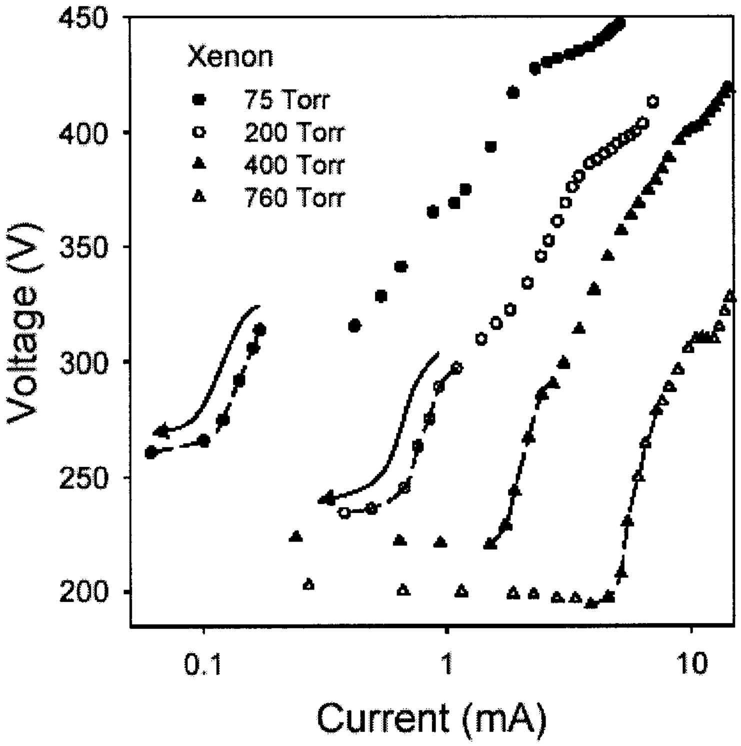

Fig 6.2 Voltage-current characteristics of xenon discharges at various pressures. The range where pattern formation is observed is indicated by connecting the data points. For lower pressures (p < 200 Torr) this range can only be reached by reducing the current (direction of arrows)[69].

increasing pressure to larger current values, current increases exponentially with voltage (region II). This is the range where pattern formation was observed. Note that at low pressure (75 and 200 Torr) stable discharges characterized by current-voltage values in range II can only be obtained by lowering the discharge current, and starting in a current range above range II. Attempts to increase the discharge current when operating the discharge in range II, led to the extinction of the discharge. After the steep increase, the current–voltage characteristics enter a phase with slower growth of voltage with current (range III). Discharges in this range seem to be abnormal glow discharges, as suggested by the photographs of the discharge (Fig. 6.3).

The results of optical studies in the visible range are shown in Fig. 6.3. A set of photographs, for the pressure values of 75, 200, 400, and 760 Torr for various currents shows the development of patterns. Beginning at high currents, a homogeneous distribution of emission in the visible spectrum is observed. The intensity of this emission decreases with decreasing current. This development corresponds to region III in the current-voltage characteristics (Fig. 6.2). Lowering the current further leads to a discharge where the plasma loses its homogeneity, and patterns begin to form; first at the periphery. At 200 Torr this occurs at a current of slightly higher than 1 mA. With further reduced current, these patterns become more distinct, and cover less and less of the available cathode surface. The formation of these patterns corresponds to region II in the current-voltage characteristics. Further reduction of current at higher pressures (> 400 Torr) causes the loss of symmetry in these patterns (region I in current-

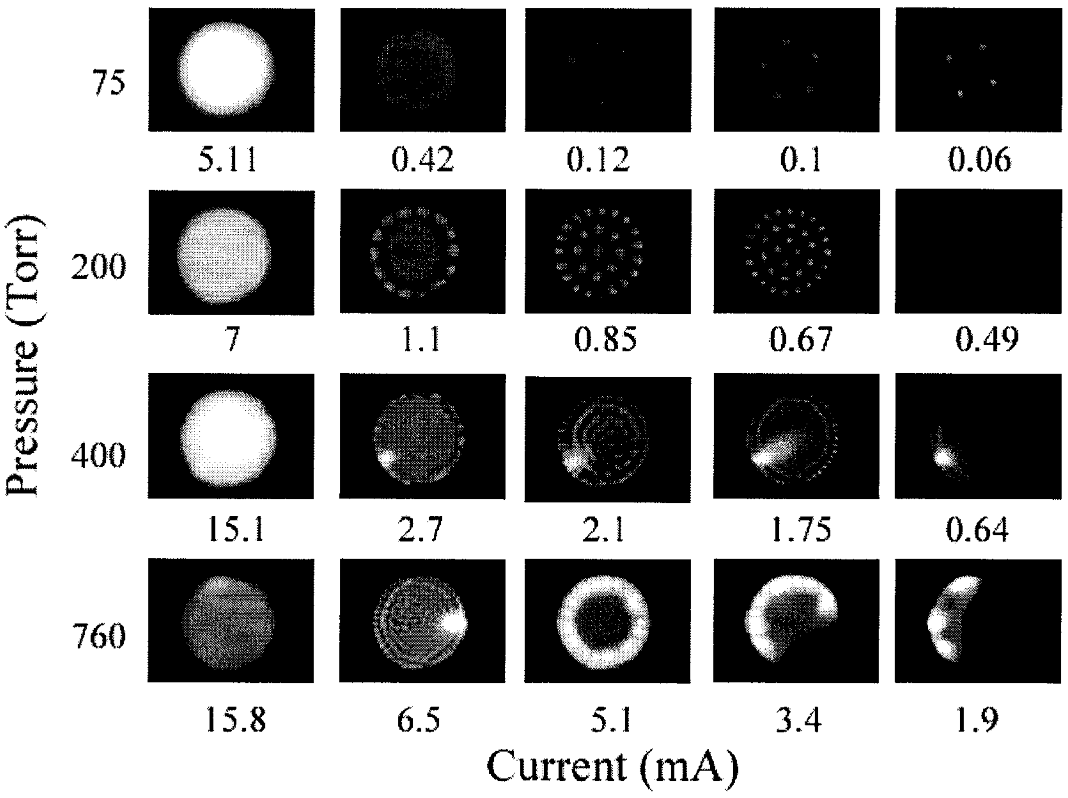

Fig 6.3 The development of the plasma observed end-on in the visible spectral range, with reducing current for various pressures. The diameter of the anode opening is 0.75 mm [69].

voltage characteristics), until the discharge extinguishes. This phase corresponds to the “normal” glow discharge as shown in Fig. 6.2. Generally, with increasing pressure, the current range where the patterns appear shifts to higher currents, patterns lose their symmetry, and the structure becomes denser. Despite this the pattern are well expressed.

Emission patterns in the low-pressure range were found to change in steps on the time scale of this observation (100 ms). The decrease in current required to change the configuration was rather small. This is shown in Fig. 6.4, where experimental results with a larger electrode geometry and a cathode opening of 1.5 mm, is shown. For a pressure of 75 Torr in xenon, changes by a few microamperes caused a complete rearrangement of the plasma.

Pattern formation is related to a strong decrease in voltage when the current is reduced. This is shown in Fig. 6.5 for the experiments at 75 Torr pressure with xenon (Fig. 6.4). Discharge voltage decreases by almost 60 V over a current range from 0.62 mA to 0.41 mA. If we assume that the luminosity of the plasma is proportional to the current density, then the current density in the luminous filaments would assume an almost constant value between 0.2 and 0.4 A/cm2. This is an order of magnitude higher than the current density value at the transition from region III (homogeneous discharges) to region II (patterned discharges). In region III the current density increases with voltage as expected from discharges operated in the abnormal glow mode.

The observed structure in the visible spectrum corresponds to structures observed in the VUV [70]. Because of the high-pressure operation, the discharge

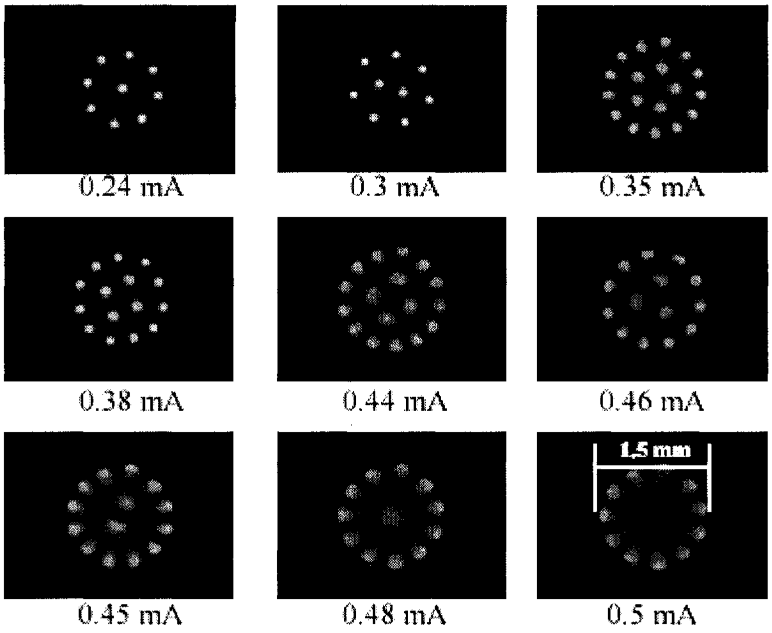
0.24 mA
0.3 mA
0.35 mA
0.38 mA
0.44 mA
0.46 mA
0.45 mA
0.48 mA
0.5 mA

Fig 6.4 Development of plasma patterns with reduced current in a xenon discharge at a pressure of 75 Torr. The diameter of the anode opening in this case is 1.5 mm [69].

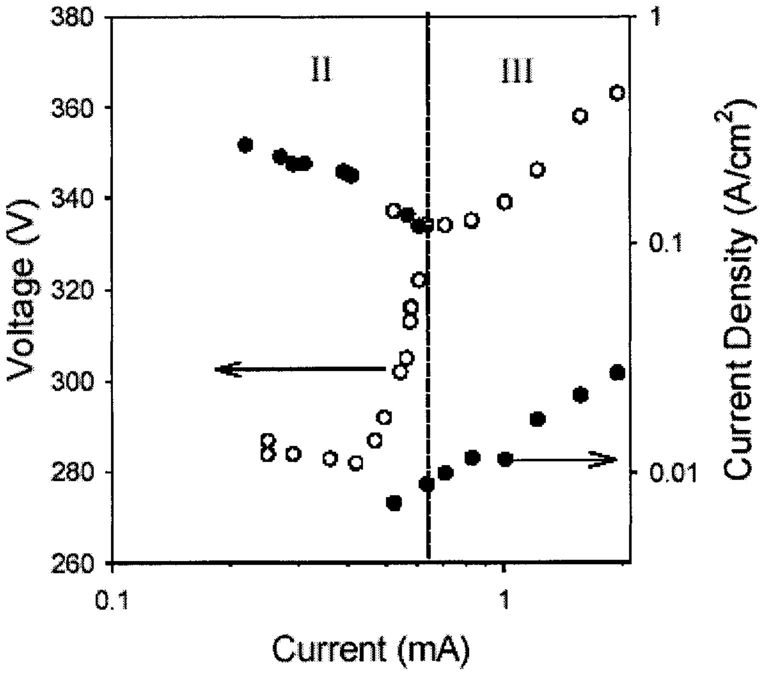

Fig 6.5. Voltage-current and current density–current characteristics of discharge in xenon at 75 Torr pressure. The current densities were estimated by assuming that the current flows through the luminous filaments only [69].

plasma is a strong source of xenon excimer radiation [4]. Recorded images in the VUV at a wavelength of 172 nm, the excimer wavelength of xenon, show similar patterns as in the visible (Fig. 6.6). The VUV images were recorded using an imaging system (ICCD camera, optical filter at 170.9 nm, and a Mg_2F lens). The system was evacuated to pressures in the mTorr range to avoid absorption. For high pressures (760 Torr), the structures observed in the visible are not seen in the VUV photographs. However, this might be due to the lower spatial resolution of the UV camera, compared to the camera used to record the visible appearance of the discharge (Fig. 6.3).

6.2. Discussion

Self-organization has been observed in various nonequilibrium systems. Best known are patterns which evolve in fluids, and are based on convection (Benard pattern) [71]. Observations of pattern formation in barrier discharges [72,73] are more recent. Barrier discharges are gas discharges, generally at high gas pressure, which are generated by applying pulsed or oscillating electric fields to electrodes, which are covered by dielectrics, or where a dielectric layer is placed between the electrodes. The lifetime of these discharges is determined by the charging time of the dielectric layer(s). The discharge current is quenched when the electric field generated by the space charge on the dielectric surface has reached values approaching that of the applied electric field. The position of the ensuing discharge for repetitively pulsed or oscillatory applied electric fields is respectively dependent on the repetition rate and oscillation frequency. If the time

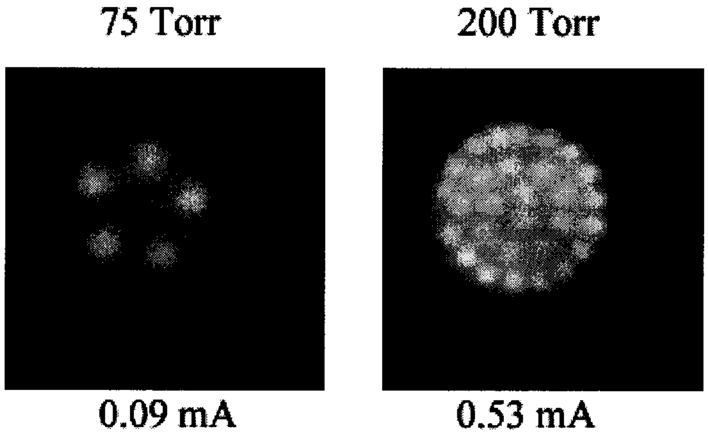

75 Torr

200 Torr

0.09 mA

0.53 mA

Fig 6.6. Examples for structures observed in the VUV (172 nm), The parameters are the same as used for the discharges shown in Fig. 6.3 [69].

between discharges is long enough such that the surface charge at the position of the preceding filament has spread over a larger surface, diffuse discharges may develop. If the space charge distribution is still nonhomogeneous, the succeeding filament tends to form where the space charge is maximum and the total electric field (sum of applied and space charge field) is minimum. In this case regularly distributed filaments have been observed, dependent on electric field and type of working gas. A model for this observed self-organization has, to our knowledge, not yet been established.

Although the patterns observed in barrier discharges look very similar to the ones seen in our microdischarges, the physics must be different. Unlike in the barrier discharges, our discharges are operated in a direct current mode, rather then pulsed; they are sustained between metal electrodes; and the electrodes are not plane parallel. However, although the ring shaped anode in our electrode configuration is not directly opposite to the planar cathode, we may assume that the negative glow, a plasma generated by the electrons accelerated in the cathode fall, will provide a planar conducting layer connected to the anode with a potential close to the anode potential. The fact that the negative glow serves as a conductor, which allows the current to flow radially to the ring shaped anode, generates a virtual electrode configuration, which is plane parallel, with a gap distance on the order of the cathode fall thickness (Fig. 6.7). The cathode fall thickness is dependent on gas and gas pressure, and on the mode of the discharge. Due to the lack of information about cathode fall thickness values for xenon gas and molybdenum electrodes, available data on argon gas with an aluminum cathode [74] were used to provide information on the order of magnitude of cathode fall thickness and negative glow thickness. For normal glow discharges in argon at a pressure of 75 Torr, where the plasma covers only part of the cathode surface, the cathode fall thickness is approximately 40 μm, and the thickness of the negative glow is approximately 270 μm. They decrease linearly with increasing pressure, and for atmospheric pressure argon, are respectively only 4 and 27 μm [74]. The cathode fall thickness decreases further when the discharge enters the abnormal glow mode.

The cathode fall voltage increases when the discharge enters the abnormal glow mode. This mode is characterized by the fact that the discharge covers the entire available cathode surface. The only way to increase current is to increase the current density, which requires an increased cathode fall voltage. Still, in this case, the negative glow continues to serve as a conductor which permits radial flow of the sum of the transverse electron and ion current, from the cathode fall to the ring shaped anode. Even in the case where pattern formation is observed, current continuity requires that the current from single filaments must flow radially through a conducting layer to the anode. We believe that a planar, but likely nonhomogeneous, plasma layer must exist in this case. In all these cases, the discharge seems to be reduced to cathode fall and negative glow, with the negative glow serving as the planar “anode” (Fig. 6.7). The discharge is reduced to the boundary layer (cathode fall and negative glow) at the cathode. We refer this discharge type as Cathode Boundary Layer discharge (CBL discharge).

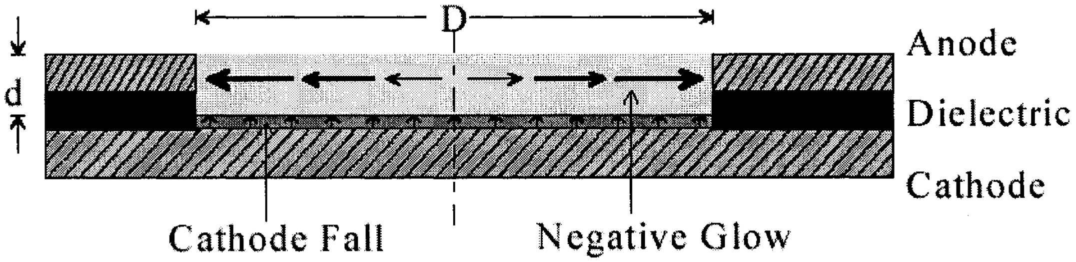

Fig 6.7. Cross-section of CBL electrode geometry, schematically showing the cathode fall layer and the negative glow region with the current directions in both layers [69].

For the case of constant current density at the cathode surface, the calculated radial current density, J_r, dependent on the distance from the discharge axis, r, in the negative glow, is:

$$J_r = J_z\left(\frac{r}{2d}\right) \tag{6.1}$$

where J_z is the current density perpendicular to the cathode surface (carried in cathode fall) and d is the thickness of the plasma layer which carries the radial current (the thickness of the negative glow). In this geometry, the current density increases linearly with r. By way of contrast in the case where the anode is on the opposite side of the cathode [66], the current density increases strongly towards the microhole. Consequently, this is a more stable planar discharge than the one with the microhole. It will become unstable if the opening of the cathode surface is so large that the current density at the outermost radius reaches a critical value, probably limiting the diameter of the anode opening.

An analytical model for the cathode fall voltage in such a “parallel plane” geometry has been developed [75, 76]. The secondary electron emission from the cathode in this model is assumed to be due to ion impact only. The increase in electron current in the cathode fall is due to ionizing electron collisions; the rate of which can be described by an ionization coefficient, α. The ion current in the negative glow, a plasma at the end of the cathode fall region, is negligible. According to this model, the current density, J, in the cathode fall is:

$$\frac{J}{p^2} = \frac{\varepsilon_0}{\ln((1+\gamma)/\gamma) - 1/(1+\gamma)} \int_0^{E_c/p} \frac{\alpha}{p} v_+\left(\frac{E}{p}\right) d\left(\frac{E}{p}\right) \tag{6.2}$$

where p is the pressure, ε_0 the absolute permitivity, γ the secondary electron emission coefficient, α the Townsend ionization coefficient, v+ the ion drift velocity, and E_c the electric field at the cathode surface.

The model assumes that the space charge field in the cathode fall is determined by a homogeneous ion density. Consequently, the electric field in the cathode fall decreases linearly with distance from the cathode. It has a gradient of E_c/l_c where l_c is the thickness of the cathode fall layer. The product of pressure and cathode fall thickness is given as:

$$pl_c = \frac{E_c}{p}\frac{\varepsilon_0(1+\gamma)v_+(0)}{J/p^2} \tag{6.3}$$

where $v_+(0)$ is the ion drift velocity at the cathode surface.

Integration over the distance from the cathode surface to the point where the electric field diminishes provides the value of the cathode fall voltage:

$$V_c = \frac{1}{2}\frac{E_c}{p}pl_c \tag{6.4}$$

Equations 6.2 through 6.4 allow us to calculate the cathode fall voltage dependence on the current density with an empirical formula for α [74]:

$$\frac{\alpha}{p} = A\exp\left(B\frac{E}{p}\right) \tag{6.5}$$

The ion drift velocity for xenon was assumed to be proportional to that of argon [77] by a factor equal to the ratio of the relative mass:

$$v_+\left(\frac{E}{p}\right) = \frac{m_{Ar}}{m_{Xe}}C\sqrt{\frac{E}{p}} \tag{6.6}$$

where m_{Ar} and m_{Xe} are the atomic mass of argon and xenon, respectively, and C was obtained from a graph [77] as 8000 $cm^{3/2}s^{-1}$ $Torr^{1/2}$ $V^{-1/2}$. The cathode fall voltage for a xenon discharge at a pressure of 100 Torr was calculated, using data for xenon [A = 26 $(cm\ Torr)^{-1}$, B = 350 V/(cm Torr)] [21] for the calculation of the ionization rate (eq. 6.5) and an assumed secondary electron emission coefficient, γ, of 0.05. This voltage is plotted in Fig. 6.8 versus current density as a solid, bold line. We did not find a value of γ for xenon gas and molybdenum electrodes, and therefore assigned a value that is in the general range of γ for glow discharges [74]. Since the following model does not claim quantitative accuracy, this assumption is not critical. The minimum cathode fall voltage represents the normal glow discharge characterized by a constant current density (increase in current is obtained by increasing the discharge area). The voltage-current density characteristic for lower current is related to an unstable glow discharge (negative slope of characteristic). The high current part of the curve represents the abnormal glow mode, where any increase in current density leads to an increase in sustaining voltage.

The only electron generation process at the cathode considered in the original von Engel/Steenbeck model [75] was secondary electron emission through ion impact. This is a reasonable assumption for low current densities, where the increase in temperature at the cathode due to ion impact is small enough that thermal electron emission can be neglected. However, with increasing current density in the abnormal glow, this assumption becomes invalid. The effect of thermal electron emission was first studied by von Engel and

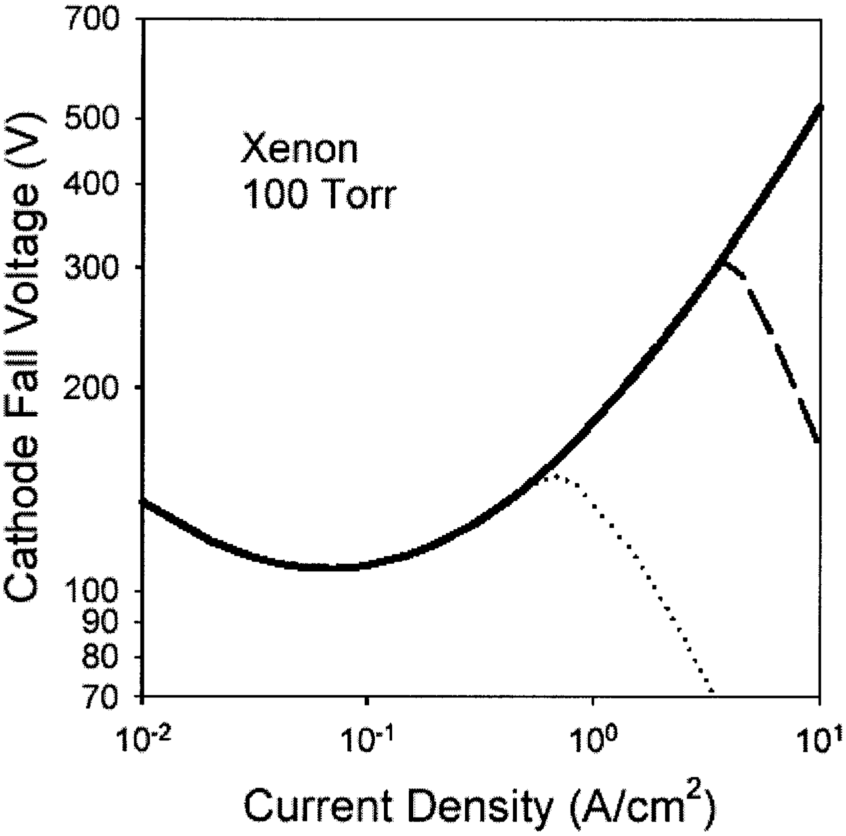

Fig 6.8 Computed voltage–current density characteristics for the cathode fall of a glow discharge in xenon at 100 Torr. The results depicted by the solid curve were obtained by assuming that the electron emission from the cathode is due to ion impact only; the dashed and dotted curves show the additional effect of thermal electron emission. For the dotted curve, the temperature at the cathode surface is determined by radiative losses [75]; for the dashed curve, additional thermal conductance losses have been considered.

Steenbeck, and also published in ref. 75. They introduced a modified secondary electron emission coefficient, γ':

$$\gamma' = \gamma + \frac{1+\gamma}{J/J_t - 1} \tag{6.7}$$

which includes the thermal electron emission current, J_t, calculated by means of Richardson's law:

$$J_t = aT^2 e^{-b/T} \tag{6.8}$$

where T is the temperature at the cathode surface and a and b are constants dependent on the electrode material.

The cathode temperature in this model is determined by the condition that the entire electrical power in the cathode fall is converted into blackbody radiation from the cathode surface:

$$JV_c = \sigma T^4 \tag{6.9}$$

where σ (5.7x10-12 W/cm2) is the radiation constant.

Despite the simplicity of this assumption, the modeling results predict the glow-to-arc transition, an effect which is observed when the current density in an abnormal glow reaches a critical value. In this phase, the thermal emission of electrons from the cathode surpasses the secondary electron emission through ion impact, and the cathode fall voltage decreases with increasing current density, as shown in Fig. 6.8 (dotted curve). The discharge becomes unstable, the plasma column contracts, and the resulting filament eventually develops into an arc.

Considering that the electrode system for the CBL discharges consists of electrodes which have a thickness of only 250 μm and are embedded in a gas which allows efficient removal of thermal energy through convection, it is reasonable to assume that thermal conduction through the electrodes plays a major role in the energy balance of such discharges. We therefore extended Engel's and Steenbeck's model [20] by adding thermal conduction through the cathode as a loss process. The processes at the cathode surface are shown schematically in Fig. 6.9. The energy loss per unit area due to radiation, σT^4, and conduction, q, through the cathode surface, is assumed to be balanced by the electrical power density in the cathode fall:

$$JV_c = \sigma T^4 + q \tag{6.10}$$

The energy loss due to thermal conduction through the cathode surface is determined by the temperature gradient normal to the surface. Since, in this extended Engel/Steenbeck model, the cathode area is assumed to be infinitely large, radial heat flow components are not considered. The heat flow into the cathode, in this case, is:

$$q = -k\frac{dT}{dn} \tag{6.11}$$

with k being the heat conduction constant. The temperature gradient, dT/dn, is the difference in the temperature at the cathode surface, T_c, to that at the opposite face of the cathode foil, T_{oc}, divided by the foil thickness, d_c:

$$\frac{dT}{dn} = \frac{T_c - T_{oc}}{d_c} \tag{6.12}$$

Assuming that the temperature T_{oc} at the cathode foil face opposite the cathode surface has values above room temperature, the linear dependence on

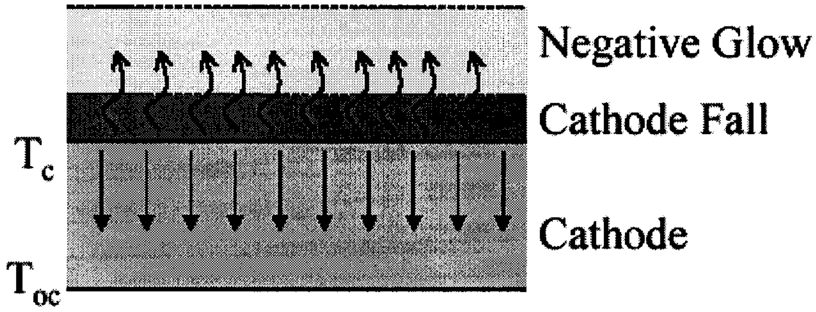

Fig 6.9 Schematic cross-section of cathode and plasma layers at the cathode. The loss processes are indicated by curved (radiation) and straight (thermal conduction) arrows [69].

temperature at the cathode surface, T_c,

$$T_{oc} = 300(1 - C_1) + C_1 T_c \tag{6.13}$$

allows us to calculate the voltage-current density characteristics of the glow discharge with the constant C_1 as a parameter. Results of this calculation, with $C_1 = 0.99$ are shown in Fig. 9 (dashed curve). Adding thermal conduction losses to the model causes a reduction in surface temperature, and, consequently, an extended range of abnormal glow operation, compared to the V-J characteristic where only radiative losses were considered. This indicates that forced cooling of the cathode foil is a good way to extend the stable region of this glow discharge.

As shown in Fig. 6.8, for both cases (radiative losses and radiative plus conduction losses), there is only one stable solution for any given cathode fall voltage. This means there is only one region, the abnormal cathode fall region, with positive slope in the voltage–current density characteristic. Branches with negative differential resistance, the subnormal glow at low current densities, and the glow-to-arc transition at high current densities, are inherently unstable. However, assuming that the spatially varying intensities correspond to current densities, the observed discharge pattern requires that two stable modes exist [73]. Another stable mode in a glow discharge, beyond the abnormal glow, would require a loss mechanism that removes energy from the plasma at a higher rate than the power required to sustain the discharge at constant voltage.

This can be achieved through forced cooling, as will be shown in the following. The temperature T_{oc} is kept constant at a certain threshold temperature by means of cooling of the cathode rather than linearly following the cathode surface temperature (eq. 6.13). This effect is shown in Fig. 6.10. Here it was assumed that the temperature, T_{oc}, is kept at 2676 K for any temperature at the cathode surface, T_c, which exceeds 2700 K. This effect clearly introduces a second stable branch in the cathode fall voltage–current density characteristic. This branch occurs for this particular case, at current densities of one to two orders of magnitude above that for the normal glow discharge. Although not shown in this figure, the discharge voltage decreases again after reaching a maximum at current densities of approximately 70 A/cm^2, and transitions into an arc as expected.

Reducing the voltage from its highest value in the abnormal cathode fall mode, as indicated by the arrow in Fig. 6.11, will initially keep the discharge in the abnormal glow mode. However, when the voltage reaches point A, the two stable branches at the same voltage allow the discharge to exist in both modes. Transition back into a single mode occurs at point B.

Although we have not actively cooled our cathode, it is reasonable to assume that with increasing temperature, the thermal conduction losses increase due to increased convection at the cathode face opposite to the discharge. This is not reflected in the calculation, where we assume an abrupt change in conduction above 2,700 K. But it is assumed that an increased convection, which would cause an increased value of C_1 with temperature could lead to a reversal in slope in the V-J characteristics.

Even if convection is not sufficient to cause stabilization of the discharge, another physical effect which will occur with increasing temperature will definitely

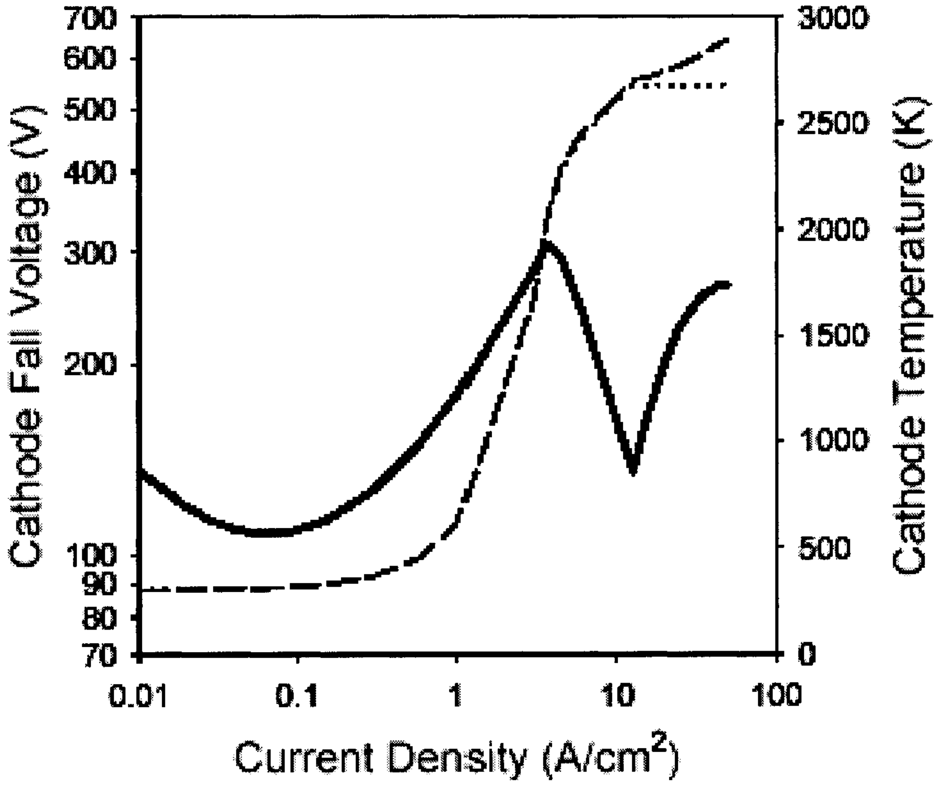

Fig 6.10. The cathode fall voltage (solid line, bold) and the temperature at the cathode surface, Tc (dashed line) and at the opposite face of the cathode, Toc, (dotted line) versus current density for a discharge with thermal electron emission from the cathode (cathode temperature determined by radiative losses and thermal conduction) with forced cooling. Up to a cathode surface temperature of 2,700 K, the temperature of the opposite face of the cathode follows the cathode surface temperature (C_1 = 0.99). For temperatures exceeding 2,700 K the cathode foil at the opposite side of the discharge is kept at a constant temperature, in this case, according to eq. 6.13, at 2676 K [69].

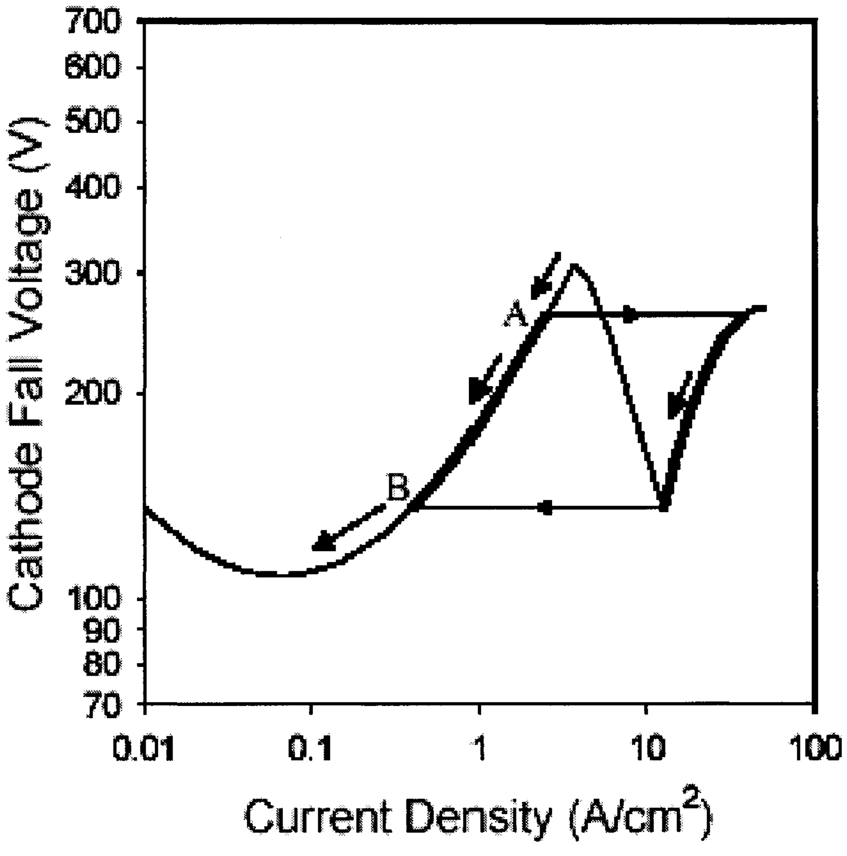

Fig 6.11 Transitions in discharge current density when the discharge mode is changed from the abnormal cathode fall mode to the normal cathode fall mode. In the voltage range from A to B the current density is double-valued [69].

force the V-J characteristic to change its slope. This change will occur when the surface temperature reaches the melting temperature of the cathode. For molybdenum, this is at T = 2,896 K. At this temperature, additional thermal energy is required to cause the phase transition from solid to liquid at the cathode surface. It can be expected that the additional loss of energy caused by the phase transition (latent heat) at the melting point causes a reversal in the slope of the voltage-current density characteristics. The variable parameter is the current density, since the area covered by the plasma is assumed to be constant. However, when we reach values of the current density where thermal effects become dominant and glow-to-arc transition (the current density at the onset of negative differential conductance) sets in, this assumption does not hold. For this range, which is characterized by the formation of filaments, i.e. a contraction of the plasma, a two dimensional treatment of the plasma is needed.

This model explains the presence of two stable regions in one cathode layer discharge. We are not able to explain the mechanism that leads to the regular pattern (self-organization). The mechanism for self-organization, the development of regularly placed plasma filaments, might also be due to thermal conduction as the loss process. Stability of the filaments with increasingly smaller diameters requires an increasing radial flow of thermal energy away from the micro-cathode spots. In order to satisfy the stability condition, the distance between filaments needs to be small such that the radial energy losses reach the level required for stable operation. This could be an explanation for the observed spatial distribution of filaments.

CHAPTER VII

SUMMARY AND CONCLUSIONS

7.1 MHCD Arrays / Parallel operation

The voltage-current (V-I) characteristics of microhollow cathode discharges show three distinct modes of operation: (1) the Townsend mode at low currents; (2) the hollow cathode discharge and normal glow discharge modes, which have negative or flat I-V slopes; and (3) a mode at high currents with a V-I characteristic which resembles that of an abnormal glow discharge with a positive dV/dI.

In the Townsend discharge mode, the electric field in the gap is not distorted by the space charge. The Townsend discharge is characterized by a high operation voltage and a positive I-V slope. The positive differential resistance in this mode allows us to operate microhollow cathode discharges in parallel without individual ballasting. Stable DC parallel operation of MHCDs in Ar and Xe gas were achieved up to pressures of 400 Torr. In this mode, the current per discharge is on the order of several micro-ampere to several hundred micro-ampere. The electrode geometry could be simplified by using a metal mesh cathode and a planar anode separated by an alumina spacer with an opening. For its low current density operation, it has been run for more than 24 hours continuously.

When the discharge operates at higher current, the sustaining voltage drops due to the hollow cathode effect and the discharge quickly enters the normal glow discharge mode. In this mode plasma extends over the cathode surface around the cathode hole. With increasing current the discharge voltage stays almost constant. Only single discharge operation is possible in this mode because of the flat differential resistance (dV/dI). To generate large-area excimer sources, single MHCDs were operated with current up to 55 mA and pulse mode was used to avoid destroying the sample [7]. A two millimeter square plasma has been generated in Xe with UV radiant density up to 15.2 w/cm^2 [7]. Multiple discharge operation requires ballasting each discharge. A distributed ballast electrode geometry with a semi-insulating silicon instead of an anode allows us operate MHCDs in parallel in normal glow mode [60]. For a large array the power consumption on the resistive electrode could be troublesome.

If the current increases to a value in which all the cathode surface is covered by plasma, the discharge transfers into an abnormal glow discharge, characterized by a positive differential resistance. In this mode it is possible to operate the MHCDs in parallel without individual ballast. But for the normal open cathode hole geometry, the cathode is so large that the sample will be destroyed before it reaches the current for abnormal glow discharge. To force the discharge to transfer to abnormal glow discharge at low current, the cathode surface must be reduced.

There are two ways to reduce the surface of MHCD. One is using a dielectric layer to cover the surface of the cathode surrounding the hole, leaving the circular surface of the cathode hole exposed. In this approach, the I-V characteristic is positive after a low onset current value (below 1 mA for most pressures). A 5X5 array discharge was operated with this method in different gases at pressures up to 400 Torr.

The other way is to use a closed-end cathode hole and leave the end on the anode side open. The anode and dielectric could both have the same desired opening pattern around the cathode holes. Then the plasma will cover the cathode surface beyond a critical current value. This configuration makes the discharge resistance on the order of several kΩ. Linear and two-dimensional arrangements both were successful in generating MHCDs arrays. The development of a radiant emission distribution in both the visible and the UV shows that homogenous plasma is established with increasing current. It was found that the highest total optical power levels in Xe at wavelength near 172 nm was reached for pressures in excess of 400 Torr. Highest excimer radiant emittance generated from a 1 cm long string discharge reaches 370 mW at 30 mA in 600 Torr Xe. This corresponds to a power density over 18 W/cm^2. The efficiency reaches 10% for dc operation. After running the discharge in this geometry for more than 5 hours, the excimer radiant emittance retained 60% of its initial level. A 10X10 MHCD array patterned discharge with radiant area of 1 cm^2 was fabricated and operated in 300 Torr Xe at current 60 mA.

7.2 Series operation of MHCDs

Series discharges were generated in a three-electrode sandwich arrangement, which allowed us to study both single discharges as well as tandem discharges (discharges arranged in series). The center electrode has a limited ring-shaped surface given by the hole radius and the foil thickness. Therefore, the discharge for configuration with center electrode as cathode is, at high currents, an abnormal glow discharge with a resistive characteristic. In the configuration, where the outer electrode serves as a cathode, the cathode fall can expand over the outer surface. The discharge in this case behaves as a normal glow discharge, with constant voltage at increasing current. The differences in optical power observed from opposite end-on directions are due to the excimer source locating at the cathode.

Forming longitudinal arrays consisting of a multi-electrode sandwich structure alternative-biased the metal foils (electrodes) is possible. In a multi-electrode configuration all the electrodes, anodes and cathodes, would be limited in surface area, due to the dielectric spacers between them. Consequently any of the discharges in this multi-electrode system would be abnormal, with resistive discharge characteristics (at higher currents), the condition for stable operation without individual ballast. Due to the negligible reabsorption of excimer radiation in the excimer gas, the irradiance generated by such a string on the axis of the hollow would for n discharges be n times that of a single discharge. Powerful flat panel excimer lamps can be generated by operating these discharge strings in parallel.

Another application for a string of discharges would be as a micro-laser medium. With gain conditions as described discharges in chapter V, lasing should be achievable if sufficient discharges are placed along the line of sight. Such lasers will be small in size (cm range) and able to operate in direct current.

7.3 CBL microdischarges

Cathode Boundary Layer Discharges (CBL) are direct current glow discharges between a flat thin cathode and an annual anode, which is placed within cathode fall region to restrict the cathode area. CBL discharges were found to be stable up to atmospheric pressure. The discharge regions seem to be reduced to only cathode fall and negative glow, with the negative glow serving to conduct the current to the anode. The CBL discharge voltage–current density (V-J) characteristic was found to have a positive slope over most of the current range, indicating that parallel operation of these discharges is possible without using individual ballast resistors. This means, that it is possible, using such electrode configurations, to generate extended plasma layers of thickness on the order of 100 μm at high pressure as flat excimer sources. The maximum diameter of the anode opening is limited in several millimeters, since the discharge will become unstable when the current density at the circumference reaches a critical value.

7.4 Self-organization in CBL microdischarges

When the current in CBL discharges is lowered below a critical value, homogeneous plasma layer will transit to a structured plasma. The plasma patterns are filament structures arranged in concentric circles. The number of filaments depends on the pressure and current. The structures are most distinct at pressures below 200 Torr. With increasing pressure, the density of the filaments increases and the structure becomes more irregular. To operate the discharge in patterned mode, it is required to run the discharge in a higher current first and then reduce the current. For low-pressure operation ($p < 200$ Torr), it was not possible to reach a discharge state with a higher number of filaments from a state with fewer.

The existence of self-organized patterns requires that at least two stable discharge modes of different current density exist at the same voltage. For conventional glow discharges, only one stable mode exists, i.e. the abnormal glow. With increasing current density, the abnormal glow transfers into an arc. In ref 75 this glow-to-arc transition was modeled by considering thermal electron emission from the cathode and the secondary electron emission. And secondary electron emission is generally assumed to be the major process of electron generation in glow discharges at the cathode. We have extended this model by including an additional thermal process, i.e. heat conduction into the cathode.

This energy loss process will, under certain circumstances, result in a second stable region in the glow discharge characteristic. The condition for stability is that the thermal energy is efficiently removed from the cathode by forced cooling. Considering the thickness of our cathodes, 250 μm, this is easily possible. Convection at higher temperature might already satisfy this condition of forced cooling. The condition that energy is removed from the plasma at such a rate that the temperature and, consequently, the thermal electron emission rate decreases for a certain range of operation is also given when the surface temperature reaches the melting point of the material.

We are not able to explain the observed self-organization so far. However, increased thermal losses, which cause stabilization, may explain the effect of pattern formation in the discharge. The increased radial heat flow from the cathode spot of an individual filament with increasingly smaller diameter might be the reason for self-organization. Sufficiently large thermal energy losses through radial conduction, a necessary condition for filament stability, require minimum separation between filaments. This separation is determined by the radial temperature distribution around the filaments.

7.5 Conclusions

Microhollow cathode discharge arrays can be generated in all discharge modes. For discharge modes where the current-voltage characteristic has a negative slope (hollow cathode discharge mode) or is flat (normal glow discharge mode) it is possible to generate arrays by using distributed resistive ballast. Using etching methods in silicon as electrode material seems to allow the manufacturing of large systems. If operated in discharge modes where the V-I characteristic has a positive slope, the discharge can be operated in parallel without individual ballast. Operating in the Townsend discharge mode requires reducing the current to small values such that space charge effects are negligible (generally < 1mA per discharge). Although the radiant efficiency can reach 9% in this mode, the irradiance is generally low for some application, and the pressure range is limited under 400 Torr. Operating in abnormal glow discharge mode requires limiting the cathode surface area. MHCD arrays with limited cathode surface can be operated up to atmospheric pressure. Besides the high power density (18.5 W/cm^2), the highest UV radiant efficiency reaches 6-9%, similar to single MHCD. Large area even patterned MHCD arrays can be easily manufactured by means of dielectric coating. The problem when operating in this mode (abnormal glow) is the reduced lifetime due to the electrode erosion at elevated current densities. By extending the MHCD to CBL discharge, the electrode structure can be further simplified. The positive V-J characteristic of CBL discharge indicates the possibility of generating CBL discharge arrays. MHCD array in series can produce higher excimer irradiance. Stimulated amplify emission is possible when enough MHCDs operate in series.

REFERENCES

1. B. Eliasson, H. Esrom, and U. Kogeschatz, *ABB Review*, **3/91**, 21 (1991).

2. K. H. Schoenbach, R. Verhappen, T. Tessnow, and F.E. Peterkin, W.W. Byszewski, *Appl. Phys. Lett.* **68**(1), 13-15 (1996).

3. K. H. Schoenbach, A. El-Habachi, W. Shi and M. Ciocca, *Plasma Sourcees Sci. Technol.* **6**, 468-477 (1997).

4. A. El-Habachi and K. H. Schoenbach, *Appl. Phys. Lett.* **72**(1), 22-24 (1998).

5. J. W. Frame, D. J. Wheeler, T. A. DeTemple, and J. G. Eden, *Appl. Phys. Lett.* **71**, 1165 (1997).

6. K. H. Schoenbach, A. El-Habachi, M. Moselhy, W. Shi, and R. H. Stark, *Physics of Plasma*, **7**(5), 2186 (2000).

7. M. Moselhy, W. Shi, R. H. Stark, and K. H. Schoenbach, *Appl. Phys. Lett.* **79**(9), 1240 (2001).

8. U. Kogelschatz, B. Eliasson, and W. Egli, *J. Phys.* **IV** 7, 47 (1997).

9. E. Kauer and E. Schnedler, *Moglichkeiten und Grenzen der Lichterzeugung Phys Bl*, **42**, 128 (1986).

10. B. Eliasson and U. Kogelschatz, *IEEE Trans. Plasma Sci.* **19**, 309 (1991).

11. R. J. Carman and R. P. Mildren, *J. Phys. D: Appl. Phys.* **36**, 1 (2003).

12. F. Vollkommer and L. Hizschke, *Proceedings of the Eighth International Symposium on the Science and Technology of Light Sources*, August 30-September 3, 1998, Greifswald, Germany, 1998, LS-8, p51.

13. Osram XERADEX Excimer Discharge Lamp, http:// www. sylvania.com

14. R. Mehnert, *UV and EB Curing Technolohy and Equipment,* John Wiley/SITA, 83 (1999).

15. R. Mehnert, *Proc. RadTech Europe,* **99**, 303 (1999).

16. J. Y. Ahang, G. Windall and I. W. Boyd, *Appl. Surf. Sci.* **186**, 568 (2002).

17. I. W. Boyd, J. –Y. Zhang and U. Kogelschatz, "Development and Applications of UV Excimer Lamp", Photo-Excited Processes, Diagnostics and

Applications, A. Peled, Ed., Kluwer Academic Publishers, The Netherlands, 161(2003).

18. H. Esrom and U. Kogelschatz, *Thin Solid Films*, **218**, 231 (1992).

19. M. Laroussi, *IEEE Trans. Plasma Science*, **24**, 1188-1191 (1996).

20. T. C. Montie, K. Kelly-Wintenberg, and J. R. Roth, *IEEE Trans. Plasma Science*, vol. **28**, 41-50 (2000).

21. H. Herrmann, I. Henins, J. Park, and G. S. Selwyn, *Phys. Plasmas*, **6**, 2284-2289 (1999).

22. M. Moisan, J. Barbeau, S. Moreau, J. Pelletier, M. Tabrizian, and L'H. Yahia, *International Journal of Pharmaceutics*, **226**, 1-21 (2001).

23. Ch. K. Rhodes, *Topics on Applied Physics: Excimer lasers,* Springer-Verlag, New York, 1984.

24. W. M. Hughes, J. Shannon and R. Hunter, *Appl. Phys. Lett.* **24**, 488 (1972).

25. P. W. Hoff, J. C. Swingle and C. K. Rhodes, *Appl. Phys. Lett.* **23**, 245 (1973).

26. H. A. Koehler, L. J. Ferderber, D. L.Redhead and P. J. Ebert, *Appl. Phys. Lett.* **21**, 198 (1972).

27. R. M. Waynant, *Appl. Phys. Lett*, **30**, 234 (1977).

28. J. M. Hoffman, A. K. Hays and G. C. Tisone, *Appl. Phys. Lett*, **28**, 538 (1976).

29. J. R. Murray and H. T. Powell, *Appl. Phys. Lett*, **29**, 252 (1976).

30. J. J. Ewing and C.A. Brau, *Appl. Phys. Lett*, **27**, 350 (1975).

31. S. K. Searles and G. A. Hart, *Appl. Phys. Lett.* **27**, 243 (1975).

32. C.A. Brau and J. J. Ewing, *Appl. Phys. Lett.* **27**, 435 (1975).

33. J. H. Parks, *Appl. Phys. Lett.* **31**, 297 (1977).

34. H. T. Powell, J. R. Murray and C. K. Rhoodes, *Appl. Phys. Lett.* **25**, 730 (1974).

35. W. M. Hughes, N. T. Olson and R. Hunter, *Appl. Phys. Lett.* **28**, 81 (1976).

36. B. Gellert and U. Kogelschatz, Appl. *Phys. B.* **52**, 14-21(1991).

37. B. Elliasson and U. Kogelschatz, Appl. Phys. B **46**, 299 (1988).

38. D.C. Lorents: *Physica* **82**C, 19 (1976).

39. C. W. Werner, E. V. George, P.W. Hoff, C. K. Rhodes: *IEEE J. QE* **13**,769 (1977).

40. K.T. Gillen, R. P. Saxon, D. C. Lorents, G. E. Ice, R. E. Olson, *J. Chem. Phys.* **64**, 1925 (1976).

41. E. Ellis, N. D. Twiddy, *J. Phys. B*2, 1366 (1969).

42. A. H. Futch, F. A. Grant, Phys, Rev. **104**, 356 (1956).

43. N. Thonnard, G. S. Hurst, *Phys. Rev.* A**5**, 1110 (1972).

44. J. W. Keto, R. E. Gleason, G. K. Walters, *Phys. Rev. Lett.* **33**, 1375 (1974).

45. D. Lindau and H . F. Doebele, *Rec. Phys. Instrum.* **59**, 525 (1988).

46. R. S. Taylor, K. E. Leopold and K. O. Tan, *Appl.Phys. Lett.* **59**, 525 (1991).

47. V. S. Skakun, M. I. Lomaev, V. F. Tarasenko, D. V. Shitts, G. L. Johnson and F. T. Wang, *Laser Particle Beams*, **21**, 115 (2003).

48. R. Stark and K. H. Schoenbach, *J. Appl. Phys.* **85**, 15(1999).

49. A. H. Mohamed, R. Block, and K. H. Schoenbach, *IEEE Trans. Plasma Sci.* **30**, 182 (2002).

50. M. Salvermoser and D.E. Murnick, *J. Appl. Phys.* **94**, 15 (2003).

51. F.Paschen, *Ann.Physik* **50**, 901 (1916).

52. G. Schaefer and K. H. Schoenbach, *Physics and applications of pseudo sparks*, Plenum Press, New York, 55 (1990).

53. H. Helm, *Z. Naturforschung*, **27A**, 1812 (1972).

54. J. W. Gewartowski, H. A. Watson, *Principles of Electron Tubes*, Princeton, N. J., Van Nostrand, 65 (1965).

55. F. W. Aston, *Proc. R. Soc*, **A79**, 80 (1907).

56. A. D. White, *J. Appl. Phys.* **30**, 711 (1959).

57. D. J. Sturges and H. J. Oskam, *Appl. Phys.* **35**, 2887 (1964).

58. A. Fiala, L. C. Pitchford and J. P. Boeuf, *Proc. XXII Conf. Phenomena in Ionized Gases*, Hoboken, 191 (1995).

59. K. H. Schoenbach, M. Moselhy, W. Shi, and R. Bentley, *J. Vac. Sci. Technol*, A **21**(4), 1 (2003).

60. W. Shi, R. H. Stark, K. H. Schoenbach, *IEEE Trans. On Plasma Sci.* **27**, 16 (1999).

61. T. Paul, R. Hartmann, J. Heberlein, W. Shi, R. Stark, and K. H. Scheoenbach, *Proc. International Thermal Spray Conference*, Essen, Germany, March, ASM International, 23 (2002)

62. J. A. R. Samson *Techniques of Vacuum Ultraviolet Spectroscopy,* Licoln, NE: Pied, 212 (1980).

63. A. El-Habachi, *Microhollow Cathode Discharge Excimer Lamps* PhD disseration, Old Dominion University (1998).

64. B.G. Salmov, S.Ellialtiglu, B. G. Akinoglu, N. N. Lebedeva, and L.G. Patriski, J Phys.D: *Appl.Phys.*, **29**, 628-633 (1996).

65. S. J. Park, J. Chen, C. Liu, and J. G. Eden, *Appl.Phys.Lett.* **78**, 419 (2001).

66. M. Moselhy, W. Shi, R. H. Stark, K. H. Schoenbach, *IEEE Trans. Plasma Sci.* **30**, 198 (2002).

67. A. El-Habachi, W. Shi, M. Moselhy, R. Stark, and K.H. Schoenbach, *J. Appl. Phys.* **88**, 3220 (2000).

68. J. T. Verdeyen, *Laser Electronics*, 3rd ed. Prentice-Hall, Englewood Cliffs, NJ, 1995, p.414.

69. K. H. Schoenbach, M. Moselhy and W. Shi, *Plasma Sources Sci. Technol.* **13**, 177 (2004).

70. M. Mosrlhy and K. H. Schoenbach, *J. Appl. Phys.* **95**, 1642 (2004).

71. E. L. Koschmieder, *Benard convection Advances in Chemical Physics*, **26**, ed I Prigogine and S. A. Rice, Chichester: Wiley, 177-212 (1974).

72. U. Kogelschatz, *IEEE Trans. Plasma Sci.* **30**, 1400 (2002).

73. W. Breazeal, K. M. Flynn and E. G. Gwinn, *Phys. Rev. E*, **52**, 1503(1995).

74. J. D. Cobine, *Gaseous Conductors: Theory and Engineering Applications*, New York: Dover, 1958.

75. A. V. Engel and M. Steenbeck, *Elekrische Physik u. Technik*, **1** and **2**, Berlin:Springer, (1932/1934).

76. Yu. D. Korolev and G. A. Mesyats, *Physics of Pulsed Breakdown in Gases*, Ekaterinburg: URO-Press, (1998).

77. Yu. D. Raiser, *Gas Discharge Physics*, Berlin: Springer, (1997).

APPENDIX

Optical Gain Measurement on Microhollow Cathode Discharges

Theoretical calculation predicted that microhollow cathode discharge (MHCD) is well suited for excitation of microlaser [67]. To explore the evidence of excited stimulated emission from MHCDs, we have done experiment to measure the gain on 308 nm emission of a XeCl discharge. In the experiment a sample MHCD was optically excited by another MHCD, which was placed close enough to transmit some 308 nm UV light through the sample discharge. By measuring the UV radiation intensity change when it passes through the sample MHCD, we can find the gain or absorption coefficient.

The test system consisted of two sets of single MHCD electrodes aligned through the micro-hollow cathode as shown in the Fig. A1. All the electrodes were 100 μm thick molybdenum foils, and the dielectric spacers between cathode and anode were 250 μm thick alumina sheets. Both of the micro-hollows were 100 μm in diameter. The sample MHCD was covered with alumina sheets on both cathode and anode sides. The two MHCD were placed about 700 μm apart. An RS Princeton Instruments ICCD-MAX intensified charge coupled device (CCD) camera was used to image the radiation from the system. The UV excimer radiation was separated from all other radiation by using an UV filter with a peak transmittance at a wavelength of 307.3 nm and a full width at half maximum (FWHM) of 24.4 nm. A fused silica lens was used to focus the UV radiation on the ICCD camera. The UV emission power was obtained by integrating the intensity of images.

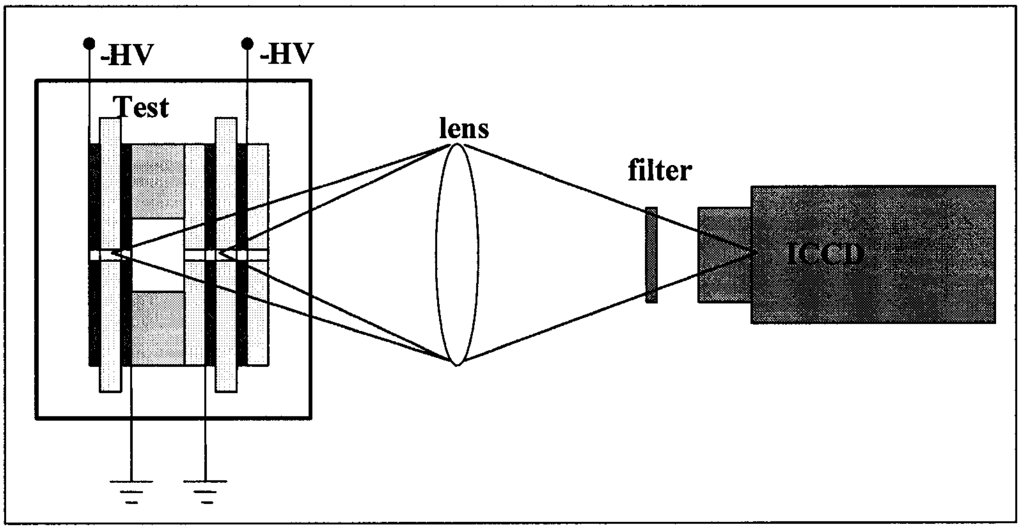

Fig A.1 Test sample geometry and experimental setup.

The two MHCDs were individually ballasted and powered by two high voltage suppliers. To prevent coupling between the two discharges, all currents through the discharges were monitored to ensure that the anode current equals the cathode current. During the gain measurement, both discharges were kept at the same current value.

The first step was to measure the excitation optical power passing through the sample microhollow. During this time the sample MHCD was not sustained. Then, with the excitation MHCD off, the sample MHCD was operated and the UV emission of this discharge was recorded. The last step was to measure the UV intensity with both MHCDs operating. The gain is calculated as

$$g = \frac{I_{both} - I_{ex} - I_{bk}}{I_{ex}} \tag{A.1}$$

where I_{ex} is the intensity from the excitation MHCD only, I_{bk} from the sample MHCD only, and I_{both} from both MHCDs.

The set of test results is shown in Fig A.2 with an image of the discharges. The measurements indicated UV emission increases by 5% to 15% when it passes through a MHCD. This could be an evidence of stimulated emission on the XeCl discharge. But if we assume the plasma column is about 350 μm, the gain will be about 1 to 3 /cm, which is too high compare with theoretical calculation (0.38/cm) [7]. This may indicate that coupling between the two discharges was possible. Further experiment with isolated excitation source and longer sample plasma column need to be done.

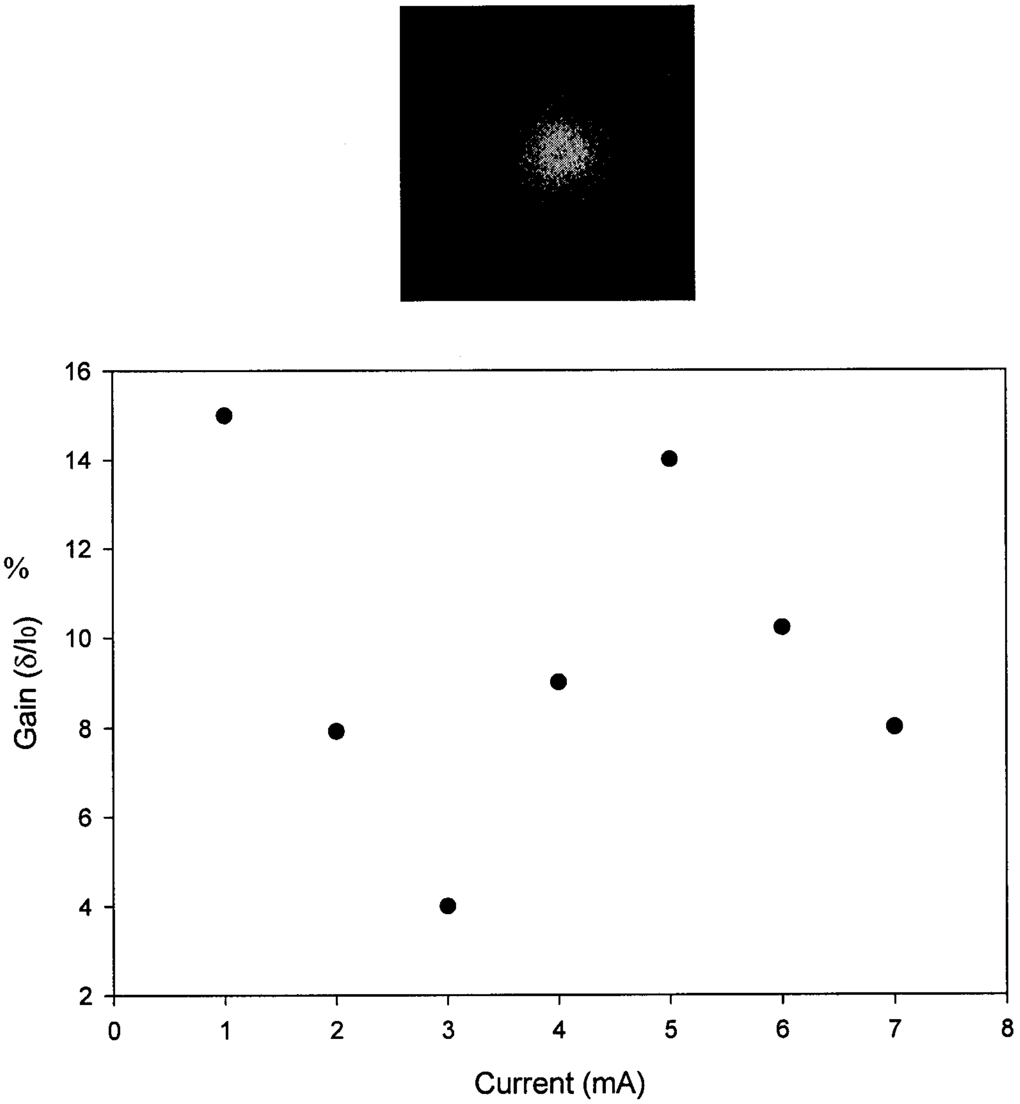

Fig. A.2 Image of XeCl discharge and gain vs current of discharges in XeCl 1000 Torr.

VITA

WENHUI SHI

Education:

Doctor of Philosophy (Electrical Engineering), Old Dominion University, Norfolk, Virginia May 2004

Master of Science (Electrical Engineering), Old Dominion University, Norfolk, Virginia August 1998

Bachelor of Science (Laser Physics), Chungchun Institute of Optics & Fine Mechanics, Changchun, China July 1987

Experience:

Optical Scientist May 2002 - Present
Science & Engineering Services, Inc, Columbia, Maryland

Research Assistant August 1996 - May 2002
Physical Electrical Research Institute, Department of Electrical Engineering, Old Dominion University, Norfolk, Virginia

Laser Engineer September 1992 – August 1996
Mars Opto-electronics Company, Wuhan, China

R&D Engineer September 1987 – September 1992
Wuhan Optics Research Institute, Wuhan China

Publication:

"High-pressure hollow cathode discharges," Plasma Sources Technol. 6, 468 (1997).

"Parallel operation of microhollow cathode discharges," IEEE Trans. Plasma Sci. 27, 16 (1999).

"Microhollow cathode discharge excimer lamps," Phys.Plasma, 7, 2186 (2000).

"Series operation of direct current xenon chloride excimer sources," J.Appl. Phys. 88, 3220 (2000).

"Xenon excimer emission from pulsed microhollow cathode discharges," Appl. Phys. Lett. 79, 1240 (2001).

"A flat glow discharge excimer radiation source," IEEE Trans. Plasma Sci.30, 198 (2002).

"Microhollow cathode discharges," J. Vac. Sci, Technol. 24, 1 (2003).

"Self-organization in cathode boundary layer microdischarges," Plasma Sources sci.Technol. 13, 177 (2004).